WSKAZÓWKI DOTYCZĄCE PRZYGOTOWANIA ARTYKUŁÓW

- Artykuły przeznaczone do opublikowania w kwartalniku „Technologia i Automatyzacja Montażu" powinny mieć oryginalny i naukowo-techniczny charakter i być zgodne z problematyką czasopisma. Redakcja przyjmuje artykuły w jęz. polskim, jęz. angielskim i jęz. rosyjskim.
- Artykuł o maksymalnej objętości 5 stron A4 wraz z ilustracjami powinien być napisany czcionką Times Roman lub Arial 12 pkt, z interlinią 12 pkt. Formatowany tekst nie powinien mieć podziału na kolumny.
- Tytuł artykułu należy podać w jęz. polskim i jęz. angielskim. Tytuł nieprzekraczający 10 słów powinien odzwierciedlać istotne elementy treści artykułu.
- Struktura artykułów naukowo-technicznych prezentujących prace autora(ów) powinna być następująca: wstęp (wprowadzenie); metodyka (badań, analiz, pracy z podaniem ewentualnie materiałów, założeń itp.); wyniki (badań, analiz); omówienie wyników; wnioski; spis literatury.
- Podpisy pod ilustracjami oraz tytuły tablic należy podać w jęz. artykułu i jęz. angielskim.
- Ilustracje należy dołączyć również jako osobne pliki w formacie: .jpg, .tiff, z rozdzielczością co najmniej 300 dpi. Wszystkie zamieszczane ilustracje powinny być własnością autora(ów) lub należy podać źródło pochodzenia rysunków.
- Wzory matematyczne pisane w edytorze równań Microsoft Equation i powinny być oznaczane kolejnym numerem w nawiasie okrągłym. Wszystkie symbole powinny być objaśnione. Należy stosować jednostki układu SI.
- Spis literatury należy podać w kolejności cytowania w tekście, a odnośniki w tekściepo winny być ponumerowane cyframi arabskimi i umieszczone w nawiasach kwadratowych. W przypadku korzystania z Internetu należy podać adres strony i datę odczytu. Liczbę autocytowań należy ograniczyć do niezbędnych.
- Do artykułu należy dołączyć streszczenie w jęz. artykułu i jęz. angielskim, zawierające minimum 200–250 słów.
- Pod streszczeniem należy podać 3–6 słów kluczowych w jęz. artykułu i jęz. angielskim, zwracając uwagę, by nie były one powtórzeniem tytułu pracy.
- Po spisie literatury zaleca się podanie źródła finansowania pracy.
- Na końcu artykułu należy podać: imiona i nazwiska autorów, tytuły naukowe lub zawodowe, telefon, faks, e-mail, miejsce zatrudnienia wraz z adresem do korespondencji.

PROCEDURA RECENZOWANIA

Procedura recenzowania artykułów w czasopiśmie jest zgodna z zaleceniami Ministerstwa Naukii Szkolnictwa Wyższego zawartymi w opracowaniu „Dobre praktyki w procedurach recenzyjnych w nauce", Warszawa 2011.

Wszystkie artykuły naukowo-techniczne publikowane w kwartalniku „Technologia i Automatyzacja Montażu" są recenzowane.

Nadesłane artykuły są poddawane redakcyjnej ocenie formalnej i otrzymują numer redakcyjny, identyfikujący je na dalszych etapach procesu wydawniczego, a redakcja wysyła do autorów informację o przyjęciu artykułu i wysłaniu go do recenzentów. Do oceny każdej publikacji powołuje się co najmniej dwóch niezależnych recenzentów. Redakcja dobiera recenzentów rzetelnych i kompetentnych w danej dziedzinie. Nadesłane artykuły nie są nigdy wysyłane do recenzentów z tej samej placówki, z której pochodzi autor. Prace recenzentów są poufne i anonimowe. Recenzja musi mieć formę pisemną i kończyć się jednoznacznym wnioskiem o dopuszczeniu artykułu do publikacji w czasopiśmie lub jego odrzuceniu. W przypadku pracy w języku obcym, co najmniej jeden z recenzentów jest afiliowany w instytucji zagranicznej innej niż narodowość autora pracy. Autorzy są informowani o wynikach recenzji oraz otrzymują je do wglądu. W sytuacjach spornych redakcja powołuje dodatkowych recenzentów.

Lista recenzentów publikowana jest w ostatnim zeszycie każdego rocznika.

**Kwartalnik „Technologia i Automatyzacja Montażu"
ukazuje się formie elektronicznej w otwartym dostępnie
(Open Access) i jest dostępny na Portalu Informacji
Technicznej Wydawnictwa SIGMA-NOT
www.sigma-not.pl**

CONTENTS / W NUMERZE

CHANGE IN THE EDITOR IN CHIEF POSITION OF THE QUARTERLY

Editorial Board of TiAM

Dear Authors and Readers,

On July 1st there was a change in the position of editor in chief of the quarterly „Technologia i Automatyzacja Montażu" ("Assembly Techniques and Technologies"). The position was taken by Katarzyna Antosz, Ph.D. D.Sc. Eng., Associate Professor from Rzeszow University of Technology, who replaced the former editor in chief Prof. Jerzy Łunarski, Ph.D. D.Sc. Eng.

The Editorial Board of the journal and its associates would like to sincerely thank Prof. Jerzy Łunarski for his remarkable contribution into the development of the journal. It was at the request of Prof. Jerzy Łunarski, which was submitted through OBR PTiKM TEKOMA Warszawa, that in 1993 a nationwide scientific and technical quarterly entitled „Technologia i Automatyzacja Montażu" was founded. Prof. Jerzy Łunarski was editor in chief for 27 years.

At the same time, showing gratitude for his efforts and commitment to creating the journal, we would like to present scientific and research achievements of Professor and his organisational accomplishments related not only to the activities of the journal.

The professional life of Professor Jerzy Łunarski is mainly related to Rzeszow University of Technology, with which he has been associated since 1964 (he worked in Huta Stalowa Wola and WSK Rzeszów before). At that time in the then Wyższa Szkoła Inżynierska (University of Engineering) in Rzeszów he started his job at the Department of Machine Technology as a senior assistant. In 1973, holding a doctorate degree, Jerzy Łunarski was appointed a head of the newly created Department of Machine Technology (ZTM). The department, then transformed into the Department of Manufacturing Processes and Production Organisation (now Department of Manufacturing Processes and Production Engineering) was headed by him up to 2007.

Apart from, being the Head of the Department, Prof. Jerzy Łunarski undertook numerous organizational and research tasks. He held various functions in the statutory bodies of the University and the Department. He was also the Scientific Secretary (deputy head of

science and research at OBR TEKOMA), a member of the Scientific Council (by choice) and the IMBIGS Warszawa Committee of Experts, a member of technical board of No. 6 "Quality Management" in PKN, a reviewer and opinion-giver of the scientific, didactic and development papers commissioned to him, and is still a member of the Academy of Engineering in Poland.

Professor was also the chairman of the Organisational Boards of 39 scientific and technical conferences nationwide and international in the field of machine technology and assembly techniques organized by Rzeszow University of Technology together with OBR TEKOMA, and then IMBIGS Warszawa. He initiated and edited many team papers, of a guide and monographic nature, providing guidance for designers, experimenters and operational staff. These include: „Automatyzacja procesów technologicznych montażu maszyn" (ed. WNT), „Automatyczne orientowanie w procesach montażu" (RUT), „Układy podawania w systemach automatycznego montażu" (WUT), „Konstrukcyjne połączenia klejowe elementów metalowych w budowie maszyn" (RzUT), „Prasowanie radialne w procesie kształtowania i łączenia małych elementów maszyn" (RzUT) and other.

He is the author of a number of monographic academic and scientific textbooks on various issues on production management, such as: „Zarządzanie jakością − standardy i zasady" (WNT 2008, 2012), „Techniczno-organizacyjne aspekty konkurencyjności − samoocena i doskonalenie" (RzUT 2008), „Zarządzanie technologiami − ocena i doskonalenie" (RzUT 2009), „Systemy jakości, normalizacji i akredytacji w zarządzaniu organizacjami" (RzUT 2009), „Zarządzanie jakością w logistyce" (RzUT 2009), „Inżynieria systemów i analiza systemowa" (RzUT 2010), „Zintegrowane systemy zarządzania − wspomaganie systemów zarządzania systemami standardowymi" (RzUT 2011), „Projektowanie procesów −technicznych, produkcyjnych i gospodarczych" (RzUT 2012, 2014), „Normalizacja i standaryzacja" (RzUT 2014), „Certyfikacja − w działalności gospodarczej i rozwojowej" (IMBIGS 2015), „Innowacje

technologiczne w przedsiębiorstwach – projektowanie, wdrażanie i użytkowanie" (IMBIGS 2016).

He received many awards and distinctions for his work i.e. the Honorary Professor of the Rzeszow University of Technology, Golden Cross of Merit, Medal of National Education, Meritorious for Rzeszow Voivodeship, Meritorious for Rzeszow University of Technology, Golden Badge of the Institute of Mechanised Construction and Rock Mining in Warsaw, Award of the Mayor of Rzeszów, Polish Quality Award in science and a number of diplomas and other awards.

Thank You very much again!

As a new editor in chief of the journal, I express my gratitude for Professor Jerzy Łunarski and IMBIGS Warszawa for their confidence in me and for entrusting me with such a distinguished position. For many years I have actively been involved in the work related to the quarterly – I was a member of the editorial board as a thematic editor in the field of reliability and maintenance.

Continuing the intention of prof. Jerzy Łuarski, I accept the commitment to further develop the quarterly. At the same time, I encourage you to disseminate information about the journal and to publish on its pages.

PROBLEMATIC ASPECTS OF NUMERICAL COMPUTATION OF THE HYBRID JOINTS

Problematyka obliczeń numerycznych połączeń hybrydowych

Marek ROŚKOWICZ   ORCID 0000-0003-0501-0622

Jarosław GĄSIOR   ORCID 0000-0003-3205-0486

A b s t r a c t: This paper presents the results of numerical calculations to compare the stress fields of hybrid (mechanical-adhesive) joints. ANSYS ver.19 was used as a computing tool with its solver based on finite element method (FEA – Finite Element Analysis). Based on the results obtained, a comparative analysis of the stresses in the adhesive joints for adhesives with different Young's modulus including different mounting schemes of mechanical fasteners and pressures caused by the assembly of the mechanical fasteners was performed. For modelling purposes of hybrid joints it is assumed that calculations will be made for single-lap joints where specimens with AW 2024T3 material parameters were joined. The adhesive layer was modelled by two layers of elements, adding i.a. pressure to the adherend caused by a preliminary tension of mechanical fasteners. In order to reduce the negative peeling effect at the ends of the adhesive layer, the case of mounting mechanical fasteners closer to the joint edge was also considered – at a distance of one diameter of the fitting instead of two. It has been found that using adhesive with lower value of Young's modulus can increase the load capacity of the joints due to possibility of absorbing higher loading by the mechanical fasteners. Moving the mechanical fasteners closer to the lap edge will result in a positive reduction of stress responsible for peeling of adhesive layer, as well as the pressure caused by the assembly of the bolts.

K e y w o r d s: hybrid joints, hybrid joint modelling, numerical computation of hybrid joints stress distribution in adhesive layer

S t r e s z c z e n i e: W pracy zaprezentowano rezultaty obliczeń numerycznych, których celem było porównanie pól naprężeń występujących w połączeniach hybrydowych (mechaniczno-klejowych). Jako narzędzie obliczeniowe wykorzystano aplikację Ansys v.19 opartą na metodzie elementów skończonych – MES (ang. FEA – Finite Element Analysis). Na podstawie otrzymanych wyników wykonano analizę porównawczą naprężeń występujących w spoinach połączeń adhezyjnych dla klejów o różnym module Younga, dla różnej geometrii montażu łączników oraz dla przypadku z uwzględnieniem nacisków wywołanych montażem łączników mechanicznych. W modelowaniu połączeń hybrydowych przyjęto, że obliczenia zostaną wykonane dla połączeń jednozakładkowych, w których łączone były elementy o parametrach materiału AW 2024T3. Spoinę połączenia klejowego modelowano jedną warstwą elementów, obciążając ją dodatkowo m.in. naciskami wywołanymi napięciem wstępnym łączników mechanicznych. W celu zmniejszenia negatywnego zjawiska oddzierania występującego na końcach zakładki połączenia adhezyjnego przeanalizowano również przypadek montażu łączników mechanicznych bliżej krawędzi połączenia – w odległości równej jednej średnicy łącznika zamiast dwóch. Stwierdzono, że zastosowanie kleju o mniejszym module może zwiększyć nośność połączeń ze względu na większe wytężenie łączników mechanicznych. Przesunięcie łączników mechanicznych bliżej krawędzi zakładki wpływa pozytywnie na obniżenie naprężeń wywołujących zjawisko oddzierania spoiny klejowej, podobnie jak naciski wywołane montażem śrub.

S ł o w a   k l u c z o w e: połączenia hybrydowe, modelowanie połączeń hybrydowych, rozkład naprężeń w spoinie połączenia adhezyjnego

Introduction

Hybrid joints as a combination of adhesive and mechanical joints are an interesting alternative to joining components made of both metal and composite materials. Especially when connecting components made of polymer composite materials that are more susceptible to bearing stresses than metals, the use of adhesive in addition to mechanical joints allows increasing load capacity joints without damaging composite material as a result of exceeding the allowable pressures. And as aerospace manufacturers are increasingly interested in polymeric composites for airframe construction [19], the problem of effective composite assembly is now up to date.

In addition to the technical problems [4], the assembling of aviation constructions also has formal problems due to limited confidence in the use of adhesive joints in the main structures. There is also a technical barrier for the non-destructive testing of adhesive joints in used machinery effectively (e.g. aircraft) [7]. Therefore, the guidelines defined by the aviation authorities favour the use of hybrid joints instead of just adhesives [10].

Studies on hybrid joints show that they have improved strength characteristics compared to mechanical and adhesive joints in both static and durable area [3, 6, 9].

As the authors of [1, 4, 5, 16, 17] indicate, one of the reason for their increased fatigue life is the lower stress peaks that occur in the vicinity of the assembling holes for mechanical fasteners.

The load capacity and fatigue life of hybrid joints depend on the strength and geometric parameters of the adhesive layer (including the susceptibility of the adhesives to deformation), but also on the arrangement of the mechanical fasteners in the joint. As the experimental interaction between mechanical and adhesive interface parameters in a hybrid joints is burdensome, modern numerical solving tools can be used to optimize the load capacity of the hybrid joints.

The purpose of the calculations was to compare the stress distributions of the hybrid joint for adhesives with different Young's modulus and to evaluate the stress changes in the adhesive layer when the mechanical fasteners were moved closer to the edge of the lap. The calculation also takes into account the effect of the pre-loading caused by the assembly of the mechanical fasteners on the load capacity of hybrid joint. Also, the differences in stress values were assessed if a default tetragonal mesh and a more advanced hexagonal mesh are used to build the numerical model.

Numerical model of joint

The numerical calculations were performed for a single-lap hybrid joint model, made up of two elements with dimensions of 100 x 25 x 2 mm. The length of

the lap was 50 mm and the thickness of the adhesive 0.1 mm. The adhesive was modelled with two layers of finite elements, while the adherends are modelled with five layers of elements. The diameter of the holes for mechanical fasteners is 3 mm. Two fasteners were modelled by placing them over a distance measured from the lap edge to the hole's axis and equal to one mandrel diameter of the fastener (1d) or two diameters (2d). The fastener model had two solutions. In the first solution, it was a single body fitting made up of a 3 mm diameter shank and 5.4 mm diameter heads and 2 mm high (Fig. 1a), while in the second solution it was made up of two parts: the head with the shank and the ring, which being able to move in relation to the shaft of the shank (Fig. 1b). This allows simulating continuous load occurring in the mechanical (bolt) joint after its assembly. Figure 2 shows an example of the geometric model of a hybrid joint created in the ANSYS Workbench Design Modeller with fasteners mounted at 2d distance from the edge of the lap (2d variant).

In addition, in order to assess the influence of the finite elements mesh created in modelling joint on the results obtained, the calculations were performed for the mesh tetra type (tetrahedral) and the hexa (hexahedral) type of mesh. Figure 3 shows the models covered with tetra mesh (a) and hexa mesh (b) prepared for numerical analysis. The tetra mesh is the default grid of finite elements offered to the user by ANSYS Meshing. The main advantage of this type of grid is the relatively small amount of work in the design of the model and the shorter
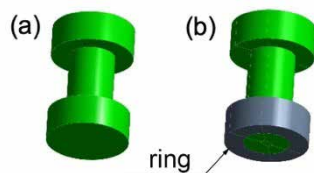
Fig. 1. Geometrical models of mechanical fasteners
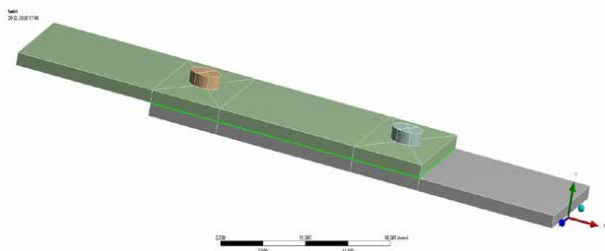
Fig. 2. Example of a geometric model of a hybrid joint in a 2d variant
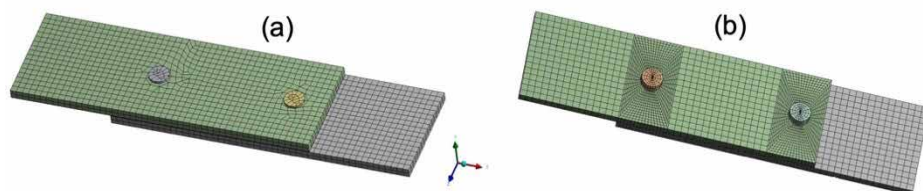
Fig. 3. Models built of Tetra mesh (a) and Hexa mesh (b)

computation time. Therefore, this solution is attractive to users and is often used by them [14].

The use of a second type of mesh – hexa – is more time consuming, but more regular mesh design has a positive effect on the quality of the results obtained. Table 1 summarizes the data for the 2d variant specimen to reflect the effect of mesh type on the number of elements and nodes present in a joint based on the same geometric model.

The following solutions are used to define the material properties of the hybrid joint elements. The joined adherends have been given the non-linear properties of aluminium alloy series 2024T3, adhesive presents the non-linear properties of Epidian 57/Z1 and Raychem S1125, mechanical fasteners have properties of steel. Table 2 shows the material parameters of the main elements used in the joint construction.

The initial load conditions of model are based on the experimental test conditions of the joints installed in the fatigue testing machine performed by authors own [17]. Hence, the following conditions are defined in the joint model (Figure 4):

a) all degrees of freedom (D_x, D_y, D_z, R_x, R_y, R_y, $R_z = 0$) was arranged at one end of the joint to reproduce the joint conditions in the machine's handle – Fig. 4 – A,

b) for the free end of the joint, the load was defined as a force acting on the cross-section surface of the joint and degrees of freedom were blocked according to the diagram: $D_z=0$, R_x, R_y, $R_z = 0$ – Fig. 4 – B,

c) The free end of the joint has been moved by a value of the thickness of the sample (2 mm) in a direction perpendicular to the direction of the force applied, thereby reproducing the axial conditions of mounting joint in the holder of the machinery during experimental tests – Fig. 4 – C,

d) The pressure generated by the mechanical fasteners after its assembly has been reproduced by the surface load of the head and the ring of the mechanical fastener – Fig. 4 – D ÷ G. The head and ring loads have opposite directions so the resultant load is reset. The load values are based on the measured torque appeared during assembly of the mechanical fasteners – approximately 2 Nm. When taking into account the torque value and the external diameter of the thread, it has been estimated that the nut tightening force is 3,3 kN.

Table 1. Compare the number of entities and the compute nodes of the connection model for Tetra and Hexa meshes

Sample model	Number of elements – Tetra grid	Number of cells – Hexa grid	Number of Nodes – Tetra grid	Number of Nodes – Hexa grid
2d	9971	28792	41963	140946

Table 2. The parameters used to define the material properties of each main element in the hybrid joint

Adherends AW 2024 T3	σ[MPa]	0	330,0	348,5	366,0	411,0	469,0	507,0	540,0	540,0	-	-
	ε	0	0,005	0,010	0,020	0,040	0,080	0,120	0,160	0,192	-	-
Adhesive Epidian 57/Z1	σ [MPa]	0	20,830	40,344	58,82	69,913	72,951	74,690	75,453	-	-	-
	ε	0	0,010	0,020	0,030	0,040	0,050	0,00	0,650	-	-	-
Adhesive Raychem 1125	σ [MPa]	0	0,50	0,75	1,00	1,20	1,35	1.,50	1,70	1,85	2,00	2,20
	ε	0	0,001	0,002	0,003	0,004	0,005	0,006	0,007	0,008	0,009	0,01
Fasteners Steel	E [GPa]	200										
	υ	0,3										

B: NL_25x50_3mm_2dh_p_fnal
Pressure 4
Time: 1, s
08.10.2019 23:41

[A] Fixed Support
[B] Force: 5000, N
[C] Displacement

[D] Pressure: 131, MPa
[E] Pressure 2: 131, MPa
[F] Pressure 3: 187, MPa
[G] Pressure 4: 187, MPa
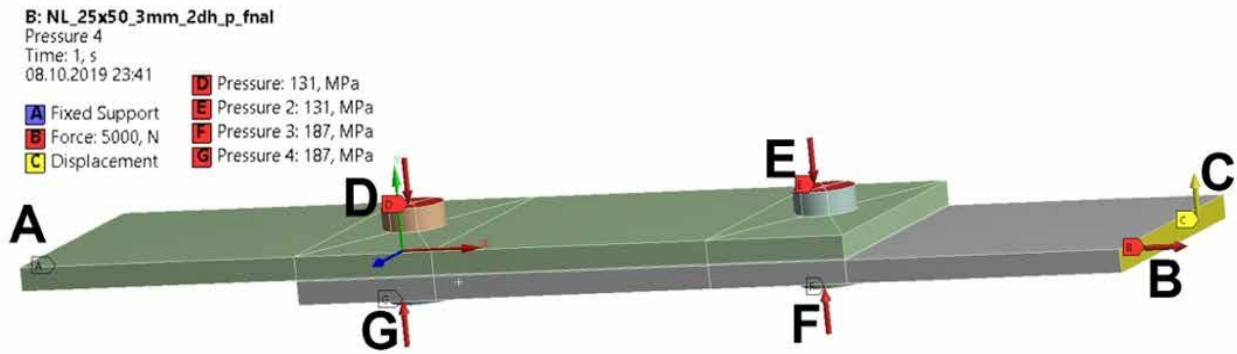
Fig. 4. Boundary conditions set in the sample calculation process

Table 3. Types of contact elements defined in the connection

Combined elements (CE)	Area of CE – adhesive layer	Heads of mechanical fasteners – CE	Tie rod spindles – internal hole surfaces	Mechanical coupler rings – mating surfaces	Mechanical coupler rings – mandrel surfaces
Contact type	Bonded	Frictional f=0,2	Frictional f=0,02	Frictional f=0,2	Frictional f=0,02

Since the hybrid joint is made up of several bodies, it was necessary to define the contact elements between the adjacent planes of the specimen elements. The types of contact elements used in the joint are shown in Table 3.

The calculation was performed in a non-linear range.

Calculation results

Experimental studies show that the destruction of a hybrid joints is a two-stage process, firstly the adhesive joint is damaged then the mechanical joint [5, 6, 9, 18, 19]. Therefore, the changes in the adhesive layer of the hybrid joint were analysed in detail. The adhesive layer was evaluated by analysing the stress distribution fields. The main purpose of the studies was to assess the changes in the adhesive joint after assembling the fasteners closer to the lap edge (so-called 1d variant instead of the 2d variant) and after using a more deformable adhesive material (Raychem S1125 instead of Epidian 57/Z1). In addition, changes in the adhesive stress fields as a function of the type of used finite element mesh were also tested during the calculation taking into account the pressures from the assembly of mechanical fasteners. The results of the calculations are presented below, taking into account the objectives of the studies adopted, including:

A) The type of mesh

The comparative calculations used a finite elements mesh of tetra to build the computing model, which is used by ANSYS as the default. Selecting and using this type of grid for calculations does not require a lot of work, but at the same time in complex geometry areas can lead to the formation of singular points. Because there are holes in the samples the usage of tetra mesh causes specific grid deformation, it was also decided to use hexa-type mesh. The mesh of hexa elements is much more demanding in terms of designer skills and time consuming, but the quality of the calculation site is higher. In the present case, the use of the hexa mesh also allowed to concentrate its elements in the vicinity of the holes for mechanical fasteners (Figure 5). Hence, there are more elements and nodes in this type of mesh which implicates increase quality of results.
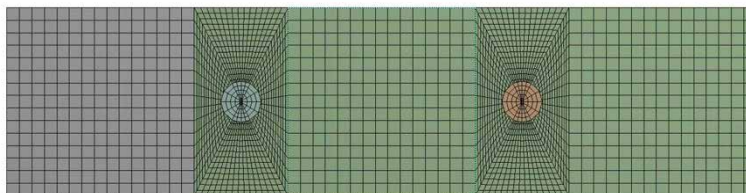
Fig. 5. Hexa mesh view with visible concentration of computing elements near holes
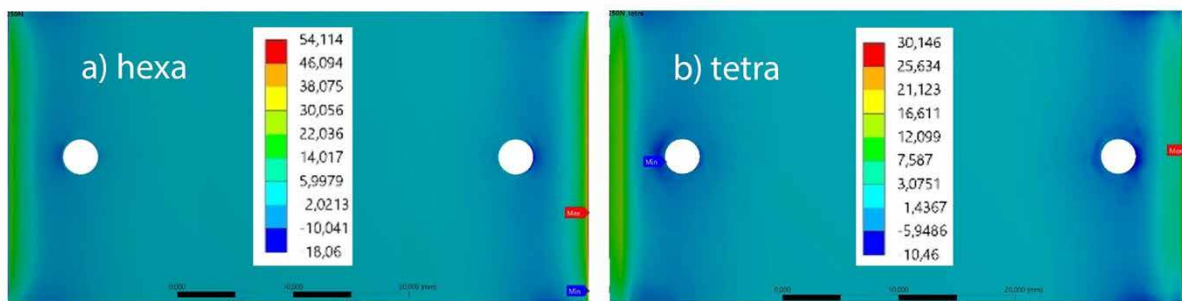
Fig. 6. Compare the distribution of normal stresses perpendicular to the adhesive layer

Using the models covered with two types of mesh, calculations were made according to the above conditions, assuming a force value equal to the joint load capacity (for hybrid joints with Epidian 57/Z1 adhesive, the mean load capacity value determined in the experimental tests was 8250 N) [17]. The calculations were performed by assigning the properties of Epidian 57/Z1 to the adhesive joint. Examples of normal stress distributions perpendicular to the adhesive layer (which are a measure of the magnitude of the peeling effect in the adhesive) are shown in Figure 6. For a model with a hexa mesh,

the maximum stress values are almost twice as large and have a value close to the stress values of butt joints, bonding with Epidian 57/Z1 [7].

Figure 7 shows maps of the distribution of the maximum principal stresses in the adhesive joint for models built on a mesh of tetra and hexa. For a model with a hexa mesh, the maximum principal stresses, which are a measure of adhesive cohesion, are lower at the ends of the lap and are closer to the actual values of adhesive decohesion. Therefore, it was decided to use models based on the hexa mesh for further calculations.
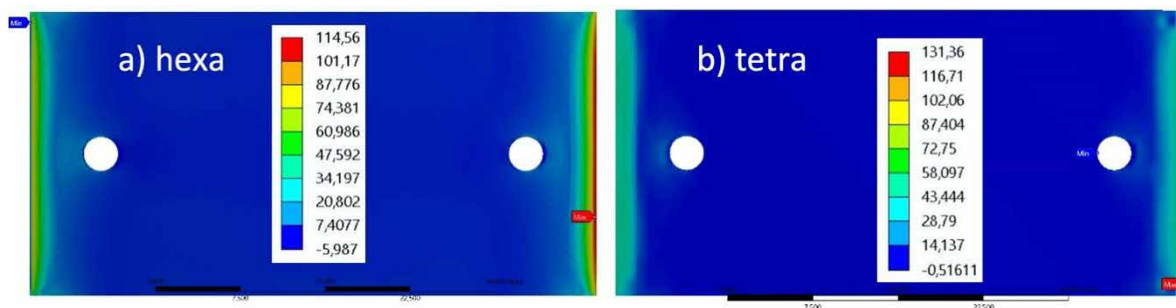
Fig. 7. Distribution of the maximum principal stresses present in the adhesive joint

B) Influence of assembly pressures

The numerical calculations for hybrid joints often exclude the effects of high torque mechanical fasteners on the adhesion layer [12, 15]. Usually the fasteners are modelled, without the pre-tension in the fasteners resulting from the way they are assembled is not taken into account (e.g. in the case of bolts, this is the torque which causes the bolt spindle to stretch and compress the fasteners on a samples surface equal to the surface

area of the heads). A comparison calculation was performed of a model constructed with hexa mesh, reproducing the pressures that result from the nut and head on the combined elements – boundary condition d), Section: Numerical model of joint. The calculations were made for Epidian 57/Z1 adhesive, loading the model with force 8250N. The distributions of the normal, shear and maximum principal stresses are shown in Figures 8, 9 and 11.
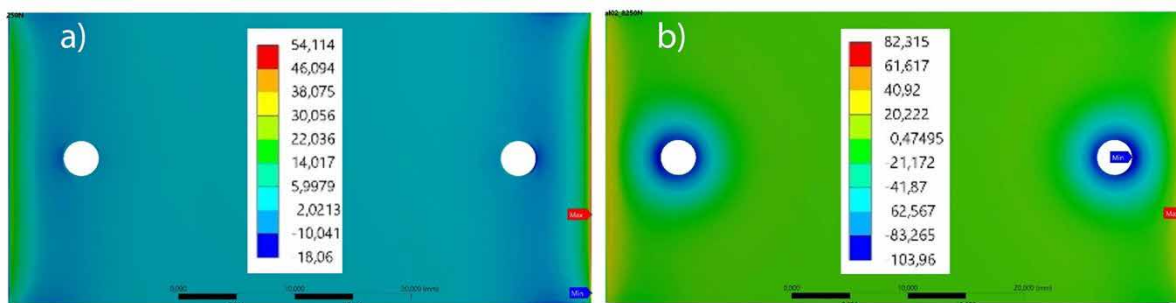
Fig. 8. Comparison of the distribution of normal stresses perpendicular to the adhesive joint
(a) without mounting pressures from the bolts, (b) taking into account the mounting pressures from the bolts
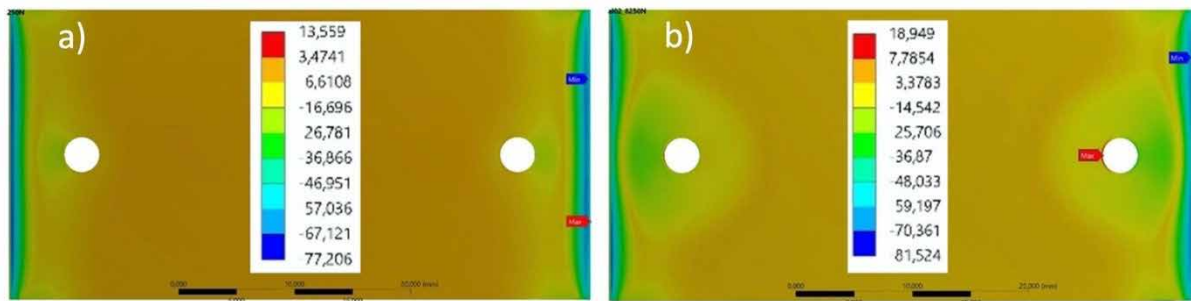
Fig. 9. Comparison of the shear stress distribution in the adhesive joint
(a) without the mounting pressure from the bolts, (b) taking into account the mounting pressure from the bolts
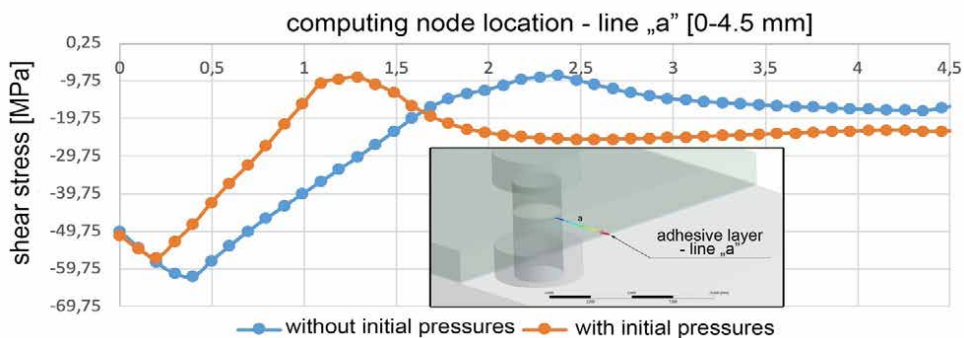
Fig. 10. Comparison of the distribution of the shear stresses on the line "a" adhesive joint
(a) without the initial (assembly) pressures, (b) taking into account the initial (assembly) pressures
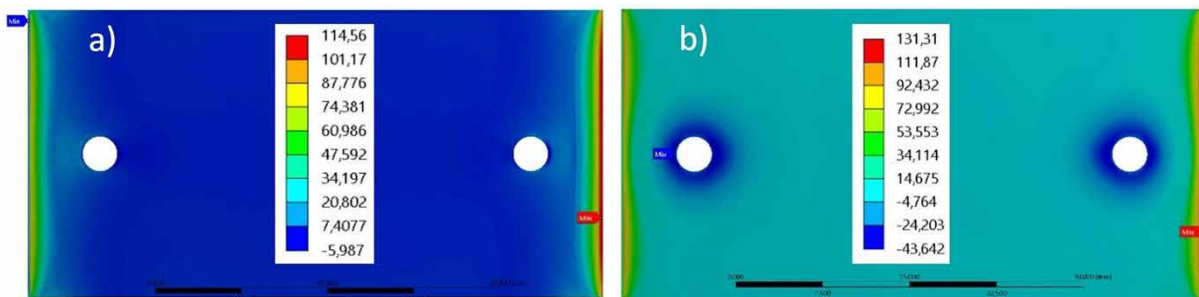
Fig.11. Comparison of the distribution of the maximum principal stresses in the adhesive joint
(a) without pressure from the fasteners, (b) taking into account the pressure from the fasteners

Analysis of the resulting distributions shows a significant effect of assembly pressures on changes not only in the distribution of normal stresses perpendicular to the adhesive in the vicinity of the holes for the fasteners – values increased (Figure 8), but also in the increase of stress values at the ends of the lap. In the area of shear stresses there is a clear zone of their variation that radiates from the holes – Figure 9. In addition, the shear stress values at the lap ends are lower as well as the difference between the stress at the lap ends and the hole area – Figure 10.

The distribution of the maximum principal stresses in the lap also changes due to assembly pressures – Fig. 11. The concentration zone at the ends of the lap is narrower and further narrowed at the middle end of the lap due to assembly pressures.

C) Assembling of mechanical fasteners – 1d and 2d option

Experimental studies [6, 12, 17] show that in the two-stage destruction of a hybrid joint, the adhesive joint is damaged firstly, then the mechanical joint is destroyed. As the results of the calculations presented above show, the positive effect of mechanical fasteners on the stress distribution in the adhesive joint is limited close to a circle with radius of approximately 1,5 diameter. According to the assembling conditions guidelines for mechanical joints, the minimum installation distance from the edge of
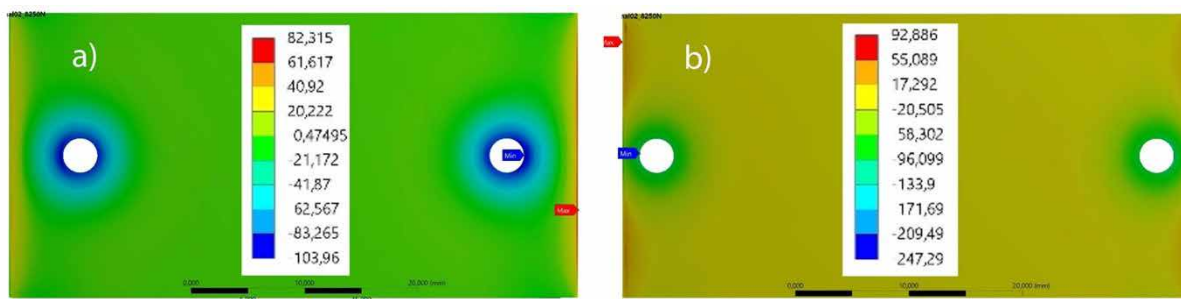
Fig. 12. Comparison of the distribution of normal stresses perpendicular to the adhesive joint
a) variant 2d, b) variant 1d
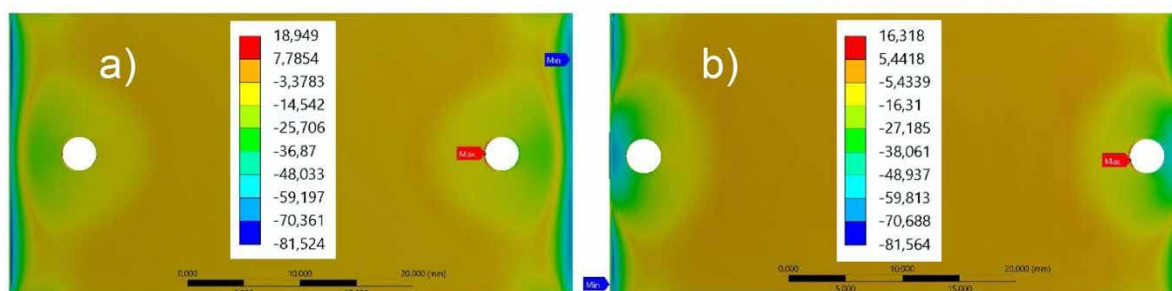
Fig. 13. Comparison of the shear stress distribution of the adhesive joint
a) variant2d, (b) variant 1d
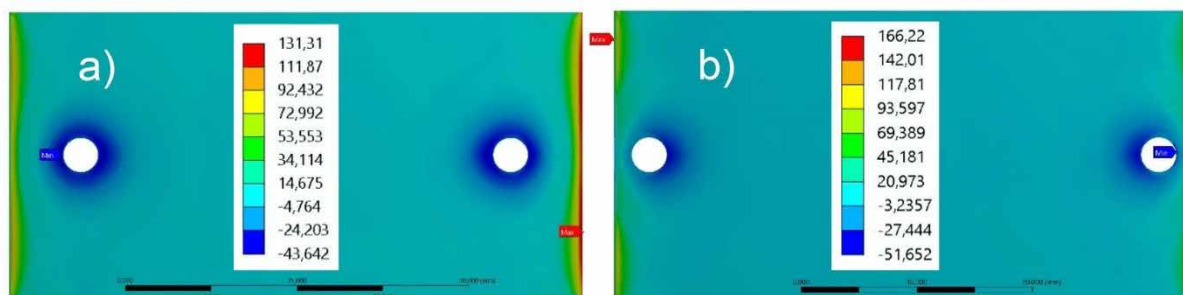
Fig. 14. Comparison of the maximum principal stress distribution of the adhesive joint
a) variant 2d, b) variant 1d

the lap should be 2d (2d variant) and this diagram was used in the calculations above. However, considering the field size where the fasteners have a positive effect on the adhesive joint, it was decided to perform calculations for a scheme where the mechanical fastener will be mounted closer to the edge of the lap at a distance of one diameter (1d variant) from the edge of the lap. It was assumed that the presence of fasteners closer to the edge will reduce the negative stress peaks at the ends of the lap and the mechanical properties of the hybrid joints, e.g. its load capacity, will be improved. The computations were made for model with Epidian 57/Z1 adhesive, loading the joint with a force of 8250 N. The distributions of the normal,

shear and maximum principal stresses are shown in Figures 12, 13 and 14.

When analysing the results obtained, it was found that moving the fasteners closer to the lap edge separates the stress concentration zone into two parts and creates a much smaller area around the holes. Therefore, there is no continuous stress concentration zone at the ends of the lap as in the 2d variant, but two smaller zones symmetrically aligned with the hole's axis. The magnitude of the stress concentration field in variant 1d is then lower compared to the 2d variant. The own experimental studies [17] show a significant improvement in the load capacity of hybrid joints when the modified installation scheme 1d variant is used – Figure 15.
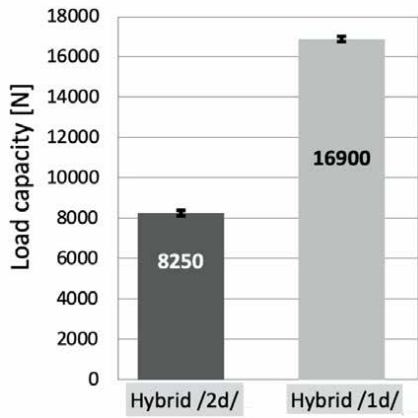
Fig. 15. Comparison of joint load capacities for the variant 2d and 1d [17]

D) Type of adhesive material

The proper use of the mechanical parameters of the hybrid joints is primarily based on the optimal distribution of the total load between the adhesive and mechanical joints, in order to different types of joints, i.e. the adhesive and mechanical joints as combination forming the hybrid joint, present properly load sharing to create homogenous stress distribution. Using a simplified hybrid joint model (Figure 16) as the authors of the publication [9, 15], it can be assumed that the use of a more deformable adhesive (i.a. lower value of Ea_d) should result in a higher absorbing and load sharing by the mechanical joint and as a consequence higher load capacity the hybrid joint

The research presented in [1, 2] shows that the adhesive parameters have a significant effect on the level of load absorption by mechanical fasteners. In order to achieve the condition that at least 10% of the load in the hybrid joint is transferred to mechanical fasteners, the authors recommend the use of deformable adhesive materials. In own calculations, the hybrid joint was modelled with using two adhesives, of which Epidian 57/Z1 was a highly rigid, while Raychem S1125 was a flexible one. The distribution of the shear and maximum principal stresses for the 5000 N load in variant 1d with initial pressures is shown in Figures 17 and 18.
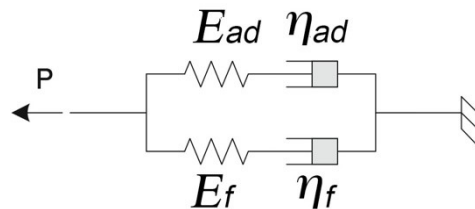
Fig.16. Simplified hybrid joint model (E_{ad} E_f - elastic modules of adhesive and mechanical fasteners, η_{ad}, η_f - viscosity coefficients of adhesive and mechanical fasteners [9]
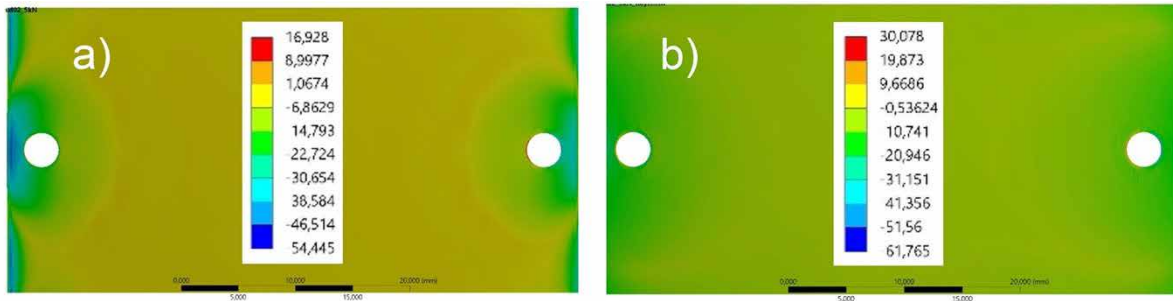
Fig. 17. Comparison of the shear stress distribution of the adhesive joint
a) Epidian 57/Z1, variant 1d, (b) Raychem S1125 variant 1d
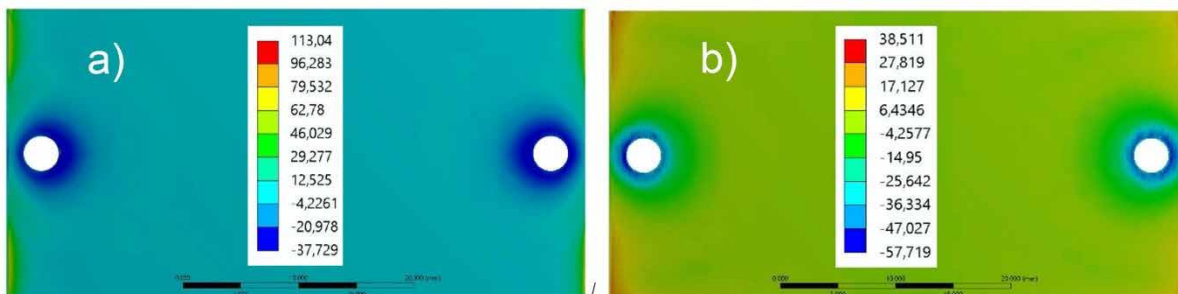
Fig. 18. Comparison of the maximum principal stress distribution of the adhesive joint
a) Epidian 57/Z1, variant 1d, b) Raychem S1125, variant 1d
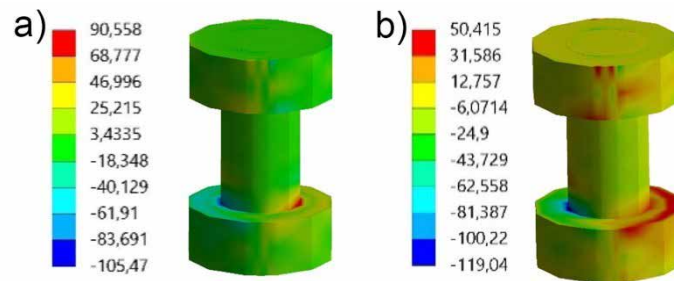
Fig. 19. Shear stress distribution in mechanical fasteners in the hybrid joint with (a) adhesive Epidian 57/Z1, (b) adhesive Raychem S1125

For the model with Raychem S1125 adhesive properties, the variation in stress distribution in the adhesive layer is lower. For hybrid joints, the smaller differences between the stress values at the ends and at the centre of the lap mean i.a. their increased of fatigue life [13]. In addition, the shear stress values in the mechanical fasteners in the model with Raychem S1125 adhesive are almost twice higher, which means that the fasteners are more effort – Figure 19.

Conclusions

On the basis of the computations made, it was found that:

- On the one hand, the density of the mesh elements and their regular shape around the holes (hexagonal mesh) result in a significant increase of the calculation task and increase of the time taken to prepare the model and perform the calculations by about 5 times compared to the model with the tetragonal default grid. On the other hand, the results obtained, e.g. the stress distribution in the hybrid joint are more similar to the stress values estimated from experimental studies.
- The pre-load of the hybrid joint including adhesive is the result of the assembly process of the mechanical fasteners. And since the calculated stress status of the adhesive joint is the basis for estimating the fatigue life of the hybrid joint, the assembly pressures should be taken into account in defining the boundary conditions of this type of joint (if a model with a limited number of mechanical fasteners is considered, the so-called higher level model in the form of a sample or a smaller part of the structure).
- The results of the computations obtained for the two assembly variants of the fasteners (1d and 2d) do not clearly indicate that there is a significant reduction in stress at the lap ends, but when the fasteners are moved closer to the lap edge, it separates the stress accumulation zone into two parts reducing the negative stress peaks. Additionally, the areas with significantly less uneven stress distribution are created around the holes, what positively affects the load capacity and durability of hybrid joints.

- The results of the computations made also indicate that the use of adhesive material more susceptible to deformation is a positive factor in solving the stress compensation problem on lap length. For this material, the process of "passing" the load from the adhesive to the mechanical fasteners is more efficient and results in a higher absorbing as well as load sharing by the mechanical joint. The consequence is higher load capacity the hybrid joint.

References

[1] Bodjona K., Raju K., Lim G.H., Lessard L. 2015. „Load sharing in single-lap bonded/bolted composite joints. Part I: Model development and validation". Composite Structures 129: 268-275.

[2] Bodjona K., Lessard L. 2015. „Load sharing in single--lap bonded/bolted composite joints. Part II: Global sensitivity analysis". Composite Structures 129: 276-283.

[3] Brotherhood C.J., Drinkwater B.W., Dixon S. 2003. „The detectability of kissing bonds in adhesive joints using ultrasonic techniques". Ultrasonics 41:521-529.

[4] Caliskan M. 2006. „Evaluation of bonded and bolted repair techniques with finite element method". Materials and design 27: 811-820.

[5] Chowdhury N., Chiu W. K., Wang J., Chang P. 2015. „Static and fatigue testing thin riveted, bonded and hybrid carbon fiber double lap joints used in aircraft structures". Composite Structures 121: 315-323.

[6] Da Silva L. F. M., Pirondi A., Ochsner A. 2011. Hybrid Adhesive Joints. Berlin: Springer.

[7] Godzimirski J., Komorek A., Rośkowicz M., Smal T., Tkaczuk S. 2010. Adhesives – use in the technical maintenance. Warsaw: Scientific – Technical Publications. ISBN 978-83-204-3605-1.

[8] Godzimirski J., Rośkowicz M., Tkaczuk S. 2009. Fatigue life of adhesive joints. Warsaw: Military University of Technology.

[9] Gómez S., Onoro J., Pecharroman J. 2006. „A simple mechanical model of a structural hybrid adhesive/riveted single lap joint". Internal Journal of Adhesion & Adhesives 27: 263-267.

[10] Hart-Smith L.J. 1973. Adhesive-bonded double-lap joints. Technical report NASA CR-112235.

[11] Kelly G. 2005. „Load transfer in hybrid (bonded/bolted) composite single-lap joints". Composite Structures 69: 35-43.

[12] Kelly G. 2006. „Quasi-static strength and fatigue life of hybrid (bonded/bolted) composite single-lap joints". Composite Structures 72: 119-129.

[13] Matwijenko W.A. 1994. „Influence of the construction and technological factors for fatigue life of adhesive-rivet joints". Technology and Automation of Assembly 2: 33-35.

[14] Mohamed Bak K., Prasanna Venkatesn K., Kalai Chelvan K. 2012. „Parametric study of bonded, riveted and hybrid composite joints using FEA". Journal of Applied Sciences 12(10): 1058-1062.

[15] Paroissien E., Sartor M., Huet J. 2007. „Hybrid (Bolted/Bonded) Joints Applied to Aeronautic Parts: Analytical One-Dimensional Models of a Single-Lap Joint". W Advances in Integrated Design and Manufacturing in Mechanical Engineering II, 95-110. Springer.

[16] Rośkowicz M., Chudowolska J. 2018. „The influence of mechanical fasteners for hybrid joint load capacity". Technology and Automation of Assembly 1: 52-54.

[17] Rośkowicz M., Gąsior J. 2019. „Load capacity and fatigue life of hybrid joints". Technology and Automation of Assembly 2: 30-33.

[18] Sadowski T., Kneć M., Golewski P. 2010. „Experimental investigations and numerical modelling of steel adhesive joints reinforced by rivets". International Journal of Adhesion & Adhesives 30: 338-346.

[19] Stere M., Baran D. 2011. „Calculation of hybrid joints used in modern aerospace structures". INCAS BULLETIN 3(4): 161-169.

Marek Rośkowicz, DSc.
The Institute of Aviation Technology, Military University of Technology in Warsaw
ul. gen. Sylwestra Kaliskiego 2, 00-908 Warsaw, Poland
email: marek.roskowicz@wat.edu.pl

Jarosław Gąsior, M.Sc., Eng.
The Military Centre for Standardization, Quality and Codification
ul. Nowowiejska 28A, 00-909 Warsaw, Poland
email: j.gasior@ron.mil.pl

ANALYSIS OF THE IMPACT OF SURFACE ROUGHNESS ON THE BEARING CAPACITY OF LAP ADHESIVE JOINTS FROM ALUMINUM ALLOY 2024

Władysław ZIELECKI   ORCID 0000-0002-7864-5525

Andrzej DZIERWA   ORCID 0000-0003-4545-1748

Ewelina GUŹLA   ORCID 0000-0002-7359-6007   DOI: 10.15199/160.2020.3.2

A b s t r a c t: The article presents the analysis of the impact of surface roughness on the load capacity of lap adhesive joints from aluminum alloy 2024. The surfaces of the samples were prepared to bond using mechanical treatment methods, such as milling and abrasive blasting. The surface roughness of the samples for different pre-treatment variants, measured in the 2D system, was found in the range of: Rp=19,4÷60,6 [µm], Rv=16,5÷88,1 [µm], Rz=35,9÷147,0 [µm], Rc=32,2÷103,3 [µm], Rt=37,1÷174,7 [µm], Ra=8,91÷22,73 [µm], Rq=10,50÷27,33 [µm], Rsk=-0,2260÷0,6487, Rku=1,78÷5,85, RSm=0,1207÷0,7337 [mm], Rdq=23,4÷198,7 [˚]. Strength tests showed an increase in the bearing capacity of joints the surfaces of which were subjected to both milling and abrasive blasting.

K e y w o r d s: surface roughness, milling, abrasive blasting, adhesive joints, bearing capacity

S t r e s z c z e n i e: W artykule przedstawiono analizę wpływu chropowatości powierzchni na nośność zakładkowych połączeń klejowych stopu aluminium 2024. Powierzchnie próbek zostały przygotowane do klejenia z zastosowaniem metod obróbki mechanicznej, takich jak frezowanie i piaskowanie. Chropowatość powierzchni próbek dla poszczególnych wariantów obróbki, zmierzona w układzie 2D, mieściła się w przedziale: Rp=19,4÷60,6 [µm], Rv=16,5÷88,1 [µm], Rz=35,9÷147,0 [µm], Rc=32,2÷103,3 [µm], Rt=37,1÷174,7 [µm], Ra=8,91÷22,73 [µm], Rq=10,50÷27,33 [µm], Rsk=-0,2260÷0,6487, Rku=1,78÷5,85, RSm=0,1207÷0,7337 [mm], Rdq=23,4÷198,7 [˚]. Badania wytrzymałościowe wykazały wzrost nośności połączeń, których powierzchnie poddawane były zarówno frezowaniu, jaki i piaskowaniu.

S ł o w a   k l u c z o w e: chropowatość powierzchni, frezowanie, piaskowanie, połączenia klejowe, nośność

Introduction

The technological process of adhesive bonding is carried out in several stages in a strictly defined order. The first and one of the most important stages of adhesive bonding is the surface pre-treatment - without proper preparation of the adhered surface, it would be impossible to activate the necessary binding mechanisms (mechanical, physical and chemical) and to create a durable joint [3, 5]. Therefore, the surface should be prepared in a way that ensures:
- removal of all surface contaminants from the connected elements,
- appropriate surface activation,
- required surface wettability,
- good surface development [6, 8].

According to the mechanical theory of adhesion, the geometric structure of the surface affects the strength of adhesive joints. Due to irregularities on the adhered surface it is possible to form mechanical anchors between the surface and the adhesive. These anchors are capable of carrying significant loads [1, 8]. However, in some cases, surface irregularities decrease the ability for adhesive penetration (when there are too many pores and when they are too narrow) and may weaken the connection [7, 8]. Hence, it is reasonable to search for such values of roughness parameters and such surface treatment methods that would guarantee obtaining optimal joint strength.

Material and methods

The aim of the study was to analyze the impact of the geometric structure of the surface on the bearing capacity of single-lap adhesive joints from aluminum alloy 2024. Aluminum alloy 2024 is characterized by a high strength to weight ratio and good fatigue resistance. This alloy is non-weldable and difficult to process. It is also resistant to high temperatures and has a low corrosion resistance [2, 4]. The chemical composition of this alloy is shown in Table 1.

Table 1. The chemical composition of aluminum alloy 2024 [2]

Component, weight %											
Si	Fe	Cu	Mn	Mg	Cr	Ni	Zn	Ti	V	Others*	Al
max 0,50	max 0,50	3,8 - 4,9	0,30 - 0,90	1,2 - 1,8	max 0,10	-	max 0,25	max 0,15	-	max 0,05	remaining

*Others, total ≤ 0,15%

Table 2. Variants of the applied pre-treatment methods [own elaboration]

No	Variant	Name	v_f [mm/min]
1.	Milling	F30	30
2.	Milling	F50	50
3.	Milling	F70	70
4.	Milling	F90	90
5.	Milling and abrasive blasting	FS30	30
6.	Milling and abrasive blasting	FS50	50
7.	Milling and abrasive blasting	FS70	70
8.	Milling and abrasive blasting	FS90	90

The first stage of the study was to prepare the surface of the samples for gluing. The adhered surface of the samples was subjected to different variants of mechanical pre-treatment, including milling and milling combined with abrasive blasting. The abrasive blasting was carried out using 95A corundum with a grain size of 0,27 mm. The duration of the treatment was 5 s. Milling was carried out at a spindle speed n = 140 r/min, depth of cut a_p = 0,4 mm and table feed vf of 30, 50 70 or 90 mm/min. All variants of the applied pre-treatment methods are presented in Table 2.

The next step was to examine the geometric structure of the surface. The tests were carried out in two-dimensional array. The contact stylus profilometer Taylor Hobson Surtronic 25 and TalyProfile Lite software were used for the tests. The evaluation length was 4 mm.

Then the samples were bonded. Adhesive joints were made using Loctite EA3430 two-component epoxy adhesive. A mixing tip was used to mix the adhesive components. The adhesive was applied to both surfaces, which were then joined. The dimensions of the adhesive joint were 25x12,5 mm. The samples were placed in a gluing appliance (Fig.1).

Fig. 1. The samples placed in a gluing appliance [own elaboration]

The samples were loaded with a constant force, using one-kilogram weights. The samples were kept in the appliance for 7 days at a temperature of 23±2 °C.

The last step was to examine the shear strength of adhesive joints. The samples were subjected to a static tensile test on a Zwick Roell Z030 testing machine. The initial force was 30 N and the test speed was 5 mm/min.

Results

The average values of roughness parameters and standard deviations for different variants of pre-treatment methods are presented in Table 3 and Table 4.

Average values were determined on the basis of three samples. Comparing the values of roughness parameters, it can be stated that the lowest values of Rp, Rv, Rz, Rt, Rq parameters occur for the F30 variant. The highest values of Rz, Rt, Ra, Rq parameters occur for the FS90 variant. Moreover, in most cases, the roughness parameter values are higher for variants with combined milling and abrasive blasting treatment than for the corresponding variants which were only milled. What is more, the surface roughness measurements for samples with combined milling and abrasive blasting are characterized by greater variability.

The selected surface profilograms, showing the differences in the geometric surface for various pre-treatment methods, are shown in Figure 2.

The results of the uniaxial static tensile test are shown in Table 5. Average values were determined on

Table 3. Average values of roughness parameters [own elaboration]

Variant	Rp [μm]	Rv [μm]	Rz [μm]	Rc [μm]	Rt [μm]	Ra [μm]	Rq [μm]	Rsk	Rku	RSm [mm]	Rdq [°]
F30	19,4	16,5	35,9	34,7	37,1	8,91	10,50	0,1587	1,89	0,2293	24,5
F50	30,5	27,0	57,5	57,1	58,1	15,10	17,27	0,1280	1,78	0,3653	25,1
F70	40,4	36,1	76,5	76,5	77,9	18,17	21,37	0,0195	1,94	0,5187	23,4
F90	60,6	42,4	102,7	103,3	105,0	21,00	26,20	0,6487	2,69	0,7337	29,6
FS30	34,9	27,2	62,1	32,2	89,0	9,26	11,40	0,1258	3,36	0,1340	60,0
FS50	33,2	46,2	79,4	48,1	95,1	13,60	16,23	-0,0570	2,67	0,1923	73,4
FS70	53,7	62,6	116,3	69,5	145,7	19,43	22,63	-0,1367	2,32	0,1953	105,0
FS90	58,8	88,1	147,0	79,8	174,7	22,73	27,33	-0,2260	2,80	0,1207	198,7

Table 4. Standard deviation values of roughness parameters [own elaboration]

Variant	S^2Rp [μm]	S2Rv [μm]	S^2Rz [μm]	S^2Rc [μm]	S^2Rt [μm]	S^2Ra [μm]	S^2Rq [μm]	S^2Rsk	S^2Rku	S^2RSm [mm]	S^2Rdq [°]
F30	0,2	0,2	0,2	0,0	0,4	0,03	0,08	0,0143	0,01	0,0005	1,9
F50	0,2	0,1	0,1	0,2	0,4	0,16	0,12	0,0078	0,01	0,0005	1,4
F70	0,3	0,1	0,2	0,2	0,4	0,19	0,05	0,0086	0,04	0,0005	2,2
F90	0,4	0,7	0,5	0,5	0,8	0,29	0,37	0,0057	0,02	0,0012	2,4
FS30	6,5	2,9	6,0	0,3	11,0	0,15	0,16	0,1873	0,64	0,0180	5,7
FS50	2,0	3,8	1,8	5,7	7,7	1,63	1,25	0,2720	0,60	0,0400	10,5
FS70	12,4	10,9	22,3	8,5	28,3	0,21	0,38	0,0460	0,40	0,0308	28,4
FS90	6,4	8,9	10,2	2,0	4,8	0,91	0,39	0,0781	0,53	0,0166	15,6
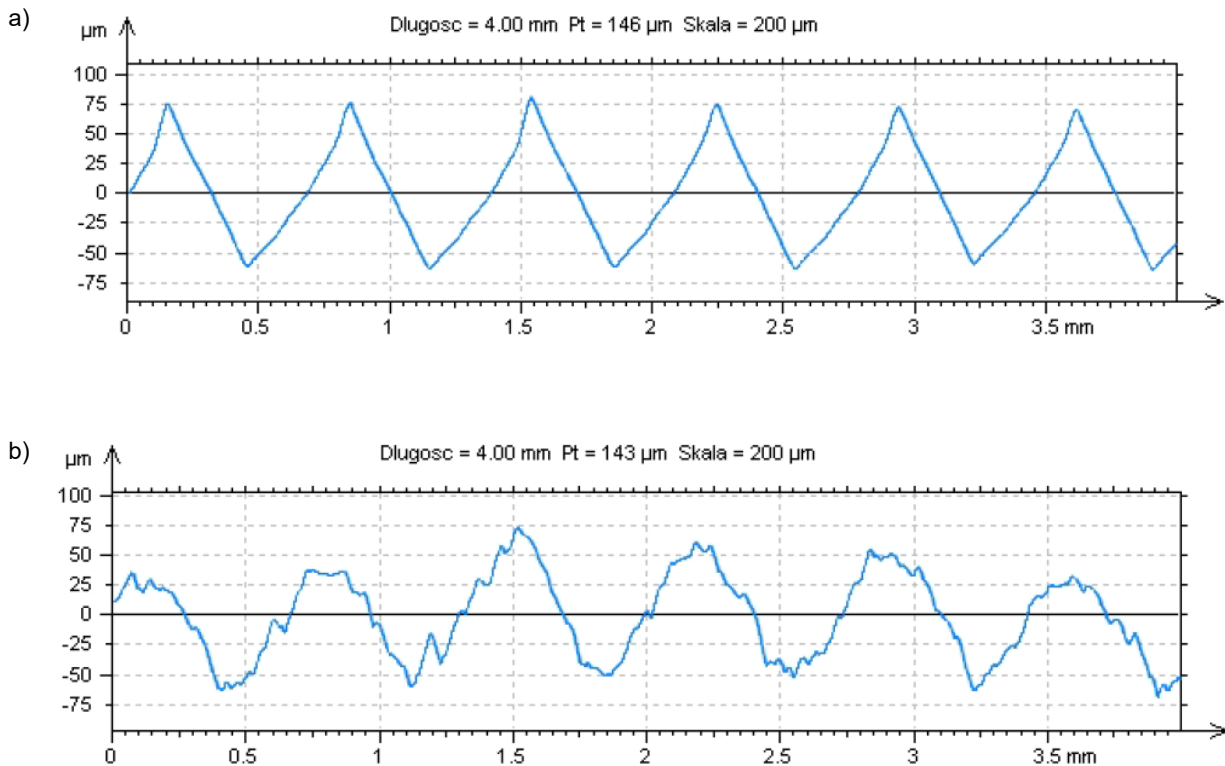
Fig. 2. Surface profilograms of the samples subjected to: a) milling – variant F90, b) milling and abrasive blasting - variant FS90 [own elaboration]

the basis of three samples. The highest values of shear strength were obtained for the samples subjected to milling and abrasive blasting. The samples which were only milled have lower shear strength values (the lower table feed, the lower shear strength). Interestingly, the bearing capacity for milled and abrasive blasted samples increased twofold (or even more) as compared to only milled samples.

Figure 3 shows a bar chart with average values of bearing capacity and standard errors. On the basis of the chart, it can be observed that the samples subjected to milling and abrasive blasting are not only characterized

Table 5. The results of the static tensile test [own elaboration]

variant	bearing capacity P [kN] – sample no 1	bearing capacity P [kN] – sample no 2	bearing capacity P [kN] – sample no 3	average bearing capacity P [kN]	standard deviation of the bearing capacity S^2P [kN]	standard error [kN]	average shear strength Rt [MPa]	increase in shear strength [%]
F30	1,48	1,11	1,61	1,40	0,26	0,15	4,48	-
F50	2,18	1,96	2,37	2,17	0,21	0,12	6,94	-
F70	2,05	1,80	1,66	1,84	0,20	0,11	5,88	-
F90	3,06	2,09	2,78	2,64	0,50	0,29	8,46	-
FS30	4,67	4,12	4,91	4,57	0,41	0,23	14,61	226,19
FS50	6,45	5,61	5,64	5,90	0,48	0,28	18,88	171,89
FS70	6,12	3,95	5,10	5,06	1,09	0,63	16,18	175,32
FS90	4,92	6,93	6,73	6,19	1,11	0,64	19,82	134,30

by higher bearing capacity, but also higher values of standard errors compared to only milled samples.

The results of measurements of surface roughness and bearing capacity were statistically analyzed using Minitab and MS Excel. The statistical research included Student's t-test, regression and correlation analysis.
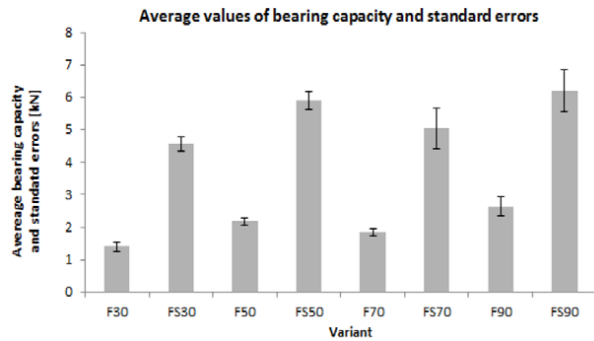
Fig. 3. Bar chart with average values of bearing capacity and standard errors [own elaboration]

The first stage of the statistical analysis was conducting Student's t-test. The Student's t-test was used to determine if the average values of bearing capacity of two different pre-treatment variants are significantly different from each other. Statistical significance α=0.05 was adopted. It means that a statistically significant difference between the obtained results occurs when the p-value < 5%. The results of Student's t-test are shown in Table 6.

Student's t-test allowed to unequivocally determining a statistically significant difference between the obtained results. P-values in most cases are lower than 5%. Therefore, the results of the Student's t-test in most cases indicate a statistically significant difference in the

bearing capacity of adhesive joints between samples subjected to milling and abrasive blasting, and samples which were only milled. The abrasive blasting of milled samples contributed to a significant increase in the bearing capacity of the joints. In the case of milled samples, the bearing capacity of adhesive joints does not show statistically significant differences between the F50 variant and variants F70 and F90, while in the case of abrasive blasted samples statistically significant differences occur only between the FS30 variant and the FS50 variant.

In the next step of the analysis, a box plot showing relationship between pre-treatment variant and bearing capacity was created (Fig. 4).

Based on the graph, it can be concluded that the largest spread of bearing capacity was obtained for variants FS70 and FS90. Samples that were exclusively milled are characterized by a smaller discrepancy in results compared to milled and abrasive blasted samples. Moreover, in the case of variants FS70 and FS90, the data distribution is the most asymmetrical.
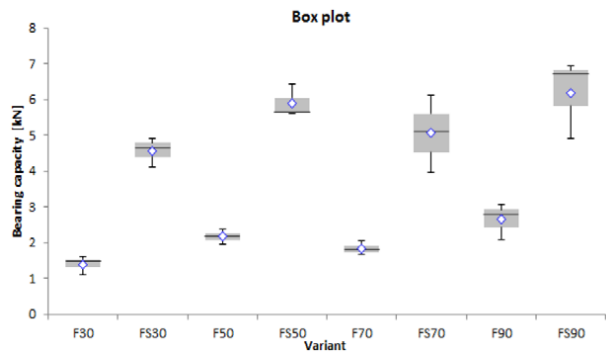
Fig. 4. Box plot showing relationship between pre-treatment variant and bearing capacity [own elaboration]

Table 6. Student's t-test results

Pv [%]	F30	F50	F70	F90	FS30	FS50	FS70	FS90
F30	x							
F50	0,870	x						
F70	4,292	5,635	x					
F90	1,564	11,868	4,624	x				
FS30	0,039	0,145	0,107	0,369	x			
FS50	0,031	0,089	0,076	0,062	1,097	x		
FS70	1,156	1,999	1,618	2,190	26,273	15,652	x	
FS90	0,682	1,067	0,915	0,891	5,647	35,225	13,654	x

As a result of regression analysis, regression equations showing the relationship between the bearing capacity of adhesive joints and roughness parameters were obtained. The calculated values of the Pearson correlation coefficients show the degree of linear relationship between the variables. The effects of regression and correlation analysis are shown in Table 7. and in Figure 5.

Based on Table 7, it can be concluded that in most cases the correlation between bearing capacity and surface roughness parameters is positive. It means that in the adopted area of variability, the bearing capacity of the connection increases with an increase of the surface roughness parameters (exceptions are Rsk and RSm parameters). The strongest correlation occurs between

Table 7. The results of correlation and regression analysis [own elaboration]

Roughness parameter	Linear regression equation	Pearson correlation coefficient r	p-value
Rp	$y_P = 1{,}83 + 0{,}0457\ x_{R_p}$	0,364	0,080
Rv	**$y_P = 1{,}06 + 0{,}0615\ x_{Rv}$**	**0,727**	**0,000**
Rz	$y_P = 0{,}870 + 0{,}0337\ x_{Rz}$	0,623	0,001
Rc	$y_P = 3{,}62 + 0{,}0016\ x_{Rc}$	0,020	0,928
Rt	**$y_P = 0{,}518 + 0{,}0327\ x_{Rt}$**	**0,758**	**0,000**
Ra	$y_P = 2{,}06 + 0{,}104\ x_{Ra}$	0,273	0,197
Rq	$y_P = 2{,}07 + 0{,}0863\ x_{Rq}$	0,274	0,195
Rsk	$y_P = 4{,}02 - 3{,}62\ x_{Rsk}$	-0,537	0,007
Rku	$y_P = 0{,}19 + 1{,}45\ x_{Rku}$	0,500	0,013
RSm	$y_P = 5{,}39 - 5{,}38\ x_{RSm}$	-0,584	0,003
Rdq	**$y_P = 2{,}03 + 0{,}0251\ x_{Rdq}$**	**0,779**	**0,000**

a)

b)

c)

d)
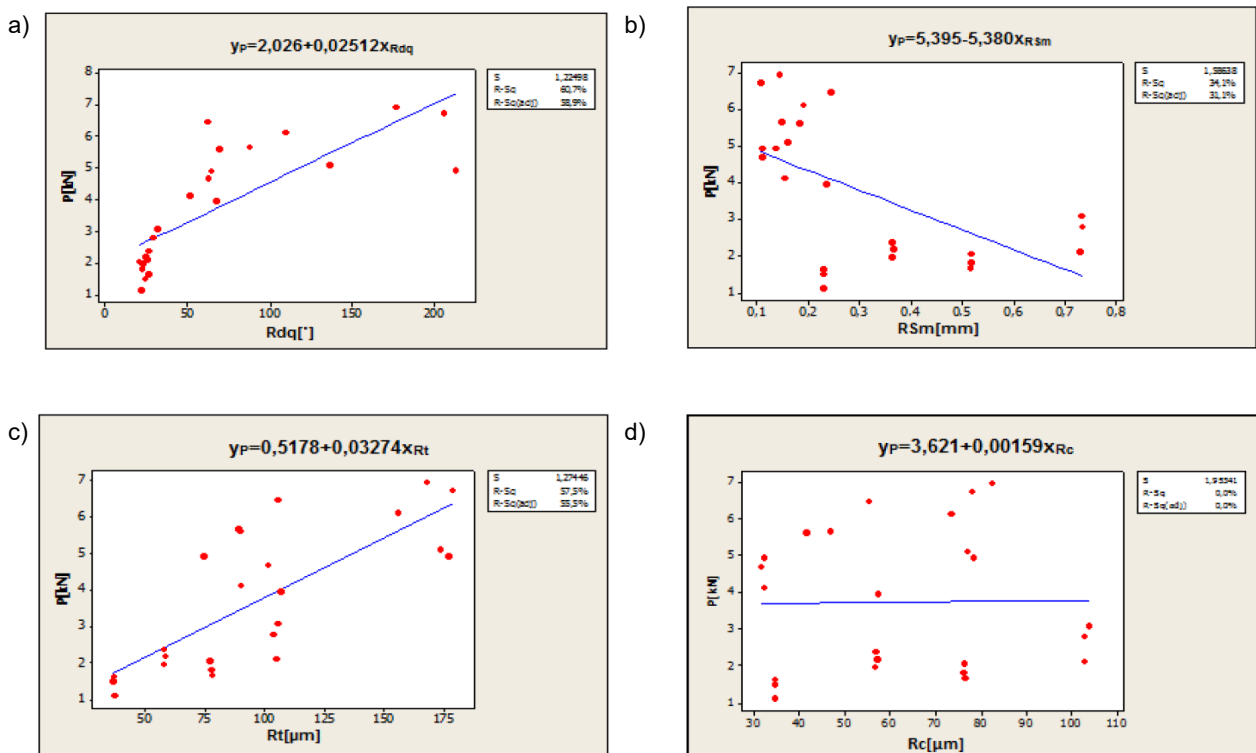
Fig. 5. Graphs of regression equations showing the relationship between the bearing capacity P and selected roughness parameters: a) Rdq, b) RSm c) Rt, d) Rc. [own elaboration]

the variables P and Rv (r = 0,727), P and Rt (r = 0, 758), as well as P and Rdq (r = 0, 779).

Conclusions

The analysis allowed determining the effect the surface roughness, obtained as a result of milling and milling combined with abrasive blasting, on the bearing capacity of lap adhesive joints from aluminum alloy 2024.

Based on the results of surface roughness tests, it can be stated that subjecting milled samples to abrasive blasting contributes to an increase in the values of most of the tested roughness parameters. What is more, the samples subjected to milling and abrasive blasting have a higher bearing capacity than samples whose surfaces were only milled. The highest bearing capacity of the connection was obtained for variant which was milled with the highest adopted table feed (v_f=90 mm/min) and abrasive blasted. The lowest bearing capacity was obtained for variant milled with the lowest assumed table feed (v_f=30 mm/min). It means that in the adopted area of variation, increasing the table feed contributes to increasing the bearing capacity of the connections. Apart from that, regression and correlation analysis showed that the bearing capacity of joints increases with the increase in the value of surface roughness parameters, apart from RSk and RSm (in the adopted area of variation).

The largest correlation occurs between the bearing capacity P of adhesive joints and the roughness parameters Rv, Rt, Rdq (r=0.727÷0.779). These roughness parameters could be used to predict the bearing capacity of the adhesive joints.

References

[1] Baldan A. 2012. „Adhesion phenomena in bonded joints". International Journal of Adhesion and Adhesives 38: 95-116.

[2] Dobrzański L. 2010. Leksykon Materiałoznawstwa. Praktyczne zestawienie norm polskich, zagranicznych i międzynarodowych. Cz. 4, rozdział 1: Metale nieżelazne i ich stopy. Warszawa: Wydawnictwo Verlag Dashofer.

[3] Godzimirski J., Kozakiewicz J., Łunarski J., Zielecki W. 1997. Konstrukcyjne połączenia klejowe elementów metalowych w budowie maszyn. Rzeszów: Oficyna Wydawnicza Politechniki Rzeszowskiej.

[4] Kuczmaszewski J., Pieśko P., Zawada-Michałowska M. 2016. „Surface roughness of thin-walled components made of aluminium alloy EN AW-2024 following different milling strategies". Advances in Science and Technology Research Journal 10(30): 150-158.

[5] Rudawska A. 2010. „Wpływ sposobu przygotowania powierzchni na wytrzymałość połączeń klejowych blach ze stali odpornej na korozję". Technologia i Automatyzacja Montażu (3): 36-40.

[6] Rudawska A. 2014. „Selected aspects of the effect of mechanical treatment on surface roughness and adhesive joint strength of steel sheets". International Journal of Adhesion and Adhesives 50: 235-243.

[7] Rudawska A., Danczak I., Müller M., Valasek P. 2016. „The effect of sand blasting on surface properties for adhesion". International Journal of Adhesion and Adhesives 70: 176–190.

[8] Zielecki W., Pawlus P., Perłowski R., Dzierwa A. 2013. „Surface topography effect on strength of lap adhesive joints after mechanical pre-treatment". Archives of Civil and Mechanical Engineering 13: 175–185.

dr hab. inż. Władysław Zielecki, prof. PRz
Wydział Budowy Maszyn i Lotnictwa Politechniki Rzeszowskiej, Katedra Technologii Maszyn i Inżynierii Produkcji
al. Powstańców Warszawy 8, 35-959 Rzeszów, Polska
e-mail: wzktmiop@prz.edu.pl

dr hab. inż. Andrzej Dzierwa, prof. PRz
Wydział Budowy Maszyn i Lotnictwa Politechniki Rzeszowskiej, Katedra Technologii Maszyn i Inżynierii Produkcji
al. Powstańców Warszawy 8, 35-959 Rzeszów, Polska
e-mail: adzierwa@prz.edu.pl

mgr inż. Ewelina Guźla
Wydział Budowy Maszyn i Lotnictwa Politechniki Rzeszowskiej, Katedra Technologii Maszyn i Inżynierii Produkcji
al. Powstańców Warszawy 8, 35-959 Rzeszów, Polska
e-mail: e.guzla@prz.edu.pl

INFLUENCE OF COEFFICIENT OF FRICTION ON TI-6AI-4V TITANIUM ALLOY TURNING PROCESS – FEM ANALYSIS

Joanna LISOWICZ   ORCID 0000-0002-9467-721X

A b s t r a c t: The good properties of Ti-6Al-4V titanium alloy make it widely used, but at the same time, make it difficult to machine. One of the factors which influence the machinability of metal alloys is coefficient of friction, which can be lowered by multiple cooling and lubricating methods. In the present work the influence of coefficient of friction on the turning process of Ti-6Al-4V was analyzed based on the FEM simulations conducted in DEFORM 2D/3D software. It was proven that the coefficient of friction influenced the cutting force and thrust force. It was also shown that the coefficient of friction had a significant impact on the chip compression ratio.

K e y w o r d s: Ti-6Al-4V, turning, coefficient of friction, FEM analysis

S t r e s z c z e n i e: Dobre właściwości stopu tytanu Ti-6Al-4V decydują o jego szerokim zastosowaniu, lecz jednocześnie wpływają na trudnoobrabialność. Jednym z czynników, który wpływa na obrabialność stopów metali jest współczynnik tarcia, którego wartość może być obniżana dzięki zastosowaniu różnych metod chłodzenia i smarowania. W niniejszej pracy przeanalizowano wpływ wartości współczynnika tarcia na przebieg procesu toczenia stopu Ti-6Al-4V, na podstawie symulacji MES przeprowadzonych w programie DEFRORM 2D/3D. Pokazano, iż współczynnik tarcia ma wpływ na wartość siły skrawania i siły odporowej. Uwidoczniono również istotny wpływ wartości współczynnika tarcia na współczynnik spęczenia wióra.

S ł o w a k l u c z o w e: Ti-6Al-4V, toczenie, współczynnik tarcia, analiza MES

Introduction

Use of titanium alloys has been increasing in the recent years due to their excellent properties such as high specific strength, low density and exceptional corrosion resistance. The major field of application of titanium alloys includes aerospace, but they are also used in medical applications, automotive, marine industry and others [24].

Ti-6Al-4V is the most common titanium alloy accounting for more than 50 % of global production. The major fields of application (80%) is aerospace and medical industry [31]. Its particular characterization ($\alpha+\beta$ phase) provides unique strength due to the stable structure [18]. Table 1 shows some of the properties of Ti-6Al-4V titanium alloy at a room temperature.

Metal cutting process is one of the oldest methods of reducing a metal workpiece to a given shape and features in the manufacture of most of the items, also those made of titanium alloys [4]. However, the properties which cause the wide use of titanium alloys make them also hard-to-cut material [13, 26, 34]:

- Low thermal conductivity –the thermal conductivity of titanium materials is relatively low in comparison with steel and aluminum alloys. This causes heat concentration on the tool cutting edge and face.
- High chemical reactivity – titanium with common gases (oxygen, hydrogen and nitrogen) and cutting tool material at tool operation temperatures. Formation of oxides, hydrides and nitrides cause the embrittlement and decrease of the fatigue strength of the alloy.

Table 1. Properties of Ti-6Al-4V titanium alloy [22]

Density ρ [g/cm3]	Young's modulus E [GPa]	Tensile strength R_m [MPa]	Yield strength $R_{p0.2}$ [MPa]	Elongation A [%]
4.42	106 – 114	987 – 1205	828 – 1075	10 – 18

Reactivity with cutting tool material causes galling, smearing and chipping of the workpiece surface and rapid tool wear.

- Low elastic modulus – leads to a low rigidity and allows deflection of slender and thin-walled workpiece under tool pressure, including chatter and tolerance problems.
- High temperature hardness and strength – causing deformation of the cutting tool because of high cutting forces required.
- Work hardening – causes absence of built-up edge in front of the cutting tool and increase of the shearing angle, which in turn induces a thin chip to contact a relatively small area in the cutting face, resulting in high bearing loads per unit area. The high bearing stress, combined with the friction between the chip and bearing area causes a significant heat raises in a very small area of the cutting tool and production of cratering close to the cutting edge, resulting in rapid tool breakdown. However, the formation of built-up edge is referred to be detrimental for tool coating.

The friction between workpiece and tool is one of the factors that affect machinability. To reduce friction coefficient and therefore improve machinability, various cooling and lubricating methods are applied [17]. The impact of different coolants and different cooling strategies is of interest of many scientists [10, 14 , 20]. Deiab et al. [11] have revealed that the cooling strategies had an impact on the tool wear, surface roughness and energy consumption during turning Ti-6Al-4V. Bermingham et al. [6] compared the tool life during laser assisted milling, dry milling, milling with flood emulsion, milling with minimum quantity lubrication and a hybrid laser + MQL process. It was found that conventional coolants worked well at the standard cutting speeds recommended by the tooling manufacturer, but at higher cutting speeds the coolant deteriorated tool fife due to thermal shock/fatigue. Raza et al. [28] evaluated tool wear patterns when turning titanium alloy Ti6Al4V under six lubrication techniques: Flood Cooling, Dry Machining, Vegetable Oil MQL Machining, Cooled Air Lubrication, Cryogenic Machining (with liquid Nitrogen), Vegetable Oil + Cooled Air/MQCL machining. It has been concluded that vegetable oil is a sustainable alternative to synthetic cooling in terms of tool wear and surface roughness. Rahim and Sasahara [25] studied the effect of palm oil as MQL lubricant on high speed drilling of titanium alloy Ti-6Al-4V. It was concluded that MQL with palm oil produced lower cutting forces and workpiece temperatures than MQL with synthetic ester, almost equal to the flood condition.

Multitude of researches on the impact of different types of coolants and different cooling strategies leads to the conclusion that the coolant plays an important role during machining. However, there are only a few publications where results of machining tests were referred to the coefficient of friction obtained as a result of tribological tests for specific material pairs and cooling conditions.

The machinability of material can be assessed by analysis of cutting forces values and chip shape among others [33]. In this work, the impact of the coefficient of friction on cutting forces and chip shape during Ti-6Al-4V titanium alloy turning will be checked. It will be also checked if this effect changes with the cutting speed.

Coefficient of friction in metal cutting

There are basically two types of friction: dry and viscous. Friction of dry and boundary- lubricated surfaces may be classified as Coulomb friction [30]:

$$\mu_f = \frac{F}{N} \qquad (1)$$

where N is the normal force acting at the considered interface and F is the frictional force at this interface (Figure 1).
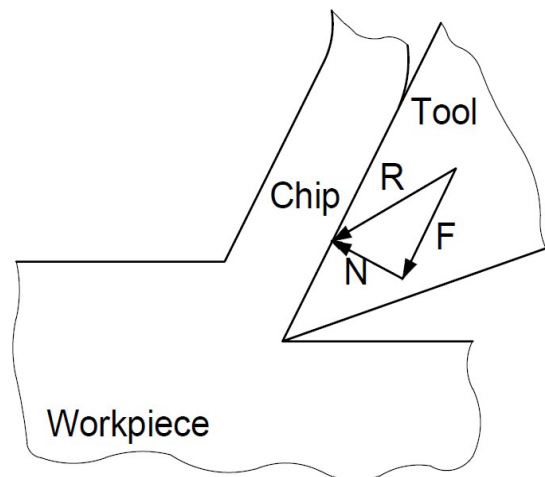
Fig 1. Normal force N and frictional force F in metal cutting (based on [2])

The regime of boundary lubrication is that the surfaces are separated by at most a few layers of lubrication molecules [23].

It is well-known that the contact between the two bodies is limited to only few microscopic high points (asperities). However, the stresses are customarily calculated by assuming that the forces are distributed over the total contact area. Due to a high contact pressure in real machining, the actual and apparent contact areas are practically the same. Therefore, the above approximation is not far from reality and numerator and denominator from of equation (1) can be divided over the tool-chip contact area A_c and then recalling than the mean normal stress at the interface is $\sigma_c = N/A_c$ and the mean shear (frictional) stress at the interface is $\tau_c = F/A_c$, one can obtain [3]:

$$\mu_f = \frac{\tau_c}{\sigma_c} \qquad (2)$$

Values for coefficient of friction are conveniently tabulated and incorporated into engineering books. However, the engineers and scientists confronted with real friction problems in machinery or industrial processes often find this simple approach insufficient to explain observations or to enable them to select from among numerous candidate materials and lubricants. Furthermore, different tabulations of friction data list different values even for (supposedly) the same sliding materials with the same lubricant (Table 2) [7].

Table 2. Values of coefficient of friction for material pair Ti-6Al-4V / WC-Co with various lubricants

Lubricant	Testing method	Coefficient of friction	References
Dry	ball-on-flat	0.42	[21]
Dry	tribometer based on a numerically controlled lathe	0.2-0.35 depending on sliding velocity (apparent friction coefficient)	[12]
Water	ball-on-flat	0.26	[21]
Deionized water	block on ring	0.34	[35]
Water	ball on disc	0.7	[37]
Water	ball on disc	0.47	[38]
Water	ball on disc	0.7	[36]
Commercial emulsion diluted to the concentration of 5 wt%	ball on disc	0.2	[38]
polyalkylene glycol (PAG) dissolved in deionized water at concentration of 10%	ball on disc	0.6	[37]
Castor oil sulfated sodium salt (CSS) aqueous solution at low concentration (5 wt%)	ball on disc	0.18	[37]
Pure castor oil	ball on disc	0.2	[37]
Cryogenic cooling	calculated on the base of cutting forces	0.42-0.54 dependent on the cutting parameters	[5]
Cryogenic cooling	rotating disk rubs on a flat specimen with a controlled normal force	0.12-0.18 depending on the method of feeding LN2	[16]
Paraffin	ball on disc	0.66	[36]
PAO40	ball on disc	0.5	[36]
self-emulsifying ester (SEE)	ball on disc	0.2	[36]
SEE aqueous solution with small concentration of 1 wt%	ball on disc	0.17	[36]
Nonylphenol polyoxyethylene ether phosphate ester (PPE) diluted to the concentration of 1 wt% by deionized water.	ball on disc	0.14	[38]

Experimental Design

The experiment was designed with three-level factors in Statistica software (Table 3). Basing on literature review the range of cutting speed was assumed as 60-150 m/min [15, 27, 29] and the range of coefficient of friction was assumed as 0.12-0.7 (based on the Table 2). Other parameters such as heat convection coefficient and tool geometry (rake angle = 7°, flank angle = 7° and cutting edge radius = 0.04 mm) have not changed in individual cases. The feed was at constant level of 0.1 mm/rev.

Table 3. The design of experiment with Statistica software

Standard Run	Cutting speed v_c [m/min]	Coefficient of friction μ
5	115	0.41
7	150	0.12
9	150	0.70
1	80	0.12
3	80	0.70
2	80	0.41
8	150	0.41
6	115	0.70
4	115	0.12

The simulations of the orthogonal turning process of Ti-6Al-4V titanium alloy taking into account the influence of coefficient of friction were held in the DEFORM 2D/3D software. The material was selected from the DEFORM database: Ti6Al4V-machiningSFTC. Material constitutive model was changed to Johnson-Cook model [39, 40], expressed by the following expression of the equivalent stress:

$$\bar{\sigma}_{JC} = A + B(\bar{\varepsilon})^n \cdot [1 + C \ln(\dot{\bar{\varepsilon}}/\dot{\bar{\varepsilon}}_0)] \cdot \left[1 - \left(\frac{T_w - T_0}{T_m - T_0}\right)^m\right] \quad (3)$$

where: $\bar{\sigma}_{JC}$ – Johnson-Cook plastic equivalent stress [MPa], A – initial yield stress [MPa], B – hardening modulus [MPa], C – strain rate dependency coefficient [MPa], m – thermal softening coefficient, n – work-hardening exponent, T_w – workpiece computed temperature [°C], T_m – melting temperature [°C], T_0 – room temperature [°C], $\bar{\varepsilon}$ – plastic strain, $\dot{\bar{\varepsilon}}$ – equivalent plastic strain rate [s^{-1}], $\dot{\bar{\varepsilon}}_0$ – reference plastic strain rate [s^{-1}].

The above model provides a satisfactory description of the behavior of metals and alloys since it considers large strains, high strain rates, and temperature dependent visco-plasticity [39]. The values of coefficients A, B, n, C, m for the Ti-6Al-4V titanium alloy are presented in Table 4 at the base of [40].

Table 4. Johnson-Cook model coefficients for Ti-6Al-4V

Material	A [MPa]	B [MPa]	n	C	m
Ti-6Al-4V	1098	1092	0.93	0.014	1.1

Experimental results and discussion

Table 5 shows the mean values of cutting force (X load) and thrust force (Y load) obtained as the result of simulations. In order to access validity of the results of simulations the results of experimental research are shown in Table 6. The experiment was conducted with use of CCMT 120408–MM 1105 cutting insert and following cutting parameters were indicated: v_c = 80 m/min, f = 0.1 mm/rev and a_p = 1 mm. The experiment was conducted in flood cooling conditions.

Table 5. List of cutting force and feed force values obtained on the basis of simulations in the DEFORM 2D/3D software

Standard Run	Cutting speed v_c [m/min]	Coefficient of friction μ	X load F_c [N]	Y load F_T [N]
5	115	0.41	176.35	135.73
7	150	0.12	134.88	111.59
9	150	0.70	174.81	133.60
1	80	0.12	190.49	140.65
3	80	0.70	217.53	111.18
2	80	0.41	194.04	129.41
8	150	0.41	159.95	137.44
6	115	0.70	193.96	123.49
4	115	0.12	168.69	141.32

Table 6. Cutting force and thrust force values obtained in experimental research

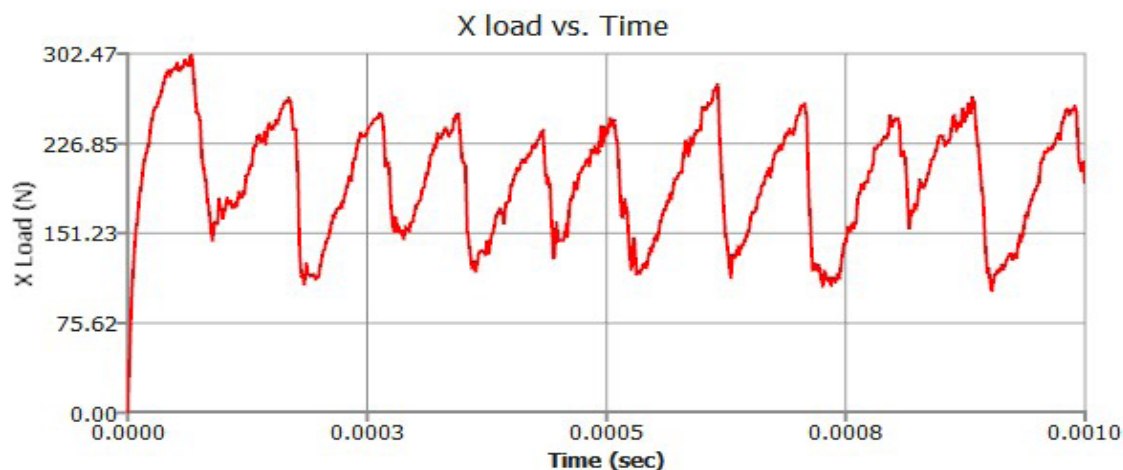| Cutting speed v_c [m/min]	Feed f [mm/rev]	Depth of cut a_p [mm]	Cutting force F_c [N]	Thrust force F_T [N]
80	0.1	1	249.15	171.52

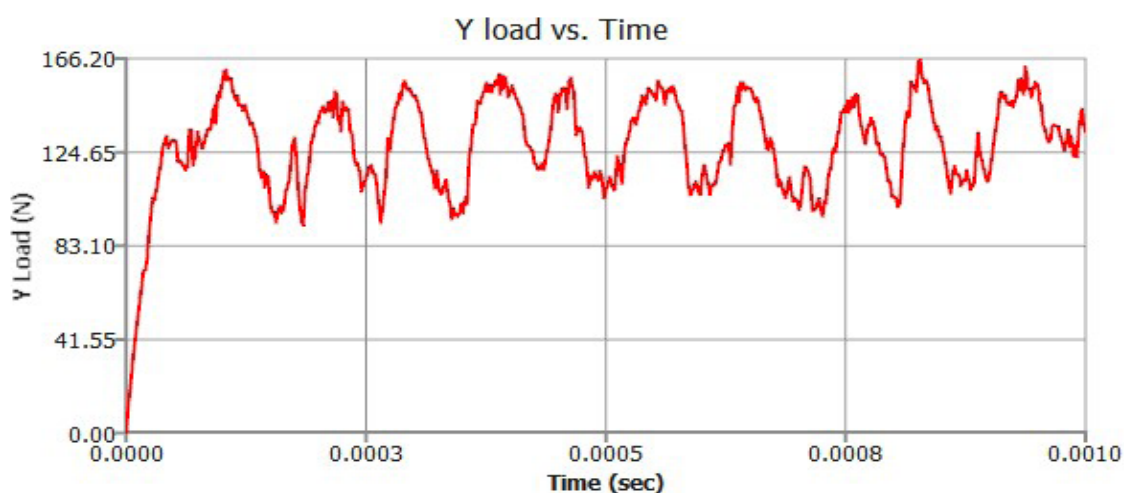Figure 2. X load (cutting force) versus time graph (v_c = 80 m/min, μ= 0.41)

Figure 3. Y load (thrust force) versus time graph (v_c = 80 m/min, μ= 0.41)

Figure 2 and Figure 3 show the sample graphs of cutting force and thrust force versus time for cutting speed 80 m/min and coefficient of friction of 0.41 generated in DERORM 2D/3D software. It can be seen that the cutting force is periodic due to a segmented chip formation.

It can be seen that the difference between the experimental and simulation results of the cutting force value is about 22 % for v_c = 80 m/min and coefficient of friction μ = 0.41. For the thrust force this difference is about 25 %.

The friction coefficient had a significant influence on the cutting force and thrust force regardless of the cutting speed value (Figure 4 and Figure 5). With increase of the coefficient of friction the cutting force increased and the thrust force decreased. This dependence is confirmed by Amrita et. al. [1], who studied the influence of the addition of nanographite to the soluble oil on the coefficient of friction and cutting forces for AISI 1040

steel. It was confirmed that for fluid with nanoparticles the coefficient of friction and cutting forces were decreased in comparison to conventional soluble oil. Talib and Rahim [32] examined the coefficient of friction of crude jatropha oil, synthetic ester and modified jatropha oils at various molar ratios of jatropha methyl ester. It was shown that the coefficient of friction was minimized for modified jatropha oil with the highest molar ratio of jatropha methyl ester (MJO5) and the highest value of coefficient of friction was obtained for the synthetic ester. Turning of AISI 1045 steel tests generally confirm the dependency of increase in cutting forces with increase of coefficient of friction with exception of machining with synthetic ester.

Moreover, it can be seen that increasing cutting speed increased cutting force. The same dependence was observed by Khan and Maity [19] during finish turning of CP-Ti grade 2 under different cooling conditions.
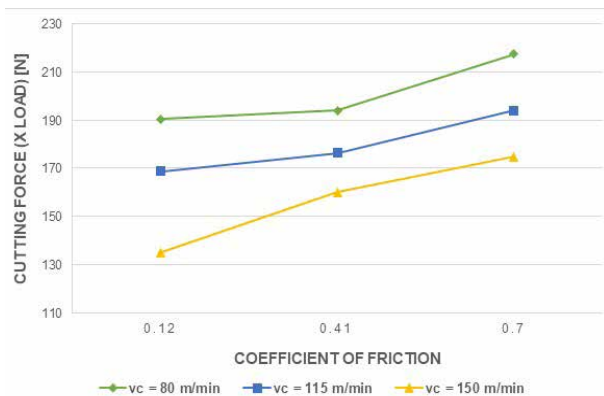
Fig. 4. Influence of coefficient of friction and cutting speed on the cutting force
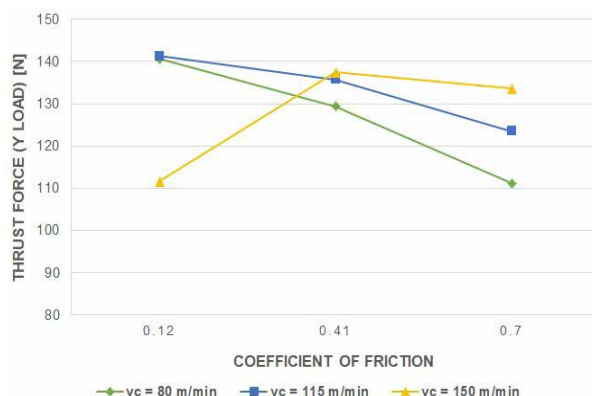
Fig. 5. Influence of coefficient of friction and cutting speed on the thrust force

Figure 6 shows the influence of coefficient of friction on the chip formation process. The segmented chips were obtained in the entire range of tested parameters. Segmented chip formation is a two stage process in which workpiece material is plastically deformed ahead of the tool causing it to bulge. Catastrophic failure occurs and a shear band is formed extending from the tool tip to the workpiece surface when a critical strain level is reached. The resulting chips consist of moderately deformed chip segments separated by narrow bands of intensely sheared material [9].
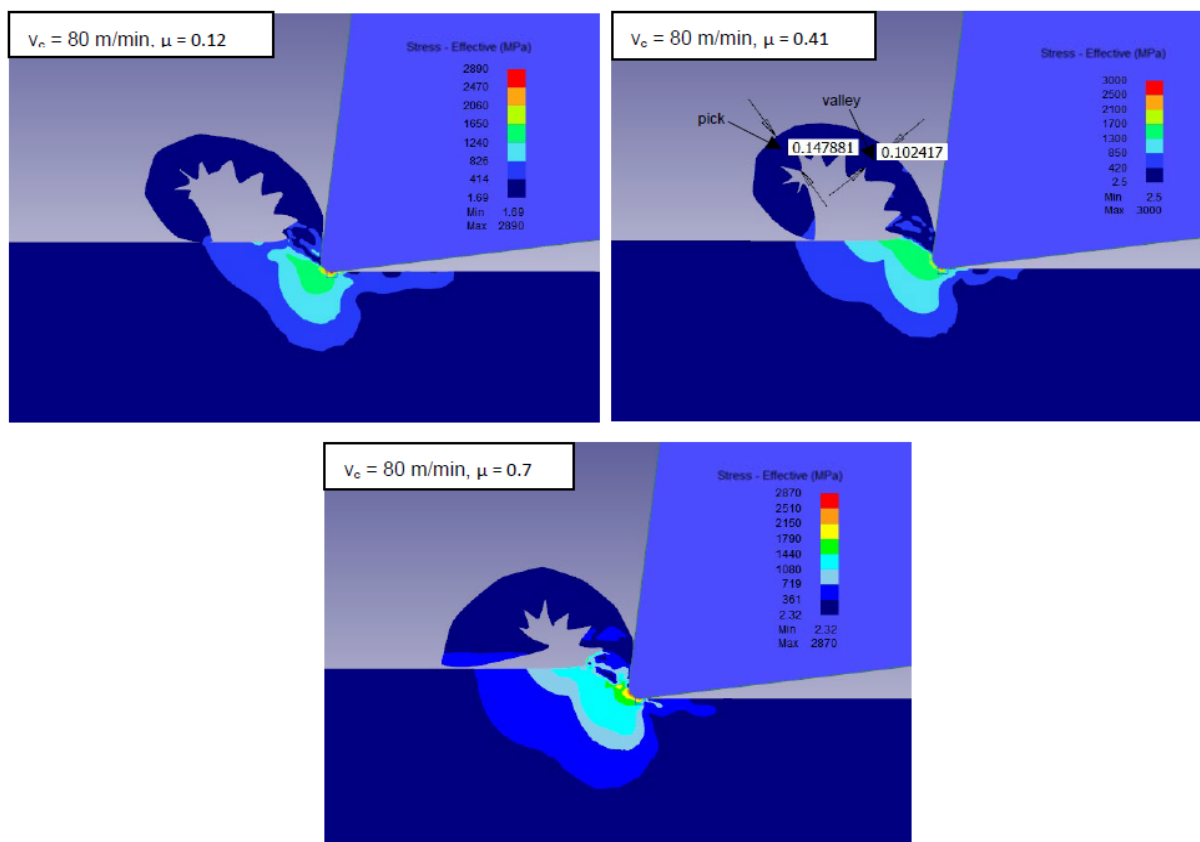
Fig. 6. The influence of coefficient of friction on chip formation process

The chip compression ratio λ_h also increased with increase of coefficient of friction. Table 7 shows values of the deformed chip thickness and the chip compression ratio. The chip compression ratio was calculated as [8]:

$$\lambda_h = \frac{h_c}{h} \qquad (4)$$

The deformed chip thickness hc was calculated as the average value of five picks' heights and five valley heights (Figure 6) and the undeformed chip thickness h was equal to the value of feed (h = 0.1 mm). Moreover it can be seen that the chip compression ratio decreased with increase of cutting speed value (Figure 7).

Table 7. List of deformed chip thicknesses and chip compression ratios calculated on the basis of simulations in the DEFORM 2D/3D program

Standard Run	Cutting speed v_c [m/min]	Coefficient of friction μ	Deformed chip thickness h_c [mm]	Chip compression ratio λ_h
5	115	0.41	0.1120	1.1195
7	150	0.12	0.1003	1.0028
9	150	0.7	0.1102	1.1016
1	80	0.12	0.1061	1.1916
3	80	0.7	0.1416	1.4160
2	80	0.41	0.1221	1.2209
8	150	0.41	0.1010	1.0096
6	115	0.7	0.1197	1.1975
4	115	0.12	0.1152	1.1520

Fig. 7. The influence of coefficient of friction and cutting speed on the chip compression ratio

Conclusions

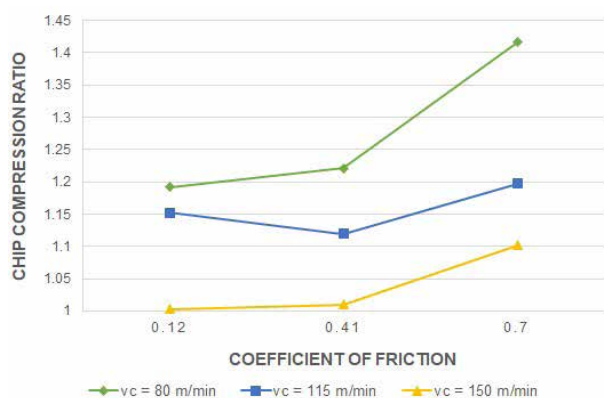Based on the results of the simulations presented above, it can be concluded that the coefficient of friction plays a significant role during Ti-6Al-4V titanium alloy machining. With the increase of friction coefficient, the cutting force and the thrust force increase significantly.

Irrespectively of the cutting parameters, the segmented chip was produced; however the coefficient of friction and cutting speed value influenced the chip compression ratio.

Based on the discussed research it is worth noting that the coefficient of friction is important factor in Ti-6Al-4V alloy machining. On the other hand it is worth pointing out that the different tabulations of friction data list different values even for the same sliding materials with the same lubricant. This leads to the conclusion that much attention should be paid to the determination of coefficient of friction for the specific cooling and lubricating methods. Knowledge of the specific values of coefficient of friction for the specific conditions will allow simulating the process closer to a real one.

On the basis of the experimental results and literature overview it can be concluded that the results of simulations can be a reliable starting point for further experimental research.

References

[1] Amrita M., Srikant R.R., Sitaramaraju A.V. 2014. "Performance evaluation of nanographite-based cutting fluid in machining process". Mater. Manuf. Process. 29(5): 600–605. DOI: 10.1080/10426914.2014.893060.

[2] Astakhov V.P. 2006. "Chapter 1 - Generalized model of chip formation". In Tribology of Metal Cutting, 1–68.

[3] Astakhov V.P. 2006. "Chapter 3 - Tribology of the tool-chip and tool-workpiece interfaces". In Tribology of Metal Cutting, 124–219.

[4] Bailey J.A. 1975. "Friction in metal machining-Mechanical aspects". Wear 31(2): 243–275. DOI: 10.1016/0043-1648(75)90161-1.

[5] Bermingham M.J., Kirsch J., Sun S., Palanisamy S., Dargusch M.S. 2011. "New observations on tool life, cutting forces and chip morphology in cryogenic machining Ti-6Al-4V". Int. J. Mach. Tools Manuf. 51(6): 500–511. DOI: 10.1016/j.ijmachtools.2011.02.009.

[6] Bermingham M.J., Sim W.M., Kent D., Gardiner S., Dargusch M.S. 2015. "Tool life and wear mechanisms in laser assisted milling Ti-6Al-4V". Wear 322–323: 151–163. DOI: 10.1016/j.wear.2014.11.001.

[7] Blau P.J. 2001. "The significance and use of the friction coefficient". Tribol. Int. 34(9): 585–591. DOI: 10.1016/S0301-679X(01)00050-0.

[8] Cotterell M., Byrne G. 2008. "Characterisation of chip formation during orthogonal cutting of titanium alloy Ti-6Al-4V". CIRP J. Manuf. Sci. Technol. 1(2): 81–85. DOI: 10.1016/j.cirpj.2008.09.017.

[9] Cotterell M., Byrne G. 2008. "Dynamics of chip formation during orthogonal cutting of titanium alloy Ti-6Al-4V". CIRP Ann. - Manuf. Technol. 57(1): 93–96. DOI: 10.1016/j.cirp.2008.03.007.

[10] Debnath S., Reddy M.M., Yi Q.S. 2014. "Environmental friendly cutting fluids and cooling techniques in machining: A review". J. Clean. Prod. 83: 33–47. DOI: 10.1016/j.jclepro.2014.07.071.

[11] Deiab I., Raza S.W., Pervaiz S. 2014. "Analysis of lubrication strategies for sustainable machining during turning of titanium ti-6al-4v alloy". Procedia CIRP 17: 766–771. DOI: 10.1016/j.procir.2014.01.112.

[12] Egaña A., Rech J., Arrazola P.J. 2012. "Characterization of Friction and Heat Partition Coefficients during Machining of a TiAl6V4 Titanium Alloy and a Cemented Carbide". Tribol. Trans. 55(5): 665–676. DOI: 10.1080/10402004.2012.692007.

[13] Ezugwu E.O., Bonney J., Yamane Y. 2003. "An overview of the machinability of aeroengine alloys". J. Mater. Process. Technol. 134(2): 233–253. DOI: 10.1016/S0924-0136(02)01042-7.

[14] Gajrani K.K., Ram D., Ravi Sankar M. 2017. "Biodegradation and hard machining performance comparison of eco-friendly cutting fluid and mineral oil using flood cooling and minimum quantity cutting fluid techniques". J. Clean. Prod. 165: 1420–1435. DOI: 10.1016/j.jclepro.2017.07.217.

[15] Habrat W. 2019. Analiza i modelowanie toczenia wykończeniowego tytanu i jego stopów. Rzeszów: Oficyna Wydawnicza Politechniki Rzeszowskiej.

[16] Hong S. 2006. "Lubrication mechanisms of LN2 in ecological cryogenic machining". Mach. Sci. Technol. 10(1): 133–155. DOI: 10.1080/10910340500534324.

[17] Hong S.Y., Ding Y., Jeong W. cheol. 2001. "Friction and cutting forces in cryogenic machining of Ti-6Al-4V". Int. J. Mach. Tools Manuf. 41(15): 2271–2285. DOI: 10.1016/S0890-6955(01)00029-3.

[18] Jamil M. et al. 2019. "Effects of hybrid Al2O3-CNT nanofluids and cryogenic cooling on machining of Ti–6Al–4V," Int. J. Adv. Manuf. Technol. 102(9–12): 3895–3909. DOI: 10.1007/s00170-019-03485-9.

[19] Khan A., Maity K. 2018. "Influence of cutting speed and cooling method on the machinability of commercially pure titanium (CP-Ti) grade II". J. Manuf. Process. 31: 650–661. DOI: 10.1016/j.jmapro.2017.12.021.

[20] Lawal S.A., Choudhury I.A., Nukman Y. 2012. "Application of vegetable oil-based metalworking fluids in machining ferrous metals - A review". Int. J. Mach. Tools Manuf. 52(1): 1–12. DOI: 10.1016/j.ijmachtools.2011.09.003.

[21] Niu Q.L., Zheng X.H., Ming W.W., Chen M. 2013. "Friction and Wear Performance of Titanium Alloys against Tungsten Carbide under Dry Sliding and Water Lubrication". Tribol. Trans. 56(1): 101–108. DOI: 10.1080/10402004.2012.729296.

[22] Oczoś K., Kawalec A. 2012. Kształtowanie metali lekkich. Warszawa: Wydawnictwo Naukowe PWN.

[23] Persson B.N.J. 1993. "Theory of friction and boundary lubrication B." Phys. Rev. B 48(24).

[24] Peters M., Hemptenmacher J., Kumpfert J., Leyens C. 2003. "Structure and Properties of Titanium and Titanium Alloys". In Titanium and Titanium Alloys (M. Peters and C. Leyens, Eds.), 1–36. Weinheim: WILEY-VCH Verlag GmbH.

[25] Rahim E.A., Sasahara H. 2011. "A study of the effect of palm oil as MQL lubricant on high speed drilling of titanium alloys". Tribol. Int. 44(3): 309–317. DOI: 10.1016/j.triboint.2010.10.032.

[26] Rahman M., Wong Y.S., Zareena A.R. 2003. "Machinability of titanium alloys". JSME International Journal, Series C: Mechanical Systems, Machine Elements and Manufacturing 46(1): 107–115. DOI: 10.1299/jsmec.46.107.

[27] Ramana M.V., Rao G.K.M., Rao D.H. 2013. "Effect of Process Parameters on Surface Roughness in Turning of Titanium Alloy under Different Conditions of Lubrication, 83–91". Conf. Proc. Recent Adv. Robot. Aeronaut. Mech. Eng. held Athens, Greece, May 14-16.

[28] Raza S.W., Pervaiz S., Deiab I. 2014. "Tool wear patterns when turning of titanium alloy using sustainable lubrication strategies". Int. J. Precis. Eng. Manuf. 15(9): 1979–1985. DOI: 10.1007/s12541-014-0554-z.

[29] Ribeiro M.V., Moreira M.R.V., Ferreira J.R. 2003. "Optimization of titanium alloy (6Al-4V) machining". J. Mater. Process. Technol. 143–144(1): 458–463. DOI: 10.1016/S0924-0136(03)00457-6.

[30] Saka N. 2015. "On the Laws and Theories of Sliding Friction". International Mechanical Engineering Conference & Exposition, November 13-19, Houston, Texas, USA. DOI: 10.1115/imece2015-51470.

[31] Shokrani A., Dhokia V., Newman S.T. 2016. "Investigation of the effects of cryogenic machining on surface integrity in CNC end milling of Ti-6Al-4V titanium alloy". J. Manuf. Process. 21:172–179. DOI: 10.1016/j.jmapro.2015.12.002.

[32] Talib N., Rahim E.A. 2016. "The Effect of Tribology Behavior on Machining Performances When Using Bio-based Lubricant as a Sustainable Metalworking Fluid". Procedia CIRP 40: 504–508. DOI: 10.1016/j.procir.2016.01.116.

[33] Trent E.M., Wright P.K. 2000. Machinability. In Metal Cutting, 4th ed., 251–310. Butterworth–Heinemann.

[34] Veiga C., Davim J.P., Loureiro A.J.R. 2013. "Review on machinability of titanium alloys: The process perspective". Rev. Adv. Mater. Sci. 34(2): 148–164.

[35] Xuedong W., Dapu W., Shengrong Y., Qunji X. 2000. "Tribochemical investigation of tungsten carbide/titanium alloy tribo-couples under aqueous lubrication". Wear 237(1): 28–32. DOI: 10.1016/S0043-1648(99)00288-4.

[36] Yang Y., Zhang C., Dai Y., Luo J. 2017. "Tribological properties of titanium alloys under lubrication of SEE oil and aqueous solutions". Tribol. Int. 109(November 2016): 40–47. DOI: 10.1016/j.triboint.2016.11.040.

[37] Yang Y., Zhang C., Dai Y., Luo J. 2019. "Lubricity and Adsorption of Castor Oil Sulfated Sodium Salt Emulsion Solution on Titanium Alloy". Tribol. Lett. 67(2): 1–14. DOI: 10.1007/s11249-019-1173-8.

[38] Yang Y., Zhang C., Wang Y., Dai Y., Luo J. 2016. "Friction and wear performance of titanium alloy against tungsten carbide lubricated with phosphate ester". Tribol. Int. 95: 27–34. DOI: 10.1016/j.triboint.2015.10.031.

[39] Zhang Y., Umbrello D., Mabrouki T., Rizzuti S., Nelias D., Gong Y. 2013. "On different FE-based models to simulate cutting operation of Titanium alloy (Ti-6Al-4V)". Mechanika 19(3): 349–357. DOI: 10.5755/j01.mech.19.3.4656.

[40] Zhang Y.C., Mabrouki T., Nelias D., Gong Y.D. 2011. "Chip formation in orthogonal cutting considering interface limiting shear stress and damage evolution based on fracture energy approach". Finite Elem. Anal. Des. 47(7): 850–863. DOI: 10.1016/j.finel.2011.02.016.

mgr inż. Joanna Lisowicz
Rzeszow University of Technology, Faculty of Mechanical Engineering and Aeronautics
Al. Powstańców Warszawy 12, 35-959 Rzeszów, Poland
e-mail: j.lisowicz@prz.edu.pl

EFFECT OF THE BRUSHING PROCESS ON THE STATE OF THE SURFACE LAYER OF BUTT JOINTS MADE OF USING THE FSW METHOD

Wpływ obróbki szczotkowaniem na stan warstwy wierzchniej spoiny wykonanej metodą FSW

Magdalena BUCIOR   ORCID 0000-0002-1081-5065
Rafał KLUZ   ORCID 0000-0001-6745-294X
Andrzej KUBIT   ORCID 0000-0002-6179-5359
Kamil OCHAŁ   ORCID 0000-0003-0641-0273

Abstract: Friction stir welding (FSW) is one of the most modern methods of joining metals and their alloys in a solid state. This method is particularly suitable for joining the materials that are difficult to weld, such as steels and high-strength aluminum, copper and titanium alloys, as well as some nickel, zirconium and copper alloys. It makes it possible to use this method in the production of aviation structures while reducing the labour consumption, cost and weight, while maintaining comparable or higher strength parameters compared to classic methods. However, the face of weld made using the FSW method is often uneven and moreover, the welding process itself introduces tensile stresses in the surface layer, which reduces the fatigue strength of the joints. Brushing is one of the methods of removing the welding burrs. The study investigates the effect of brushing treatment on the selected properties of the surface layer of butt welds of 2024-T3 aluminum alloy. The research was carried out with the use of wire brushes and cutting brushes with ceramic fibers. The analysis of the obtained results showed that brushing with using a wire brush at a feed rate of 70 mm/min (variant 1) introduced the most favorable residual stresses, while brushing with a ceramic brush at a feed rate of 100 mm/min (variant 4) provided the lowest roughness parameters.

Keyword: brushing, Friction Stir Welding, aluminum alloy, brush ceramic tools

Streszczenie: Zgrzewanie tarciowe z przemieszaniem FSW (ang. Friction Stir Welding) jest jedną z najnowocześniejszych metod łączenia metali i ich stopów w stanie stałym. Metoda ta jest szczególnie przydatna do łączenia materiałów trudno spawalnych, jak na przykład stale i wysoko wytrzymałe stopy aluminium, miedzi i tytanu, a także niektóre stopy niklu, cyrkonu i miedzi. Daje to możliwość stosowania tej metody przy produkcji struktur lotniczych przy jednoczesnym obniżeniu pracochłonności, kosztów i ich ciężaru, zachowując porównywalne lub wyższe parametry wytrzymałościowe w porównaniu do metod klasycznych. Lico spoiny wykonanej metodą FSW jest jednak często nierówne a ponadto sam proces zgrzewania wprowadza rozciągające naprężenia własne w warstwie wierzchniej, co skutkuje obniżeniem wytrzymałości zmęczeniowej złączy. Jednym ze sposobów usunięcia zadziorów powstałych podczas zgrzewania jest obróbka szczotkowaniem. W pracy przeprowadzono badania wpływu obróbki szczotkowaniem na wybrane właściwości warstwy wierzchniej spoin blach ze stopu aluminium 2024-T3. Badania prowadzono z wykorzystaniem szczotek drucianych oraz szczotek tnących z włóknami ceramicznymi. Analiza uzyskanych wyników wykazała, że szczotkowanie szczotką drucianą przy posuwie 70 mm/min (wariant 1) wprowadza najkorzystniejsze naprężenia własne, natomiast szczotkowanie szczotką ceramiczną firmy Xebec przy posuwie 100 mm/min (wariant 4) powoduje zmniejszenie parametrów chropowatości.

Słowa kluczowe: szczotkowanie, zgrzewanie tarciowe z mieszaniem materiału, stopy aluminium, szczotkowe narzędzia ceramiczne

Introduction

In the aviation industry, the reduction of fuel consumption and exhaust emissions is an important aspect having an impact on the environment. One of the ways to achieve this goal is, among others, the reduction of the weight of the plane while maintaining very good strength properties of the material. The weight reduction can be achieved through the use of light metals or the use of appropriate joints, while reducing labour consumption, costs and their weight, while maintaining comparable or higher strength parameters compared to the classic methods. One of the most modern methods of joining metals and their alloys in a solid state (at temperatures lower than the melting point of the material to be joined) includes friction stir welding (FSW). This method is particularly useful for joining materials which, according to traditional technologies, are difficult to weld, such as steels and high-strength alloys of aluminum [3, 5, 7], copper and titanium [2], as well as some nickel, zirconium and copper alloys [4]. However, the face of weld made using the FSW method is often uneven and moreover, the welding process itself introduces tensile stresses [10,12, 14] in the surface layer, which results in a reduction of

the fatigue strength of the joints. Brushing is one of the methods for removal of the welding burrs. This method applies removing the outer layer of the material with a rotating brush. Brushing is mainly used for burring, deburring and polishing operations. This treatment can be used to create a surface layer with appropriate physical and mechanical properties that differ from the properties of the material core or as a pretreatment the joining process [8]. The high availability and variety of brushes as tools is due to their good productivity, ease of implementation as manual or automatic surface finishing, and even distribution of cutting forces on the surface of the workpiece. As a result, it allows for a controlled removal material process, simple clamping the workpiece and a lower risk of damage to the machine tool and the workpiece [9]. Traditional tools used for surface finish work consist of steel or plastic fibres, their disadvantages are the permanent deformation of the fibres and quick wear, which in turn affects the surface quality [11]. The brushes made of ceramic material by Xebec are the alternative. They present innovative technology in the use of abrasive for surface treatment. Thanks to the unique Xebec technology, the abrasive in the form of fibres allows for a constant machining performance. The fibre abrasive is better than conventional abrasive because it does not tend to stick during treatment. Such a property of the brushes allows maintaining a constant cutting efficiency. One single fibre of the Xebec brushes has 1000 sanding edges. This property of abrasive brushes allows them to be used for precise deburring and polishing operations.

The surface condition of welded joints is crucial from the point of view of their operation. Residual stresses, the geometric surface structure or hardening of the surface layer often determine the strength properties of the weld.

Therefore, it is important to analyze the state of surface layer the welded joints.

The study focuses on the analysis of the impact of brushing treatment on the state of residual stresses and the geometric surface structure of FSW welded joints made of 2024-T3 aluminum alloy. Additionally, the possibility of removing flashes, burrs resulting from the welding process with using different kinds of brushes was investigated.

Method

The paper presents the experimental studies the aim of which was to analyze the residual stresses and the geometrical surface structure of butt joints using the FSW method after brushing. The possibility of removing flashes and micro-inequalities resulting from welding with using two types of brushes: wire and with ceramic fibres was also examined. For the tests, the specimens made of aluminum alloy 2023 in state T3 were used. This type of aluminum is employed in the elements that require good strength to weight ratio. This alloy has a low corrosion resistance and low weldability, widely used in the production of aviation components. The welding process was carried out on a universal vertical milling machine JAFO FWF32J2. The FSW process was made with a tool rotational speed of 1300 rpm (n), feed rate of 50 mm/min (f) and depth of 1.7 mm (d). Two sheets of aluminum were fixed in special device and next butt-welded. The thickness of the welded sheets was 2 mm. In the next stage, the welded sheets on the same machine were brushed using two types of brushes: wire brush (Fig. 1a) and with ceramic fibres (by Xebec) (Fig. 1b). The research was carried out according to several variants presented in Table 1.
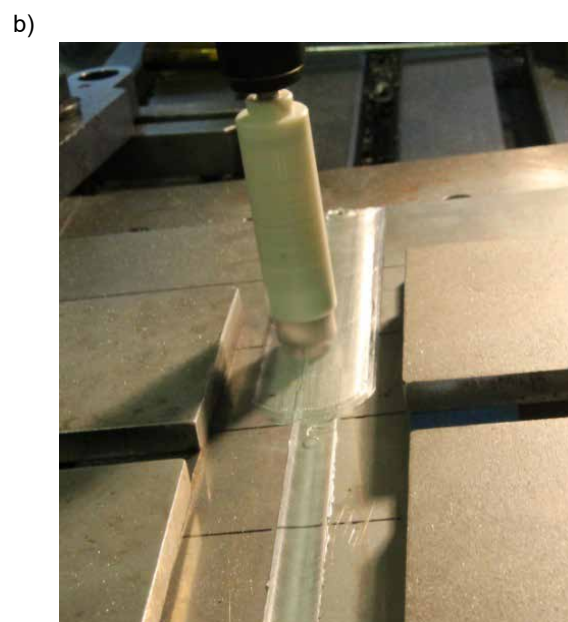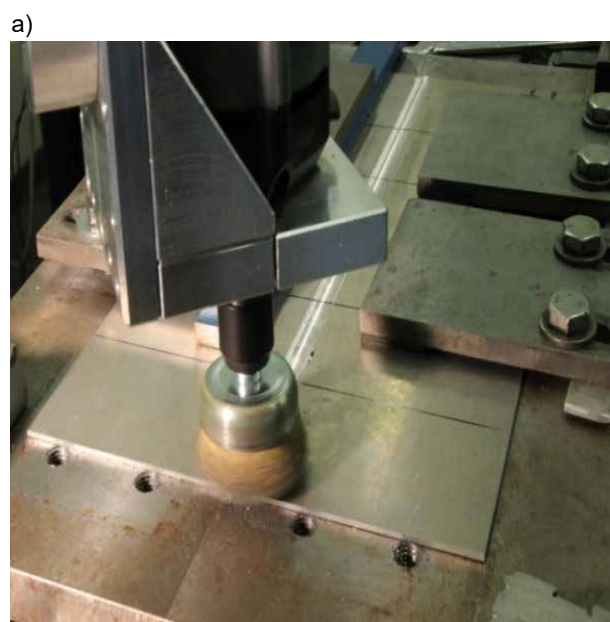
a)

b)

Fig. 1. Brushing with using of: wire brush (a) and brush with ceramic fibres (Xebec) (b)

Table 1. Variants used in the experiment

Variant	Parameters of process		Type of brush/treatment
	Feed rate f, mm/min	Rotational speed V, rpm	
1	70	10 000	Wire brush
2	100	10 000	Wire brush
3	100	10 000	Wire brush+ Xebec
4	100	10 000	Xebec
5	70	10 000	Xebec
6	-	-	Base (without treatment)

The residual stress was measured with the X-ray diffractometer Proto iXRD Combo and computer software XRD Win 2.0 by Proto Manufacturing. The research was carried out at the Department of Materials Science at Rzeszow University of Technology. This device enables measurements to be carried out directly on the tested element - it is a non-invasive test. To calculate the value of residual stresses in a given measuring point, the $\sin^2\Psi$ [1] method was used, which involves the use of symmetrical Bragg-Brentan diffraction. The Ψ-type goniometer allows obtaining appropriate inclinations of the diffraction vector by the angles Ψi in the plane perpendicular to the diffraction plane [13]. In this research was used a lamp with a chromium anode and a beam of CrKα characteristic radiation with a wavelength λ = 2.291 Å and a collimator diameter of 2 mm, an anode current of 4 mA and anode voltage of 20 kV. The stresses were determined for the constant values of the angle Ψ in the range from 25 ° to -25 °. The elastic deformations in the tested element were carried out for the diffraction line from the {311} family of planes at the angle 2θ = 139.3 °. The values of Poisson's ratio = 0.33 and Young's modulus E = 73.1 GPa were assumed in the measurements of residual stresses [6]. The residual stresses were measured on the specimen in the area of the weld at two points in the direction parallel and perpendicular to the direction of welding. The measurements were conducted for the variants after brushing and for the base surface after welding.

The study of the geometric surface structure was performed using the Taylor Hobson Talysurf CCI optical profilometer. The research included the measurements of roughness parameters, profilograms, 3D views. The surface roughness was analyzed according to the variants presented in Table 1.

Results and discussion

The presented three dimensional illustrations show that brushing with using ceramic fibres (Fig. 5 and Fig. 6) mostly removes traces of the tool used in the welding process (Fig. 7), which in effect reduces the surface roughness. For this type of brush, a decrease in the roughness parameter Ra in the range of 84 ÷ 89% (respectively variant 5 and 4) can be observed compared to the specimen without treatment (variant 6). A decreased trend can be also observed for the other amplitude parameters, for example: the Rz parameter, a decrease in the range of 76 ÷ 84% compared to variant 6. The lowest roughness was obtained for variant 4, where the feed rate was f = 100 mm/min. In turn, the largest in the case of brushing with wire brush according to variant 1, where f = 70 mm/min. For this variant, the value of the Ra parameter was 7.94 µm, which is comparable to the base variant (Ra = 8.01 µm). When comparing the roughness profiles, in the case of variant 1 (Fig. 2), we can notice a significant dimpling resulting from brushing with a using the wire brush, where the value of the parameter Rv = 27.4 µm, an increased by 34% in relation to the base surface (Fig. 7). This may be due to the properties of the welded material, which is aluminum. In all the analyzed cases, it can also be observed that the parameter describing the maximum profile peak height Rp decreased as compared to the base variant, in the range of 31 ÷ 91%, which proves that the use of brushes removes irregularities resulting from friction stir welding. The use of the Xebec brush after brushing with a wire brush (variant 3) also had a favorable effect on the roughness. In this case, the parameter Ra decreased about 35% compared to variant 2 (wire brush).

When analyzing the obtained results of roughness, the attention should be paid to the technological parameters of the brushing process. In the experiment, the variable parameter was the feed rate, adopted at two levels: 70 mm/min and 100 mm/min. Both in the case of brushing with wire brush and ceramic brush, the roughness decreases with increasing feed rate (variant 2 and 4). Summing up, it can be stated that properly selected technological parameters of the brushing process, both in the case of using wire and ceramic brushes, reduce the roughness surface of the welded joints.

In turn, the reduction of roughness has a favorable effect on the quality of the welded joints. Brushing removed flashes, notches and micro-inequalities formed during welding (Fig. 8), which could be a source of crack propagation and consequently, reduce the fatigue strength of the joint.

a)
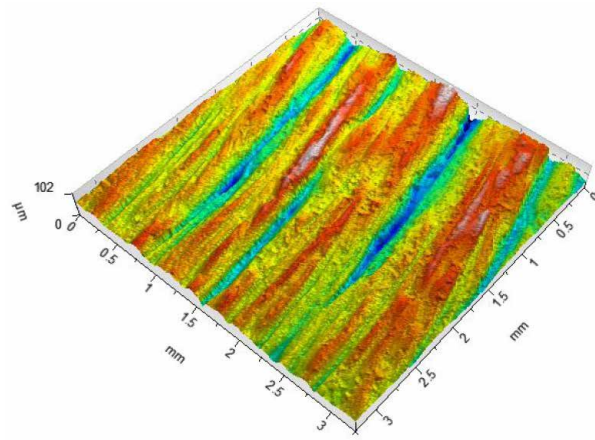
b)

Fig. 2. Three dimensional illustration (a) and surface profilogram (b) of the specimen with brushing, variant 1

a)

b)

Fig. 3. Three dimensional illustration (a) and surface profilogram (b) of the specimen with brushing, variant 2

a)

b)

Fig. 4. Three dimensional illustration (a) and surface profilogram (b) of the specimen with brushing, variant 3
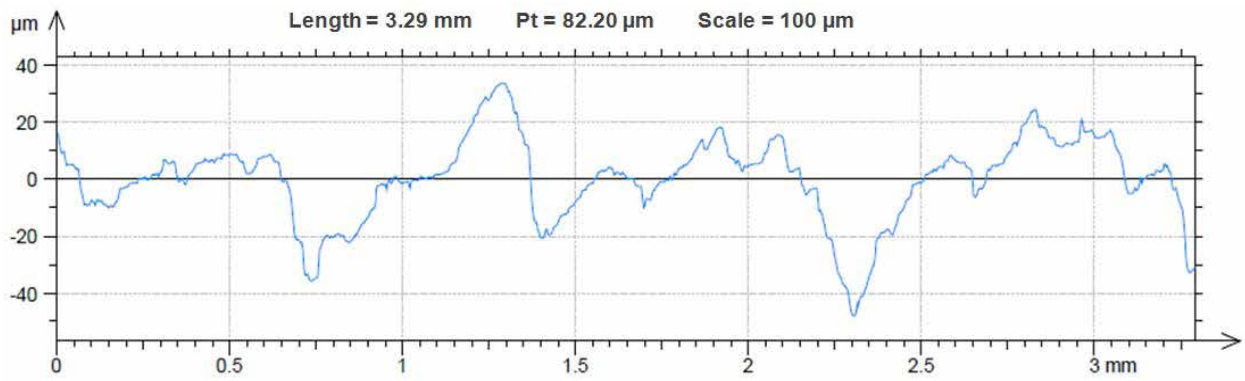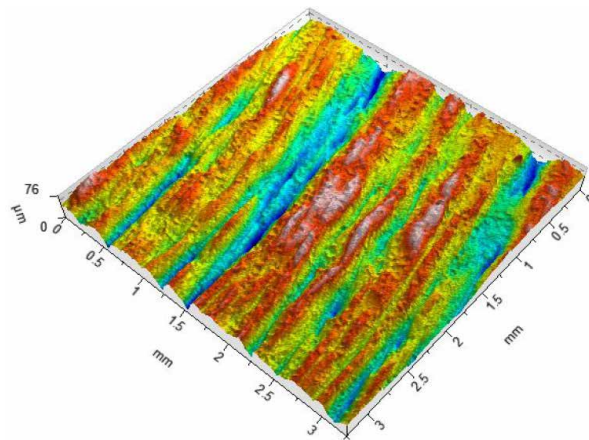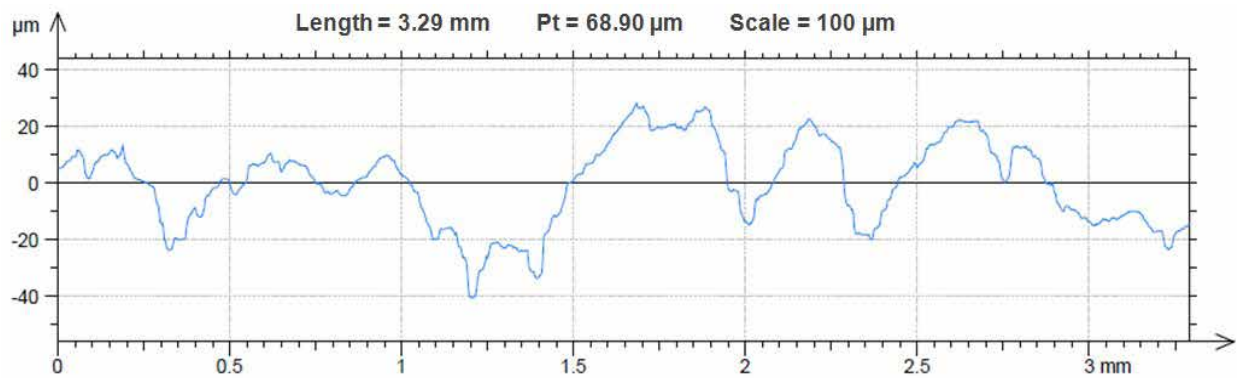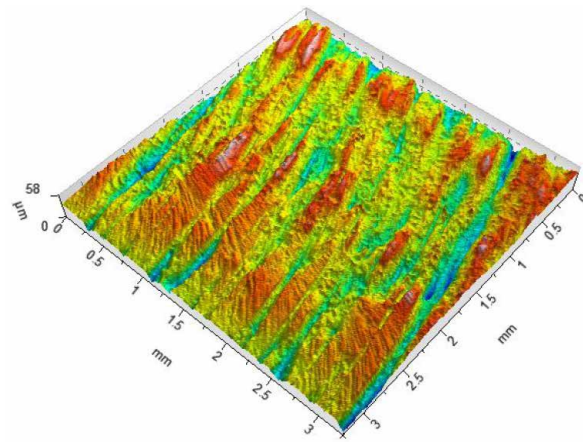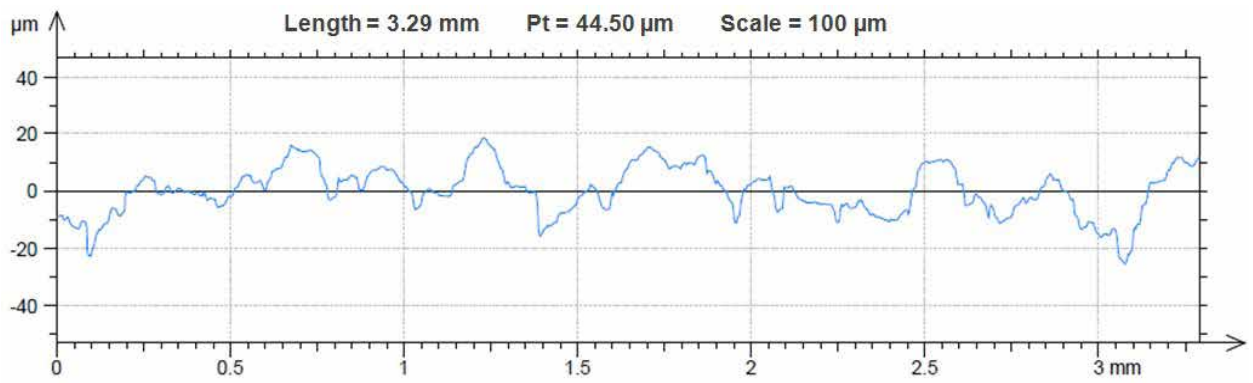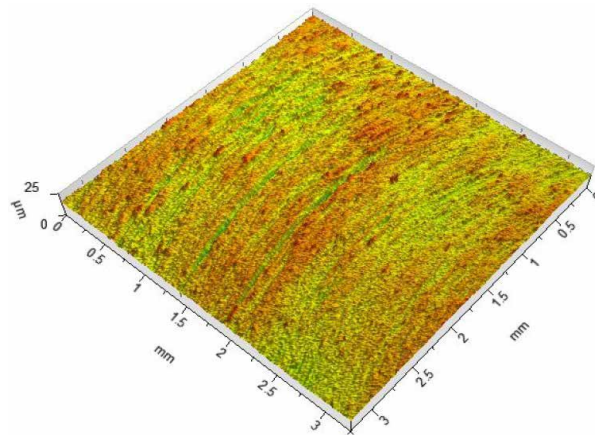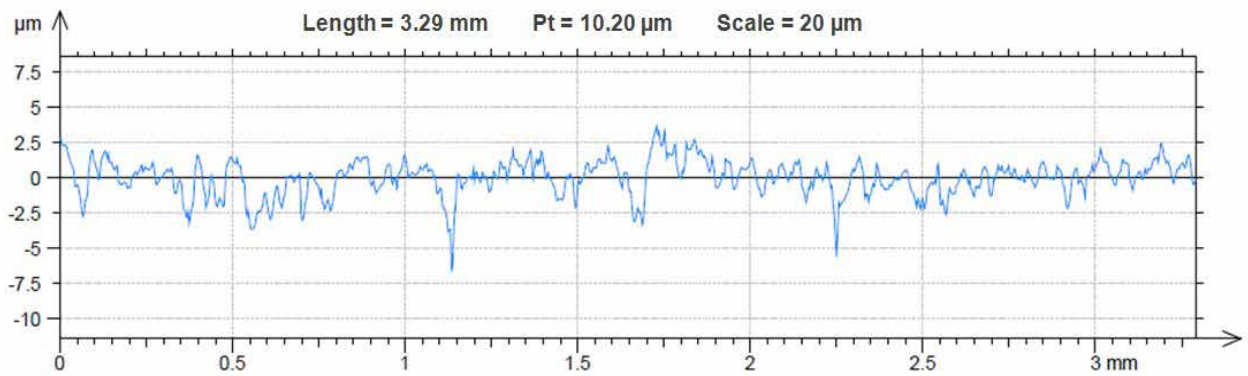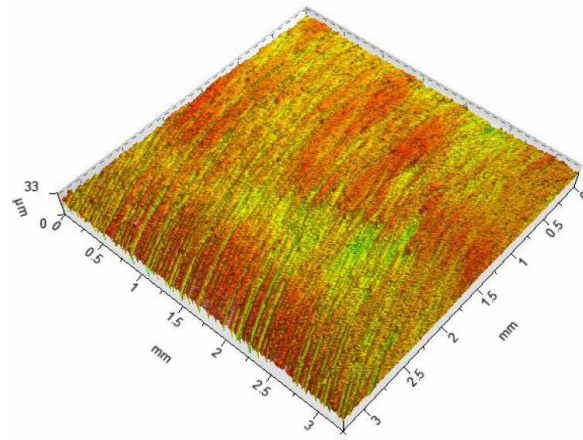
a)

b)

Fig. 5. Three dimensional illustration (a) and surface profilogram (b) of the specimen with brushing, variant 4
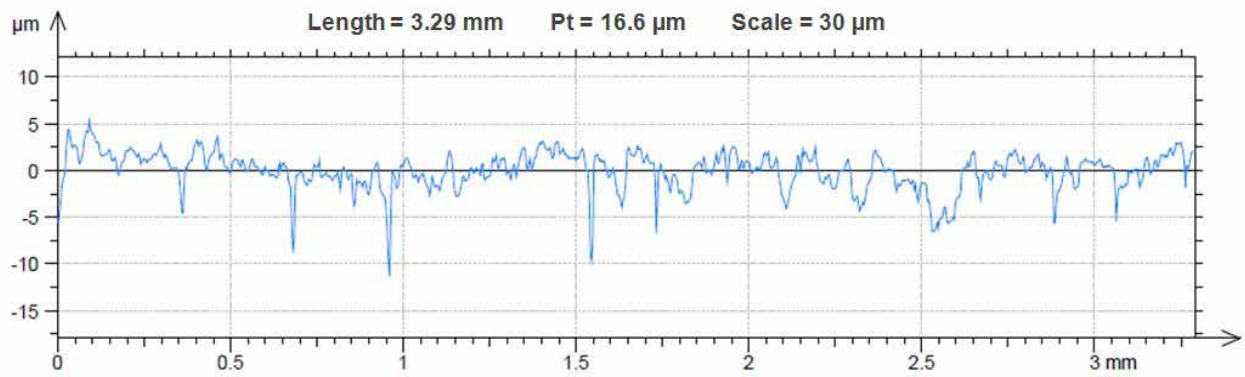
a)

b)

Fig. 6. Three dimensional illustration (a) and surface profilogram (b) of the specimen with brushing, variant 5

a)
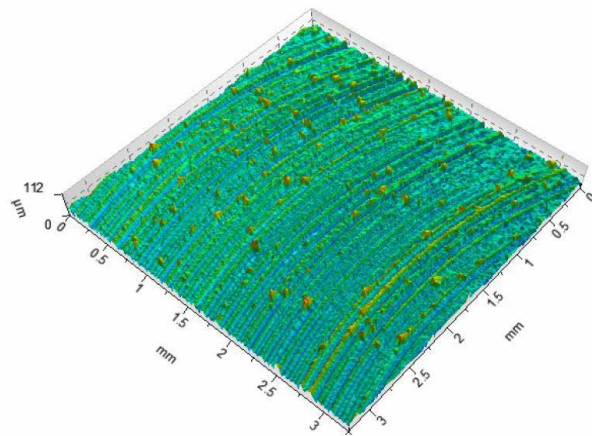
b)
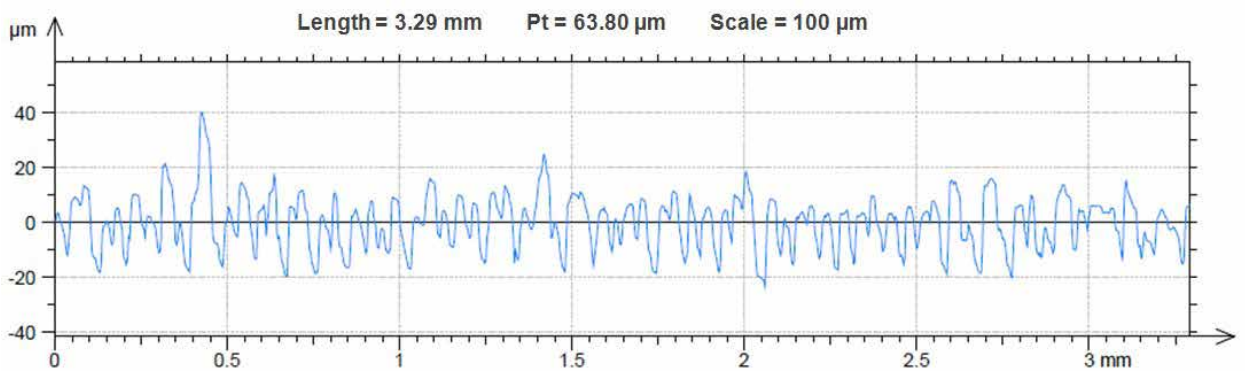
Fig. 7. Three dimensional illustration (a) and surface profilogram (b) of the specimen with welding, variant 6

Variant	Rp, µm	Rv, µm	Rz, µm	Rc, µm	Rt, µm	Ra, µm	Rq, µm
1	18.2	27.4	45.6	30	57.3	7.94	10.4
2	14.4	23	37.4	23.4	40.3	7.41	8.93
3	12.3	11.9	24.2	14.8	31.4	4.68	5.83
4	2.4	5.19	7.59	2.71	9.34	0.906	1.18
5	2.95	8.45	11.4	4.12	13.6	1.26	1.78
6	26.5	20.5	47	23.2	59	8.01	9.84

a)

b)

Fig. 8. The view of welded specimen before (a) and after brushing (b)

The residual stress research showed that brushing with a wire brush introduced compressive residual stresses in both directions. Taking into account the measurement error in the range of +/- 4 MPa, it can be concluded that, in the case of using the wire brush, the direction of stress measurement does not significantly affects the stress value. This type of brush introduces the highest compressive stresses in the direction perpendicular to the welded joint, which are σ_x = -104 MPa and σy = -98 MPa (variant 1), which is almost a 4-fold increase in stresses in the direction perpendicular and 2-fold in the direction parallel compared to the surface after welding (variant 6). Brushing according to variant 3, where two types of brushes were used, also introduced favorable compressive stresses reaching the value of σ_x = -70 MPa and σ_y = -67 MPa. In this case, when taking into account the measurement error, which was +/- 3 MPa, it can be concluded, that the direction of measurement did not significantly affect the stress value. A significant difference can be observed between the values of stresses measured in different directions in the case of brushing with the using of Xebec brush for variants 4 and 5. In the direction parallel, occurred the compressive stresses, reached the values of σ_y = -20 MPa and σ_y = -28 MPa, respectively. In turn, in the direction perpendicular occurred the tensile stresses in the range of σ_x = 10 ÷ 27 MPa. A similar relationship can be also observed after friction stir welding specimen. When analyzing the obtained test results, it can be concluded that brushing with using the wire brush, with the feed rate was f = 70 mm/min is most favorable from the point of view of residual stresses.
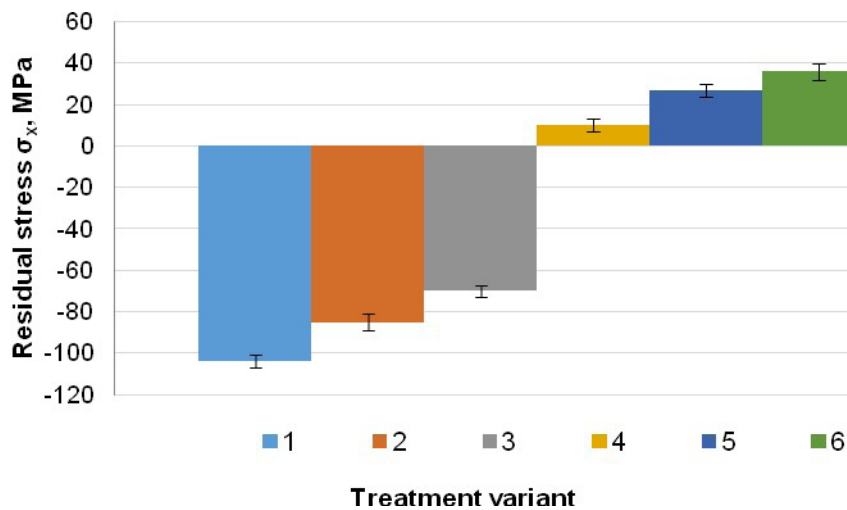
Fig. 9. Effect of treatment variant on the value of residual stresses in the perpendicular direction to the welding direction
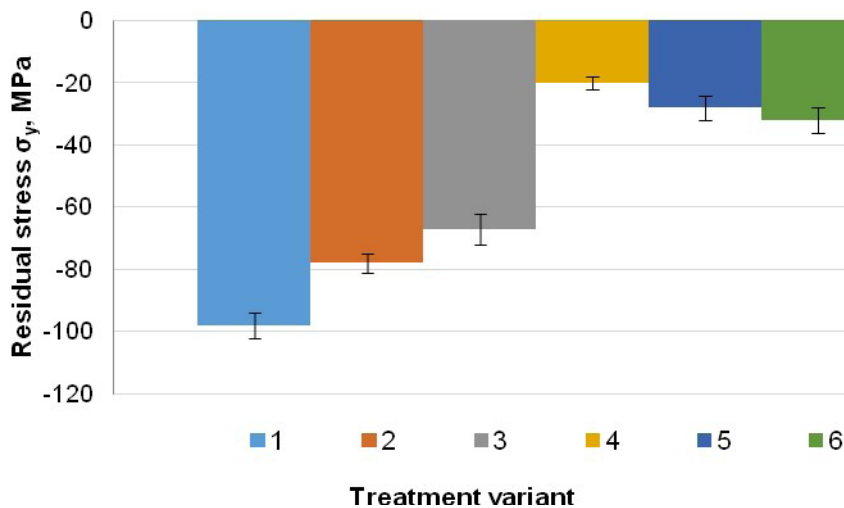
Fig. 10. Effect of treatment variant on the value of residual stresses in the parallel direction to the welding direction

Conclusions

Based on the investigation of the effect of the brushing treatment as a method to improve the condition of surface layer after welding in aluminum 2024-T3, the following conclusions can be made:

- The lowest roughness was obtained for the surface after brushing with the brush by Xebec, where the feed rate value was 100 mm/min (a decrease of 89% compared to the base specimen).
- Brushing with using two types of brushes, in the first step with wire brush and then with ceramic fibres (variant 3), resulted in a decrease in roughness by 42%, from Ra = 8.01 µm for the base specimen to Ra = 4.68 µm. In this case, there were also obtained

the beneficial compressive stresses with the values of $\sigma_x = -70$ MPa and $\sigma_y = -67$ MPa.

- The use of wire brush had a positive effect on the state of stresses in the surface layer of welded joints, for brushing according to variant 1, compressive stresses reached the value of $\sigma_x = -104$ MPa and $\sigma y = -98$ MPa.
- Brush with ceramic fibres can be used to remove micro-inequalities, burrs or flashes resulted during FSW process.
- When taking into account the obtained measurement results of the residual stress, the further stage of the research should include carrying out the fatigue tests of the welded joints after brushing.

References

[1] Bonarski J. 2013. Measurement and use of the texture-stress microstructure characteristics in materials diagnostics. Cracow: Institute of Metallurgy and Materials Science of the Polish Academy of Sciences.

[2] Buffa G., Fratini L., Micari F. 2012. "Mechanical and microstructural properties prediction by artificial neural networks in FSW processes of dual phase titanium alloys". Journal of Manufacturing Processes 14(3): 289-296. https://doi.org/10.1016/j.jmapro.2011.10.007

[3] Cao J. Y.,Wang M., Kong L., Zhao H.X., Chai P. 2017. "Microstructure, texture and mechanical properties during refill friction stir spot welding of 6061-T6 alloy". Materials Characterization 128:54–62. https://doi.org/10.1016/j.matchar.2017.03.023

[4] Khodaverdizadeh H., Mahmoudi A., Heidarzadeh A., Nazari E. 2012. "Effect of friction stir welding (FSW) parameters on strain hardening behavior of pure copper joints". Materials & Design 35: 330-334. https://doi.org/10.1016/j.matdes.2011.09.058

[5] Kluz R., Bucior M., Kubit A. 2019. "Identifying optimal Friction Stir Welding process parameters for 2024 Al alloy butt joint". Advances in Science and Technology-Research Journal 13(4): 48-53. https://doi.org/10.12913/22998624/110740

[6] Kłysz S. 2015. Basics of strength of materials. Warsaw: Technical Institute of Air Forces.

[7] Kubit A., Bucior M., Wydrzyński D., Trzepieciński T., Pytel M. 2018. „Failure mechanisms of refill friction stir spot welded 7075-T6 aluminium alloy single-lap joints". Int J Adv Manuf Technol 94:4479–4491. https://doi.org/10.1007/s00170-017-1176-2

[8] Matuszak J., Zaleski K. 2009. "Effect of technological parameters brushing steel S235JR roughness of the machined surface and the mass of material removed". W Zastosowanie informatyki w inżynierii produkcji, 69-80. Lubelskie Towarzystwo Naukowe. http://bc.pollub.pl/Content/567/PDF/zastosowania.pdf#page=69

[9] Matuszak J., Zaleski K. 2016. Deburring after milling aluminum and magnesium alloys. Lublin: Politechnika Lubelska. http://bc.pollub.pl/Content/12904/PDF/usuwanie.pdf

[10] Prime M., Gnäupel-Herold T., Baumann J., Lederich R., Bowden D., Sebring R. 2006. "Residual stress measurements in a thick, dissimilar aluminum alloy friction stir weld". Acta Materialia 54(15): 4013-4021. https://doi.org/10.1016/j.actamat.2006.04.034

[11] Sałaciński T., Pająk P. 2015. "Ceramic tools for surface finish deburring and polishing operations." Mechanik 10: 762-765. https://www.researchgate.net/publication/282834174_Ceramic_tools_for_surface_finish_deburring_and_polishing_operations

[12] Shen Z., Chen Y., Hou J.S.C., Yang X., Gerlich A.P. 2015. "Influence of processing parameters on microstructure and mechanical performance of refill friction stir spot welded 7075-T6 aluminium alloy". Sci Technol Weld Join 20:48–57. https://doi.org/10.1179/1362171814Y.0000000253

[13] Skrzypek S. 2002. New possibilities of measuring macro stress of materials using X-ray diffraction in the geometry of a constant angle of incidence. Cracow: AGH.

[14] Yang H.G., Yang H.J. 2013. "Experimental investigation on refill friction stir spot welding process of aluminum alloys". Appl Mech Mater 345:243–246. https://doi.org/10.4028/www.scientific.net/AMM.345.243

dr inż. Magdalena Bucior
Politechnika Rzeszowska, Wydział Budowy Maszyn i Lotnictwa, Katedra Technologii Maszyn i Inżynierii Produkcji
Al. Powstańców Warszawy 12, 35-959 Rzeszów, Polska
e-mail: magdabucior@prz.edu.pl

dr inż. Rafał Kluz
Politechnika Rzeszowska, Wydział Budowy Maszyn i Lotnictwa, Katedra Technologii Maszyn i Inżynierii Produkcji
Al. Powstańców Warszawy 12, 35-959 Rzeszów, Polska
e-mail: rkluz@prz.edu.pl

dr inż. Andrzej Kubit
Politechnika Rzeszowska, Wydział Budowy Maszyn i Lotnictwa, Katedra Technologii Maszyn i Inżynierii Produkcji
Al. Powstańców Warszawy 12, 35-959 Rzeszów, Polska
e-mail: akubit@prz.edu.pl

mgr inż. Kamil Ochał
Politechnika Rzeszowska, Wydział Budowy Maszyn i Lotnictwa, Katedra Nauki o Materiałach
Al. Powstańców Warszawy 12, 35-959 Rzeszów, Polska
e-mail: kochal@prz.edu.pl

THE ANALYSIS OF THE GEAR'S GEOMETRY MEASUREMENT WITH VARIOUS MEASURING SYSTEMS

Analiza pomiaru geometrii koła zębatego różnymi systemami pomiarowymi

Jarosław TYMCZYSZYN   ORCID 0000-0003-2972-5112

Abstract: The paper presents a comparison between contact and optical measuring systems, which can be implemented to measure the shape and dimensional accuracy. The comparison included the MarSurf XC20 contact system, the iNEXIVE optical microscope and the MCA II measuring arm with the MMDx100 laser head as well as the ATOS II Triple Scane structured light scanner. The measurements were conducted on a part of a gear rim. The assessment of the measuring accuracy in relation to the nominal model was performed in the GOM Inspect software. The parametric model of the gear created in the NX software was adopted as the nominal model. According to the obtained reports, it results that the MarSurf XC20 is the most accurate 2D measuring system whereas the ATOS II Triple Scane is the most accurate 3D measuring system.

Keywords: measuring systems, optical scanners, reverse engineering, gear

Streszczenie: W artykule przedstawiono porównanie pomiarowych systemów; stykowych oraz optycznych, możliwych do wykorzystania przy weryfikacji dokładności wymiarowo-kształtowej. Porównanie obejmowało system stykowy MarSurf XC20, mikroskop optyczny iNEXIVE , ramię pomiarowe MCA II z głowicą laserową MMDx100 oraz skaner światła strukturalnego ATOS II Triple Scane. Pomiary przeprowadzono na fragmencie wieńca koła zębatego. Ocenę dokładności pomiaru w odniesieniu do modelu nominalnego przeprowadzono w programie GOM Inspect. Za model nominalny przyjęto model parametryczny koła zębatego stworzonego w systemie NX. Według otrzymanych raportów wynika, że najbardziej dokładnym systemem pomiarowym 2D jest MarSurf XC20, a systemem pomiarowym 3D ATOS II Triple Scane.

Słowa kluczowe: systemy pomiarowe, skanery optyczne, inżynieria odwrotna, koło zębate

Introduction

Modeling of the elements and machine parts is traditionally carried out with the use of computer aided design systems (CAD), which are presently commonly implemented in the design of industrial products. It all begins with the idea of the designer who then models the part in a virtual environment. The concept is made possible with the use of the techniques, available on the market. Many a time during the design and manufacturing process, there is no full technical, construction or material documentation for a given product. Thanks to the increasing development of coordinate measuring techniques, data processing software [27] as well as modern manufacturing methods, the solution to this problem has become available with the reverse engineering (RE) [12]. The process allows for the reconstruction of a part's geometry in aviation [13], architectural [10] and medical [8] industries. The aim of reverse engineering is to transform the existing model into its digital counterpart, which constitutes the basis of the further work of the designers. The finished digital model can be produced using modern manufacturing techniques [6]. The most common methods include additive [3, 5, 14, 20] and subtractive [20] manufacturing. When creating a gear's model, we may implement one of the two paths (Fig. 1). In the case of the CAD path, the designing of a gear's geometry process is made possible by the tools specially designed for the task. At the design stage, the knowledge of the basic gear's parameters is crucial [25]. In the case of the second path, the gear's geometry is recreated based on the real model measurements.

The selection of the part's recreation path depends on the complexity of the model geometry. CAD modeling of a part from the start is based on the measuring data. The first method is aimed at more experienced and knowledgeable users. The result of the recreation methods is an approximate 3D solid model. Based on the knowledge of how the part works, the part can be designed as a nominal model. At the modeling stage, any signs of wear or technological imperfections that could arise during machining can be removed. A possibility to implement changes in the design of the existing part in order to improve the operation of the device or machine is an important advantage. Based on the 3D model, the documentation can be created as well as the manufacturing of the real part can be programmed. The second method, which is RE, is based on the geometric
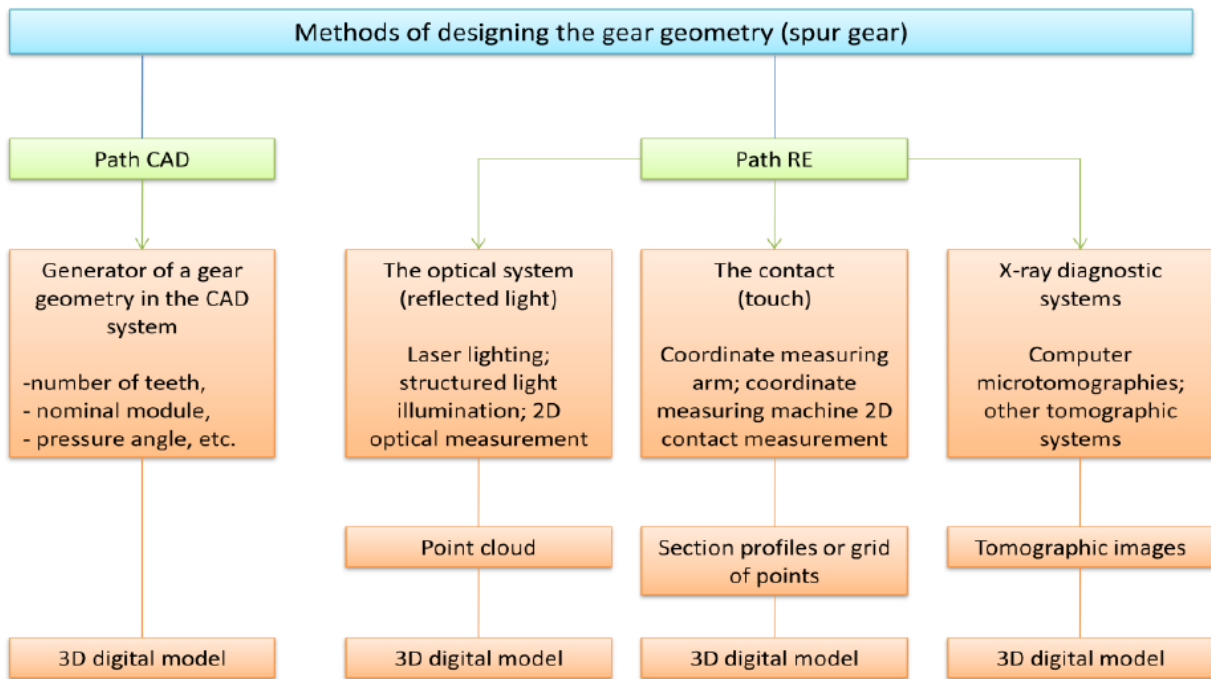
Fig. 1. Gear geometry design methods

outline of the part approximation, and then creating a surface between the generated curves. The advantages of this method include the high model accuracy as well as the short time needed to create the model. Among the disadvantages, one can include the common difficulty of creating the surface based on the measured results. Assuming that the real part has any signs of wear, they are unfortunately reproduced in the digital part. Thus, for parts that show signs of wear, the first method of CAD modeling from the start is used. The repair of worn parts is of great importance in the aviation industry in order to prolong the life cycle of aircraft elements [4, 15, 28, 31].

The increase in the manufacturing accuracy of gear's geometry needs to meet the development of modern industrial solutions. The shape and dimensional verification is conducted mainly with the use of contact coordinate measuring systems [7]. Nowadays, increasing development in optical systems based on the reflected light, as well as tomographic systems are observed. 3D optical scanning systems are commonly used and compared with each other [2, 16, 21]. Contactless techniques are increasingly used due to their advantages. With optical systems, it is possible to conduct measurements without interrupting the manufacturing process and the measuring process is performed during machining at the same station. Measurements on the CMM measuring machine require stopping the machining process [26]. Guerra [18] worked on measuring techniques suitable for the verification and repair of parts. In his work, he compared optical systems. The comparative analysis was performed for four laser scanners: linear scanner LLS, structured light scanner SLS, photogrammetric scanning system with rotational table PSSRT and laser scanning

arm LSA. Both concave and convex surfaces were analyzed. The scanned surface had a high reflection coefficient in order to identify weaknesses in optical systems. Guo [19] performed 3D measurements of the shape of a gear tooth surface with a system based on a light sensor with a linear structure with a rotational table. The gear profile errors in relation to the contact system were analyzed. He found, that the optical system was fast and accurate. Peters et al. analyzed the measurement of gears using a linear light sensor with the 2000 structure [24]. Leopold et al. and Chen et al. designed measuring devices based on the laser triangulation system [9, 22].

There are however no descriptions of the conducted experiments pertaining to a comparative analysis of the gear measuring accuracy with various contact and optical systems in the literature. The following experiments may help with the selection of such an optical measuring system, which would result in the lower measuring errors during verification of a gear geometry model. Each of the optical systems is described by parameters, such as camera resolution, depth of field or errors resulting from external sources, such as ambient light [23, 33] or surface roughness and colours [11] having an impact on the results.

Experimental results

The primary aim of the experimental tests was to compare different measuring systems used in the industry. For this purpose measuring systems with various characteristics were selected: 2D and 3D measurements, contact and optical, manual and automatic measurements.
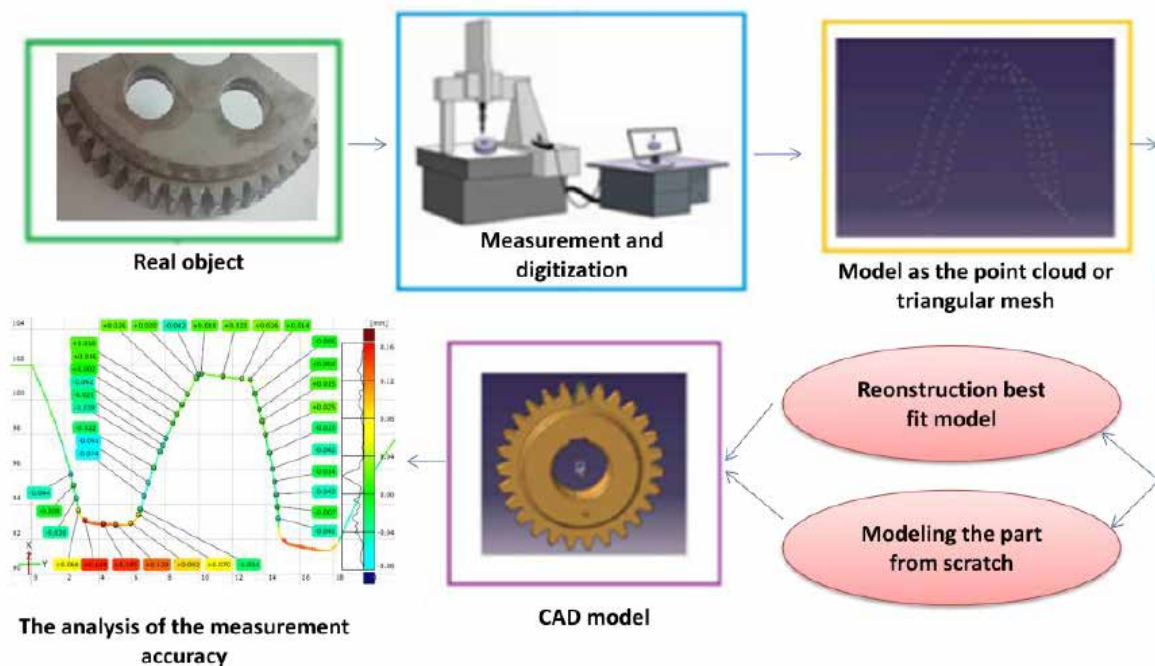
Fig. 2. Experimental tests' plan

The comparison between the systems was conducted based on the measurement of the gear part presented in Figure 2. The basic parameters of the gear are included in Table 1.

The experimental test methodology (Fig. 2) included a series of measurements of the test model using four systems of coordinate metrology and spatial reconstruction. The reconstruction was based on a point cloud in the software dedicated to the measurement system. The numerically created, based on the solid measurement were compared with the reference model in GOM Inspect software with the use of the Best fit method. As a reference, the parametric CAD model of the gear was adopted. The CAD model of the gear was created in NX 12.0 software based on the known mathematical dependencies presented in Table 1.

Table 1. Gear parameters

Lp.	Parameter	
1	Normal module	m = 4
2	Number of teeth	z = 49
3	Pressure angle	α = 20°
4	Helix angle	β = 0°
5	Material	17CrNi6-6,

The measurements were conducted at a constant ambient temperature of 20˚C. For the purpose of comparing the measurement systems, the constant value of the measurement resolution was adopted. The measured surface was covered with a thin, uniform, white layer of anti-reflective coating.

Characteristics of measuring systems

The gear geometry was measured with the use of various measurement systems, such as: the iNEXIVE optical coordinate measuring system by NIKON, the MarSurf XC20 contact system, the MCA II measuring arm with the MMDx100 laser head, the Atos II Triple Scan – structural light – Fig. 3.

The iNEXIVE optical system by NIKON (Fig. 4a) is equipped with a camera recording the outline of the element in the single measuring plane. The measurement with this method consists of determining the point cloud based on the vectors perpendicular to the measuring object's outline.

The MarSurf XC20 conturograph is a machine that allows for registering points as the measuring contact tip moves along the surface of the part. The conturograph determines single cross-sections in a given plane. The measuring tip moves at a constant speed and the displacements of the element are converted into an electrical signal. MarSurf XC20 is a technologically advanced device for the analysis of curvilinear contours. The result of the measurement is a point cloud in the x-y system – Fig. 4b.

The measuring arms MCA II (Fig. 4c) are portable devices, thanks to the appropriate design and
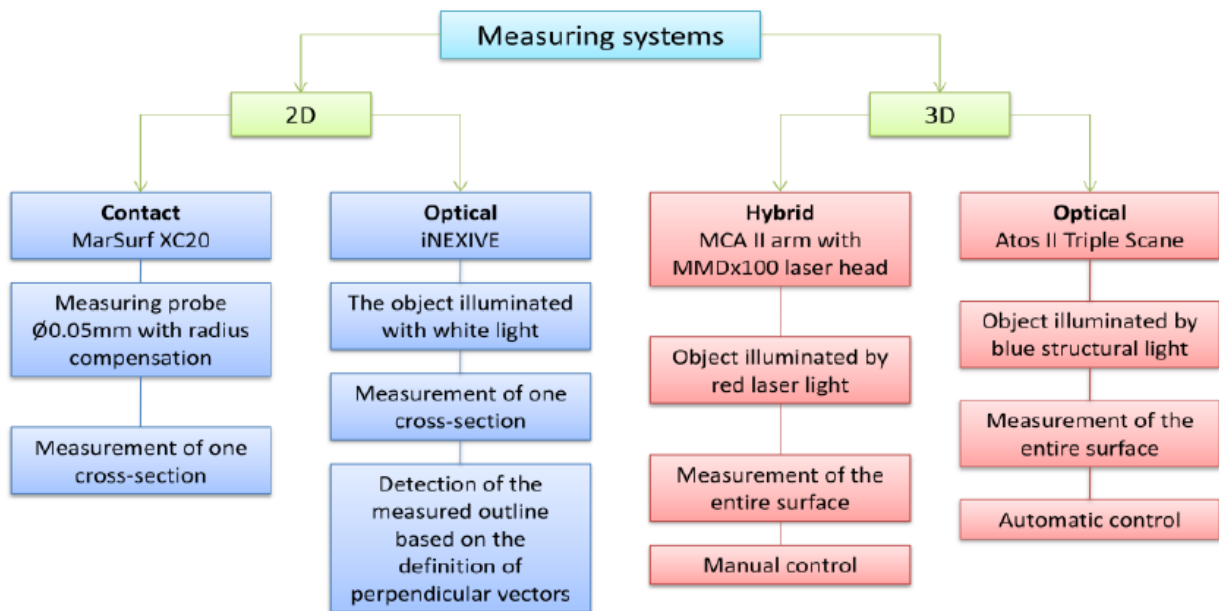
Fig. 3. Features of the compared measurement systems
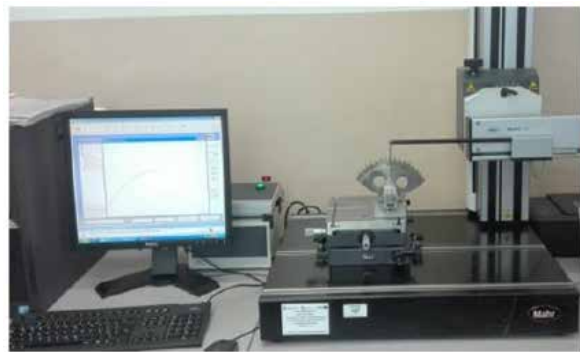
Fig. 4. The measuring stations: a) NIKON iNEXIVE optical coordinate system, b) MarSurf XC20 contact system, c) MCA II measuring arm with the MMDx100 laser head, d) Atos II Triple Scan –structured light

measurement procedure allow for work in the immediate vicinity of the element. They are used in automotive and aviation industries, and even in workshops that repair parts [27]. Systems such as measuring arm can be equipped with laser triangulation head, which enables to measure elements that are not possible to be measured with the contact methods, i.e. soft materials. The measuring arm belongs to the hybrid systems family of products. By hybrid products, one assumes measurement using the contact method as well as the optical one. For contact

measurement, a head ending with a steel or sapphire ball is used, whereas in the case of optical measurement, i.e. laser heads are adopted [29]. The MMDx100 system obtains the data from the measured geometry as a result of illuminating the object with red laser light. Laser triangulation is considered to be one of the best techniques of 3D object measurement. The technique is based on the knowledge of the geometrical dependencies between the laser beam and the coordinates of the image recorded in the detector [30]. The width of the laser beams is 100 mm, the measurement error is 10 μm and the number of scanned points on one line is 1000 at a scanning frequency of 33-150 Hz. The permissible errors of the MCA II measuring arm equipped with the laser head MDD × 100 system estimated at the confidence level of 95% are ±0,03 mm [17]. The result of the measurement is a spatial cloud of points.

The ATOS II Triple Scan Blue Light system by GOM (Fig. 4d) enables to measure the model geometry by illuminating it with a blue light and analyzing the deflection of the light lines in a series of fringe images projected on the object. The deflection of the fringes is recorded by cameras and then processed by algorithms into measuring data in the form of a set of x, y, z coordinate points that represent the measured surface. The adoption of the blue light allows for measurement regardless of the intensity of daylight or artificial (white) light. This enables to include the measurement system into a production cycle without the necessity of creating special measuring conditions. The application of blue light in the scanning process also allows for a significant reduction in the

measurement time, i.e. thanks to reducing the influence of the environment on the scanning process [11, 23, 33].

Regardless of the measurement system, the data analysis process was the same. It consisted of collecting the data in the form of point cloud coordinates. Further processing consisted of removing the areas that significantly differed from most of the results, filtering by removing noise and reducing artifacts. When data optimization was completed, the coordinate system was determined. The point cloud was triangulated and as a result, the surface mesh model was obtained.

The accuracy of the measurement systems has been tested according to dedicated standards, i.e. coordinate measuring arm is tested in relation to the ASME B89.4.22 standard [1], whereas the Atos II Triple Scan is tested according to the VDI/VDE 2634 standard [32].

Test results and discussion

The obtained measurement results allow a comparison between the measurement systems on the basis of a gear measurement to be presented. The analysis of the accuracy of geometrical dimensions of the gear was conducted with the use of the GOM Inspect V7.5 software [17]. The results of the measurement are presented in a detailed deviations map in selected profiles of the gear rim cross-sections in the plane normal to its axis. The analyzes were conducted by comparing the nominal gear CAD model with the selected point clouds obtained as a result of measurements with selected measurement systems (Fig. 5, 6).
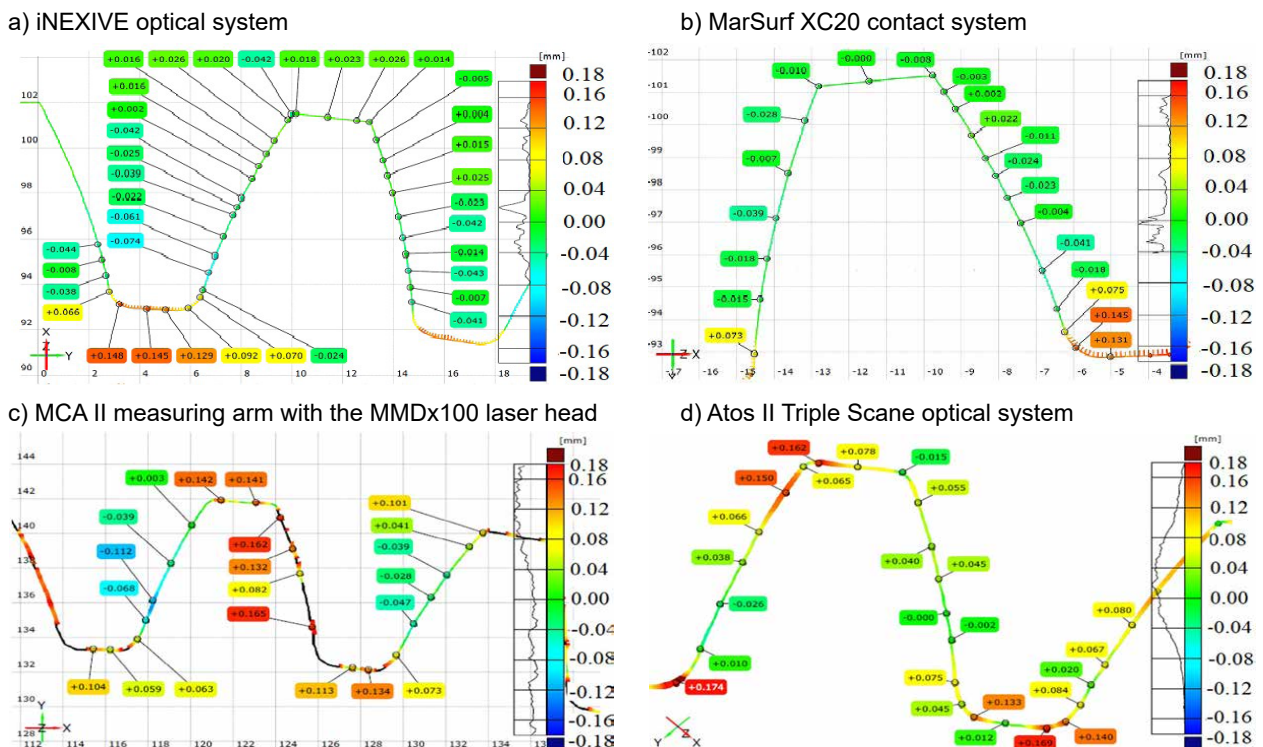

Fig. 5. The comparative analysis of measuring systems: a) iNEXIVE optical microscope, b) conturograph MarSurf XC20, c) MCA II measuring arm with the MMDx100 laser head, d) Atos II Triple Scan

Measuring Systems	Maximum/Minimum deviations		Average deviation	Standard deviation
iNEXIVE	+0,148 mm	-0,074 mm	0,026 mm	0,0698 mm
MarSurf XC20	+0,145 mm	-0,041 mm	-0,012mm	0,0472 mm
MCA II MMDx100	+0,178 mm	-0,121 mm	-0,061mm	0,1113 mm
Atos II Triple Scane	+0,174 mm	-0,084 mm	-0,054 mm	0,0915 mm

Table 2. Measured deviations of the gear

Based on the deviation maps, negative values of deviation were observed on the side of gear teeth, which can indicate wear of the tested part. Positive values of deviations were observed at the root of the tooth, which can result from the CAD model of the reference element – Fig. 5, Table 2.

The presented analysis of the gear geometry accuracy obtained by comparing the model acquired from the measurement with the NIKON iNEXIVE optical system with the reference model proved, that the deviations are in the range of +0.148 mm to -0,074 mm and the standard deviation is equal to 0.0698 mm – Fig. 5a.

The shape errors resulting from the comparison of the model obtained from the measurement with the MarSurf XC20 contact system with the reference model are in the range of +0,145 mm to -0,041 mm, whereas the standard deviation is equal to 0,0472 mm – Fig. 5b.

The map containing the shape errors obtained from the comparison between the model acquired from the MCA II optical system with the MMDx100 laser head with the reference model shows that the errors are in the range of +0,178 mm to -0,121 mm, with the standard deviation of 0,1113 mm. Based on the analysis, it was observed that in the case of the measurement with the measuring arm – laser head system, the system is not suitable for the measurement of the elements such as gears, because it does not register continuous surfaces, which leads to an incomplete model of the analyzed geometry (Fig. 5c). The incomplete point cloud proved fit to the reference model with the best fit method difficult.

The comparison between the model obtained with the Atos II Triple Scane system and the reference model is presented using the deviation map – Fig. 5d. Shape errors are in the range of +0,174 mm to -0,084 mm, whereas the standard deviation is equal to0,0915 mm.

The analysis of the deviation values obtained with various measurement systems (Fig. 6) proved that the lowest deviations were registered with the MarSurf XC20, which indicates that the contact system the most accurately reproduced the measured surface profile. The highest deviation values were obtained during the measurement with the MCA II MMDx100 system, which results from the point cloud with discontinuities and overscans. Among the three optical systems, one may distinguish the iNEXIVE optical microscope as well as the Atos II Triple Scane. The iNEXIVE measures only in one measuring plane using the white light, and the Atos II Triple Scane constitutes the blue light system that measures 3D surfaces
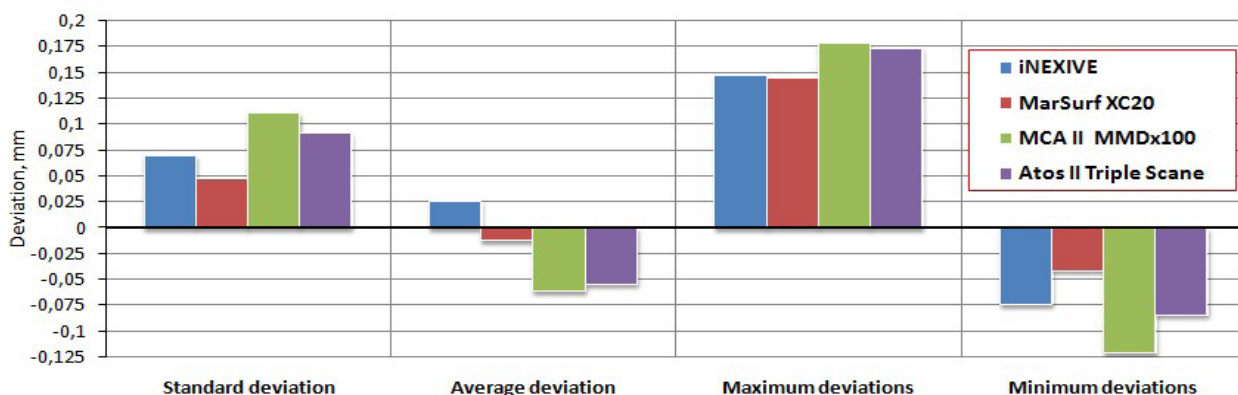

Fig. 6. The comparison between the deviations obtained from the gear measurement with various systems

Conclusions

Based on the conducted in four measurement systems experimental tests, different characteristics of the mapping deviations distribution were observed. The measurement with the MarSurf XC20 contact system proved to be the most accurate. The standard deviation and the mean deviation are the lowest. The NIKON iNEXIVE optical microscope and the MarSurf XC20 with a contact measuring probe are 2D measuring systems, which do not require the application of an anti-reflective layer. The measurement with the NIKON iNEXIVE allows for the measurement of the complete shape by changing the position of the measuring head as well as is equipped with a continuous image sharpness adjustment by changing the object illumination. In the case of the MarSurf XC20 system with a contact tip, the measurement is difficult due to the limited range of movement of the measuring probe as well as the shape of the measuring tip. In the case of the optical systems: the MCA II arm with the MMDx100 laser head and the Atos II Triple Scane, a lack of surface continuity was observed, leading to an incomplete model of the analyzed geometry, which results from the re-selectivity of the measured surface and from the difficulty for a light beam to reach all the surfaces. In the case of measurements with the MCA II arm with the MMDx100 laser head, the recorded point cloud was tainted with noise and artifacts. The measurement with the Atos II Triple Scane system using structured light is suitable for the measurement of the complex surface, because in the case of the gear measurement the resulting point cloud was uniform and continuous. The histograms for individual measurement systems have different forms. For the MarSurf XC20 contact system, the histogram is bimodal, and for the Atos II Triple Scane the histogram is in the symmetrical form.

Among the analyzed measurement systems, the most preferred optical system for 2D solids shape measurement is the NIKON iNEXIVE microscope, whereas for 3D shapes the Atos II Triple Scane system using structured light.

References

[1] ASME B89.4.22-204 Methods for Performance Evaluation of Articulated Arm Coordinate Measuring Machines.

[2] Barbero B.R., Ureta E.S. 2011. „Comparative study of different digitization techniques and their accuracy". CAD Computer Aided Design 43(2): 188–206.

[3] Brajlih T., Tasic T., Drstvensek I. et al. 2011. „Possibilities of using three-dimensional optical scanning in complex geometrical inspection". Strojniski Vestnik/Journal of Mechanical Engineering 57(11): 826–33.

[4] Brown Gordon M., Song M. 2000. „Overview of three-dimensional shape measurement using optical methods". Optical Engineering 39(1): 10.

[5] Budzik G, Przeszłowski Ł., Wieczorkowski M. et al. 2018. „Analysis of 3D printing parameters of gears for hybrid manufacturing". In: Proceedings of the 21st international ESAFORM conference on material forming, AIP Conf. Proc. 1960.

[6] Budzik G. 2011. „Metody szybkiego prototypowania". Metale & Nowe technologie 1–2: 78 – 80.

[7] Budzik G., Pisula J., Dziubek T., Sobolewski B., Zabornia M. 2011. „Zastosowanie systemów CAD / RP / CMM w procesie projektowania kół zębatych walcowych o zębach prostych". Mechanik 21: 988.

[8] Budzik G., Turek P. 2018. „Improved accuracy of mandible geometry reconstruction at the stage of data processing and modeling". Australasian Physical and Engineering Sciences in Medicine 41(3): 687–95. http://dx.doi.org/10.1007/s13246-018-0664-5.

[9] Chen Y., Chen J. 2019. „Optical inspection system for gear tooth surfaces using a projection moiré method". Sensors 19(6).

[10] Cheng X.J., Jin W. 2006. „Study on reverse engineering of historical architecture based on 3D laser scanner". Journal of Physics: Conference Series 48(1): 843–49.

[11] Dury M.R., Woodward S.D., Brown S.B., McCarthy M.B. 2016. „Surface Finish and 3D optical scanner measurement performance for precision engineering". Proceedings - ASPE 2016 Annual Meeting (November): 167–72.

[12] Dziubek T. 2012. „Analiza współrzędnościowych systemów pomiarowych kół zębatych". Politechnika Rzeszowska.

[13] Dziubek T. 2018. „Application of coordination measuring methods for assessing the performance properties of polymer gears". Polimery/Polymers 63(1): 49–52.

[14] Dziubek T., Oleksy M. 2017. „Application of ATOS II optical system in the techniques of rapid prototyping of epoxy resin-based gear models". Polimery/Polymers 62(1): 44–52.

[15] Gao J., Chen X., Yilmaz O., Gindy N. 2008. „An integrated adaptive repair solution for complex aerospace components through geometry reconstruction". International Journal of Advanced Manufacturing Technology 36(11–12): 1170–79.

[16] Geng Z., Bidanda B. 2017. „Review of reverse engineering systems–current state of the art". Virtual and Physical Prototyping 12(2): 161–72.

[17] GOM INSPECT. 2018. „Evaluation Software for 3D Measurement Data". www.gom.com/3d-software/gom-inspect.html.

[18] Guerra M.G., Lavecchia F., Maggipinto G. 2019. „Measuring techniques suitable for verification and repairing of industrial components: A comparison among optical systems". CIRP Journal of Manufacturing Science and Technology 27: 114–23.

[19] Guo X., Shi Z., Yu B., Zhao B., Li K. 2020. „3D measurement of gears based on a line structured light sensor". Precision Engineering 61: 160–69.

[20] Habrat W., Zak M., Krolczyk J., Turek P. 2018. „Comparison of geometrical accuracy of a component

manufactured using additive and conventional methods". Lecture Notes in Mechanical Engineering (201519): 765–76

[21] Intwala A.M., Magikar A. 2016. „A review on process of 3D Model Reconstruction". International Conference on Electrical, Electronics, and Optimization Techniques, ICEEOT 2016: 2851–55.

[22] Leopold J., Günther H. 2002. „Fast 3D-Measurement of Gear Wheels". Seventh International Symposium on Laser Metrology Applied to Science, Industry, and Everyday Life, Vol. 4900: 185–94.

[23] Li F., Stoddart D., Zwierzak I. 2017. „A Performance Test for a Fringe Projection Scanner in Various Ambient Light Conditions". Procedia CIRP 62: 400–404.

[24] Peters J., Goch G., Günther A. 2000. „Helical gear measurement using structured light". Proceedings of the XVI IMEKO World Congress: 2–5.

[25] PN-ISO 1328-1 Przekładnie zębate walcowe. Dokładność wykonania według ISO. Odchyłki jednoimiennych boków zębów.

[26] Quinsat Y., Dubreuil L., Iartigue C. 2017. „A novel approach for in-situ detection of machining defects". International Journal of Advanced Manufacturing Technology 90(5–8): 1625–38.

[27] Ratajczyk E. 2005. „Współrzędnościowa technika pomiarowa." Oficyna Wydawnicza Politechniki Warszawskiej.

[28] Ratajczyk E. 2012. „Współrzędnościowe ramiona pomiarowe w zastosowaniach przemysłowych". Pomiary, Automatyka, Robotyka 3: 33–39.

[29] Ratajczyk E., Adamczyk A. 2015. „Porównanie dokładności wybranych skanerów laserowych". Mechanik 12: 945–948.

[30] Ratajczyk E., Woźniak A. 2016. „Współrzędnościowe systemy pomiarowe". Oficyna Wydawnicza Politechniki Warszawskiej.

[31] Sitnik R., Karaszewski M. 2008. „Optimized point cloud triangulation for 3D scanning systems". Machine Graphics and Vision 17(4): 349–71.

[32] VDI/VDE 2634 - Optische 3-D-Messsysteme, Bildgebende Systeme mit flächenhafter Antastung.

[33] Voisin S. 2007. „Study of ambient light influence for three-dimensional scanners based on structured light". Optical Engineering 46(3): 030502.

mgr inż. Jarosław Tymczyszyn
Rzeszów University of Technology, The Faculty of Mechanical Engineering and Aeronautics
al. Powstańców Warszawy 8, 35-959 Rzeszów, Poland
e-mail: j.tymczyszyn@prz.edu.pl

EFFECT OF A TYPE OF EPOXY ADHESIVE ON THE SELECTED MECHANICAL PROPERTIES OF ADHESIVE JOINTS OF THE STEEL SHEETS

Wpływ rodzaju kleju epoksydowego na wybrane właściwości mechaniczne połączeń klejowych blach stalowych

Anna RUDAWSKA   ORCID 0000-0003-3592-8047

A b s t r a c t: The paper presents the issues related to determination of the strength of the adhesive joints of C45 steel sheets which were made using six types of epoxy adhesives. Epidian 5, Epidian 53 and Epidian 57 epoxy resins and two types of curing agents: polyamide (PAC) and amine (Z-1) were used to prepare the epoxy adhesives compounds. The adhesive joints were subjected to strength tests in accordance with DIN EN 1465. When comparing the results of the shear strength tests of single-lap adhesive joints of C45 steel sheet prepared with the use of the analyzed adhesives, it was noticed that better results were obtained with the use of the adhesive compounds containing the PAC curing agent.

K e y w o r d s: adhesive compounds, epoxy resin, curing agent , adhesive joint, strength

S t r e s z c z e n i e: W artykule przedstawiono zagadnienia związane z określeniem wytrzymałości połączeń klejowych blachy ze stali C45 wykonanych za pomocą 6 wariantów kompozycji epoksydowych. Do wykonania klejów zastosowano trzy rodzaje żywic epoksydowych: Epidina 5, Epidian 53 oraz Epidian 57 oraz dwa rodzaje utwardzaczy poliamidowy (PAC) oraz aminowy (Z-1). Połączenia klejowe poddano badaniom wytrzymałościowym zgodnie z normą DIN EN 1465. Porównując wyniki badań wytrzymałości na ścinanie jednozakładkowych połączeń klejowych blachy ze stali C45 przygotowanych za pomocą analizowanych klejów zauważono, że lepsze efekty uzyskano przy wykorzystaniu kompozycji klejowej zawierającej utwardzacz PAC.

S ł o w a   k l u c z o w e: kompozycja klejowa, żywica epoksydowa, utwardzacz, połączenie klejowe, wytrzymałość

Introduction

Adhesion is one of the more frequently employed methods in the contemporary industry for permanent joining of the elements in various constructions [1, 6, 8]. The adhesive joints may be found in most of the products with a different application, or in the machines and many constructions. If an adhesive is not used directly in the manufacturing stage or during assembling, it is employed during transport, storage or packing of the products. The frequent application of adhesive joints is affected by their advantages and characteristic properties of adhesives, including, *inter alia*, a relative easiness of performing the joints, including also dissimilar ones, and, at the same time, high resistance [2, 4 ,6]. Many different materials may be glued with different thickness may be joined using the adhesives. The discussed method of linking the elements does not cause corrosion and infringement of the structure continuity at the site of joining. Adhesion has also its defects, *inter alia* a difficult disassembling, harmfulness of chemical substances and sometimes, long time of binding of adhesive joint. The mentioned defects do not, however, disqualify the discussed method of joining in the industry; on the contrary, there is a universal application nowadays of the adhesive joints in different branches of the industry.

A high diversity of the ready-to-use adhesives, including also constructional ones and their components affects a quite wide choice of a defined type of adhesive for the specified applications. The available epoxy resins and their curing agents allow preparing the different adhesive compositions, depending on the required properties of the adhesives [3, 5, 9, 11, 13].

In the present paper, the attempt to determine the effect of a type of epoxy adhesives, containing various epoxy resins and various curing agents on the selected mechanical properties if adhesive joints of steel sheets was undertaken. The single – lap adhesive joints were subjected to shear strength tests and based upon the obtained results, the shear strength and elongation were determined.

Methodology

• The joined material

For performance of adhesive joints, the samples of the sheet of carbon, non-alloy steel C45 was used. It is the non-alloy steel of quality 1,0503 for heat improvement, according to PN-EN 10083-2 and its chemical composition is found in Tab. 1.

Type of steel	Chemical composition [%]								
	C	Si	Mn	Cr	Ni	Mo	Cu	S	P
C45 (1.0503)	0,42-0,50	0,1-0,4	0,5-0,8	Max 0,3	Max 0,3	Max 0,1	Max 0,3	Max 0,04	Max 0,04

The samples used in the tests had a shape of rectangular prism with dimensions 100 x 25 x 2 mm.

• Epoxy adhesives

During the tests, 6 two-component epoxy adhesives, consisting of epoxy resin and curing agents were used; their composition and determination is found in Tab.2.

Three epoxy resins, including non-modified epoxy resin Epidian 5 and two modified epoxy resins: Epidian 53 and Epidian 57 as well as two types of curing agent: polyamide (PAC) and amine (Z-1) were used. The mentioned products are manufactured by CIECH Sarzyna in Nowa Sarzyna (Poland).

The proportions of the mixture: resin and curing agent resulted from the stechiometric ratio, depending on the type of resin and curing agents [7].

Table 1. Chemical composition of C45 steel according to EN 10083-2 [14]

Type of resin	Type of curing agents	Weight ratio resin/ curing agents	Name of adhesive
Epidian 5	PAC	100:80	Epidian 5/PAC/100:80
Epidian 53			Epidian 53/PAC/100:80
Epidian 57			Epidian 57/PAC/100:80
Epidian 5	Z-1	100:10	Epidian 5/Z-1/100:10
Epidian 53			Epidian 53/Z-1/100:10
Epidian 57			Epidian 57/Z-1/100:10

• Shape and dimensions of adhesive joints

For strength tests, the single-lap adhesive joints with the dimensions shown in Fig.1 and Tab. 3 were prepared.

Fig. 1. The single-lap bonded joint
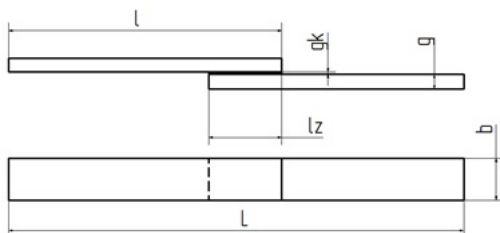
Table 3. The adhesive joints dimensions

Determination of dimension	l [mm]	b [mm]	g [mm]	L [mm]	lz [mm]	gk [mm]
Dimension	100	25	2	182	18	0,1

The length of the lap of adhesive joint was calculated from the formula for the limit length of lap joint, as presented in the work [6] and its value equal to 18 mm was adopted.

• The method of preparing the adhesive joints

The process for preparation of the surface of the steel sheet samples before adhesion covered 3 stages. The first stage consisted in a single degreasing of the surface of steel sheets with the use of acetone, by the rubbing method. After 2 minutes, the second stage of the surface preparation in a form of mechanical treatment was implemented. It was a manual abrasive dry treatment, using abrasive paper, made from corundum with granulation 320; during the mentioned treatment, 30 circulatory movements were carried out with the aim to obtain non-oriented structure. Then, the third stage of the surface preparation included the repeated degreasing, using acetone. The degreasing was performed three times, and after the last application of the degreasing agent the surfaces of the samples were left for 3 minutes to dry. The prepared samples were subjected to bonding, after the previous preparation of adhesive compositions.

For bonding of the samples, made from the steel sheets, the adhesive compositions consisting of epoxy resin and curing agent were used. The types of the employed components of the adhesives and their proportions, according to which the adhesives were prepared, are given in Tab. 2. The components of the particular adhesive compositions were measured on a balance of type TP-2/1 (FAWAG S.A., Lublin). The particular components were measured in a polymer container and then, mixed using a disc agitator at the stand for mixing of adhesives. The time of agitation was equal to 2 minutes and the time of removal of gas bubbles was also 2 minutes and the mentioned stage was implemented using a vacuum pump.

The particular adhesive compositions were evenly placed on the surface of one of the bonded samples using a special polymer spatula on the length of the anticipated lap of the adhesive joint. Then, the samples, creating the lap joint were fixed and the appropriate pressure was exerted on the bonded samples using weight of 1,5 kg. The mentioned operations were carried out in a special device where 6 samples were simultaneously tested. Then, the process of single-stage hardening on cold was carried out during 7 days. The process of adhesive preparation and surface preparation and other operations connected with the performance of adhesive joint as well as the hardening process were implemented at the ambient temperature of 22±2°C and the air humidity of 23±1%.

After the hardening process, the weight load was removed and 6 groups of adhesive joints, differing in the type of the employed adhesive composition, were created. In each group, 6 adhesive joints were performed.

• Types of the tests

During the experiment, the tests connected with the determination of the basic parameters of roughness of the surfaces of the bonded sheets and the strength tests of the adhesive joints of the steel sheets were carried out.

The measurements of the roughness parameters of the surface of the samples subjected to binding were conducted in HOMMEL – ETAMIC TURBO WAVE V.7.55 according to ISO Standard 25178.

The performed adhesive joints were subjected to strength tests according to standard DIN EN 1465 at the speed of the test equal to 5 mm/min in the strength machine. During the performance of the tests, the samples were fixed in the screw-wedge holders and were subjected to the shear strength test until the moment of destruction of the joint.

The results of the tests

• Characteristics of the surface of the bonded sheets

Tab. 4 presents the selected roughness parameters of the surfaces of the bonded sheets after the employed method of the preparation of their surface, as being described in the subsection "The method of preparing the adhesive joints", together with their mean value. The tests covered 3 samples; each of them was subjected to 8 measurements of the selected parameters. Fig. 2 illustrates the example of a profile of roughness of the sample surface after the process of the preparation of the surface.

Table 4. Surface roughness parameters of adherends

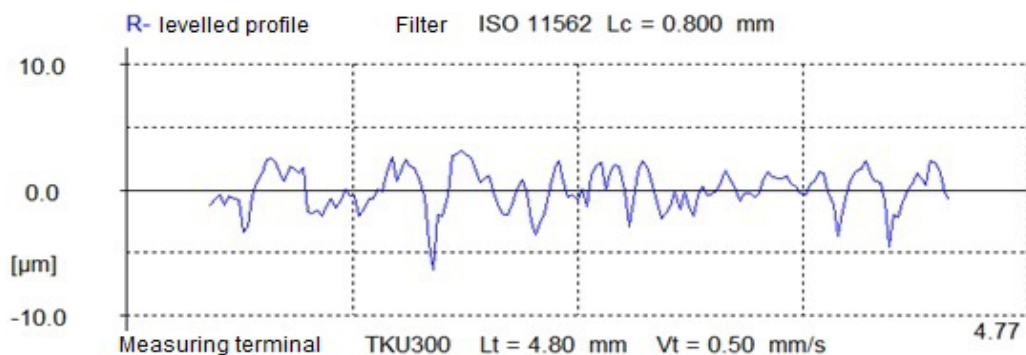| Parameter	Surface roughness parameters, mm								
	Rt	Ra	Rq	Rsk	Rz	Rp	Rmax	RSm	Rku
Value (mean)	6,87	1,11	1,34	-0,29	5,16	2,23	6,77	0,22	2,48

Fig. 2. An exemplary surface roughness profile for a sample prepared for bonding

The exemplary surface roughness profile of the sample after the employed method of preparing the surface allows a partial visualization of the state of roughness of the sample surface which was then subjected to the bonding process. Certain differences of the surface roughness profile in particular sites of the sample surface were observed what is characteristic of the manual treatment.

• **The results of the strength tests**

The presentation of the shear strength tests of the adhesive joints of steel sheets, being performed when using different adhesive combinations is given in Fig.3. in the tests, 6 variants of adhesive joints were used.

From the above presentation of the results it is followed that the adhesive joints performed with the epoxy adhesive compound, containing curing agents PAC, are characterized by considerably higher strength as compared to the joints made with the use of compounds, containing curing agent Z-1. The shear strength of the adhesive joints where curing agent PAC was employed, reaches the maximum value of 14.93 MPa whereas in the case of the adhesive joints made with the compound, containing curing agent Z-1, the maximum value of shear strength is equal to 4.60 MPa. It means that the adhesive joints performed with the application of curing agents PAC reveal 3-times higher shear strength in comparison with the adhesive joints made with the compound, containing curing agent Z-1, irrespectively of the epoxy resin. We may therefore, observe and confirm the results of the earlier studies [10, 11, 12] showing that the type of the hardener in the adhesive joints plays a significant role although the type of the employed epoxy resin is also important.

When comparing the results of the shear strength of the adhesive joints of the steel sheet, performed with the use of adhesive compounds containing polyamide hardener, we may state as follows:
• The highest shear strength was obtained in the case of the adhesive joints, made with the use of Epidian 53/PAC/100:80 (14.93 MPa) whereas the lowest value, equal to 10.33 MPa was obtained in the case of the adhesive joints performed with the use of epoxy resin Epidian 57 and curing agents PAC;
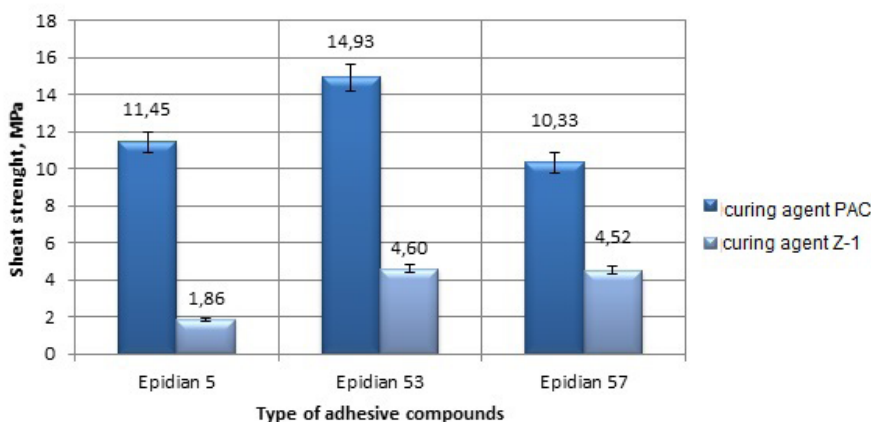

Fig. 3. Shear strength of adhesive joints of steel sheets, made with various epoxy adhesive compounds

- Value of the strength of the adhesive joints, made with the application of the compound consisting of epoxy resin Epidian 57 and curing agent PAC constitutes 90.2% of the value of strength of the adhesive joints performed with the combination of Epidian 5/PAC/100:80 and 69.2% of the value of the adhesive joints made with the use of adhesive compound Epidian 53/PAC/100:80.

When analyzing the results shown in Fig. 3 in relation to the shear resistance of the adhesive joints of the steel sheets, performed with the adhesive compounds, containing amine hardener, we may state as follows:

- The adhesive bonds performed with the use of compounds, containing epoxy resins Epidian 53 and Epidian 57, curing agents with the curing agent Z-1, reveal similar values of the shear strength. The strength of the compound Epidian 53/Z-1/100:10 is 4.60 MPa whereas that one of the compound Epidian 57/Z-1/100:10 is 4,52MPa;
- The lowest value of shear strength is equal to 1,86 and is assigned to the adhesive bonds which were performed using adhesive compound, containing epoxy resin Epidian 5;
- Value of the shear strength of the adhesive joints, made with the use of Epidian 5 and curing agent Z-1 constitutes 41,2% of the value of the strength of the adhesive joints, performed with the use of Epidian 57/Z-1/100:10 and 40,4% of the strength of the adhesive joints connected with the application of Epidian 53/Z-1/100:10.

When comparing the particular results and adopting the type of epoxy resin as a comparative criterion, we may observe the following:

- Strength of the adhesive bonds, performed with the use of compounds, containing epoxy resin Epidian 5 and hardener Z-1 is equal to 16,2% of the strength of the adhesive joints, prepared with the application of Epidian 5/PAC/100:80;
- The strength of the adhesive joints, made with the use of Epidian 53/PAC/100:80 is by ca. 70% higher than that one of the joints, performed with the compounds, containing epoxy resin Epidian 53 and curing agents Z-1;
- The strength of the adhesive joints for performance of which the compounds containing epoxy resin Epidian 57 and curing agent Z-1 were used, constitutes 43,8% of the strength of the adhesive joints prepared with the application of Epidian 57/PAC/100:80.

Fig. 4 illustrates the results of the elongation of the adhesive joints, obtained during the destruction tests of the samples of the joints, connected with the particular adhesive compounds (marking of the adhesive compounds on the diagram was presented in a simplified way, omitting the proportions of the constituents of the discussed compounds due to the readability of the diagram).

When analyzing the above discussed results, we may state that the adhesive joints, performed with the application of the epoxy adhesive compound, containing polyamide curing agents (PAC) reveal higher values of elongation in comparison with the bonds where the elements were linked with two-component adhesive and thre-ethylenoamine (Z-1) was the curing agent. Moreover, it is independent on the type of the employed epoxy resin. It means that the compounds, containing the polyamide curing agents (in relation to the analyzed epoxy resins ans the specified stechiometric relationships) are more
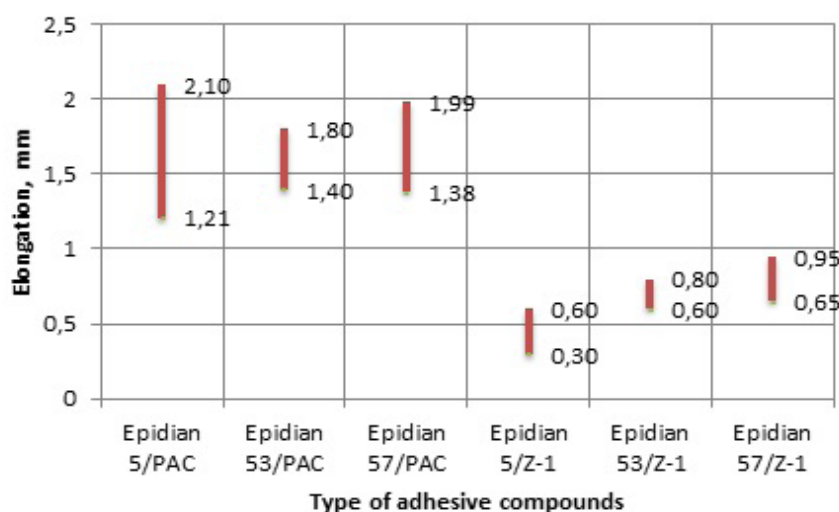

Fig. 4. Elongation at break of adhesive joints of steel sheets, made with various epoxy adhesive compounds

flexible in the adhesive joints as compared to the compounds, containing amine curing agent.

Summing up and conclusions

After conducting the comparative analysis of the results of the experimental tests, we may formulate the following conclusions:

- The adhesive bonds, being prepared with the epoxy adhesive compounds, containing curing agents PAC reveal considerably higher shear strength in comparison to the joints which were made with the epoxy adhesive compounds, containing curing agents Z-1;
- The adhesive joints in which there were used the adhesives containing curing agent PAC as well as curing agent Z-1 and the epoxy resin Epidian 53, are characterized by a higher strength in comparison to the adhesive joints , performed with the compounds containing epoxy resins Epidian 5 and Epidian 57,
- The application of curing agents PAC in the adhesive compounds with the epoxy resins cause generation of more flexible (elastic) joint than in the case of the application of curing agent Z-1.

When summing up the implemented experimental studies, we may reveal and confirm that the appropriate choice of the adhesive compounds affects significantly the strength of the adhesive joint. The precision of performing the operations during bonding process during the preparation of the surface to bonding as well as the appropriate quantity and type of the components of the adhesive compounds and its even distribution on the surface to be linked are also very important. They are the factors which may affect the strength of the adhesive joints.

The conducted tests showed that the application of the compounds, containing curing agents PAC enabled obtaining the adhesive joints of the C45 steel sheets with a higher strength than the application of the compounds with the content of curing agent Z-1.

References

[1] Brockmann W., Geiß P.L., Klingen J., Schröder B. 2009. Adhesive bonding. Materials, Applications and Technology. Weinheim, Germany: Wiley-Vch Press.
[2] Czaplicki J., Ćwikliński J., Godzimirski J., Konar P. 1987. Klejenie tworzyw konstrukcyjnych. Warszawa: WKŁ.
[3] Czub P., Bończa-Tomaszewski Z., Penczek P., Pielichowski J. 2002. Chemia i technologia żywic epoksydowych. Warszawa: WNT.
[4] da Silva L.F.M., Adams R.D. 2007. „Adhesive joint at high and low temperatures using similar and dissimilar adherends and dual adhesives". International Journal of Adhesion and Adhesives (27): 216–226.
[5] Fitton M.D., Broughton J.G. 2005. „Variable modulus adhesives: an approach to optimized joint performance". International Journal of Adhesion and Adhesives (25): 329–336.
[6] Godzimirski J., Kozakiewicz J., Łunarski J., Zielecki W. 1997. Konstrukcyjne połączenia klejowe elementów metalowych w budowie maszyn. Rzeszów: Oficyna Wydawnicza Politechniki Rzeszowskiej.
[7] Katalog: Epidian: żywice i utwardzacze, https://ciechresins.com [access: 01.10.2019].
[8] Kuczmaszewski J. 2006. Fundamentals of metal-metal adhesive joint design. Lublin: Politechnika Lubelska, Oddział PAN w Lublinie.
[9] Prolongo S.G., del Rosario G., Ureña A. 2006. „Comparative study on the adhesive properties of different epoxy resins". International Journal of Adhesion and Adhesives (26): 125 – 132.
[10] Rudawska A. 2005. „Dobór rodzaju kleju w aspekcie wytrzymałości połączeń klejowych blach ocynkowanych". Technologia i Automatyzacja Montażu (1): 28-29.
[11] Rudawska A., Cimek E. 2011. „Wpływ rodzaju kleju na wytrzymałość połączeń klejowych poliamidu PA6". Przetwórstwo Tworzyw 17(3): 198–202.
[12] Rudawska A., Kowalska B., Kubicki P. 2015. „Wytrzymałość połączeń klejowych polimerów, wykonanych za pomocą wybranych klejów sztywnych i elastycznych". Przetwórstwo Tworzyw 21(4): 343-348.
[13] Rudawska A., Kuczmaszewski J. 2012. „Badania porównawcze efektów modyfikacji żywic epoksydowych napełniaczami o dużym stopniu rozdrobnienia dla wybranych utwardzaczy". Przetwórstwo Tworzyw 18(5): 500–504.
[14] https://www.kronosedm.pl/stal-stal-c45-1-0503 [access: 01.10.2019].

Anna Rudawska, Ph.D., D.Sc., Eng.,
Associate Professor, Lublin University of Technology, Faculty of Mechanical Engineering, the Chair of Production Engineering Rudiments
ul. Nadbystrzycka 36, 20-618 Lublin, Poland
e-mail: a.rudawska@pollub.pl

APPLICATION OF CAD MODELLING IN PREPARATION OF A GRINDING WHEEL USED IN SHAPING OF A WORM THREAD OUTLINE

Leszek SKOCZYLAS   ORCID 0000-0002-2714-7155
Artur BEŁZO   ORCID 0000-0002-9414-2434
Roman WDOWIK   ORCID 0000-0002-8419-1750

A b s t r a c t: This paper presents overall description of the cylindrical worm thread grinding process. The grinding wheel CAD model was developed by the use of Boolean operation in the CAD software. The model is universal and is a basis for dressing of a grinding wheel according to the chosen shape. The tools were prepared in the way that allow to grind any contours of the worm thread.

K e y w o r d s: CAD modelling, CAD software, worm thread shape, helical surface, cutting surface of the grinding wheel

S t r e s z c z e n i e: W artykule przedstawiono ogólny opis procesu szlifowania ślimaków walcowych przekładni. Model CAD ściernicy został opracowany przy użyciu operacji Boole'a w programie CAD. Model jest uniwersalny i stanowi podstawę do obciągania ściernicy zgodnie z wybranym kształtem. Narzędzia przygotowane w sposób pozwalający na szlifowanie dowolnych geometrii zwoju ślimaka.

S ł o w a   k l u c z o w e: modelowanie CAD, program CAD, kształt zwoju ślimaka, powierzchnia śrubowa, powierzchnia tnąca ściernicy

Introduction

Advanced CAD/CAM (Computer Aided Design/ Computer Aided Manufacturing) software is nowadays one of the most significant tools of the digitalized manufacturing industry. Regardless of they function as independent software or modules of extended CAx platforms, they have become important tools of manufacturing environments. In reference to a worm gear, CAD systems, are particularly useful if a worm thread characterized by an unusual outline, is shaped. The same applies to the geometry of the tools, which are used in machining of gear wheel teeth. Modelling of complex shapes of the grinding wheel's cutting surface is one of the most difficult design issues, especially if teeth are shaped in envelope milling. For tools characterized by a simple shape, such as straight-line, the modelling process is not challenging. In this case, the standard approach in CAD software concerns the use of revolve function with reference to the appropriate sketch. The issue is complicated when the outline shape is defined by the shape of a worm thread outline. In such case, the issue is complex and requires an individual approach. It concerns the revolved curve enabling to obtain the required shape of a worn thread by the use of envelope

grinding. One of the solutions is an analytical model of the grinding wheel outline, developed on the basis of a mathematical model. The scope of their application is limited by computational complexity and workload.

The tailor-made computer programs have been developed for their effective use [9, 17, 18]. Another solution concerns the machining process simulation in CAD environment, which allows to generate a tool's outline. Advanced functions regarding solids, using Boolean operation, make it possible to create to the grinding wheel shape based on the worm thread's outline. It is a kind of reverse-engineering. The task defined as a description of tool's outline on the basis of known and nominal outline of worn thread surface may be named as a reverse task, because envelope methods have been used so far in which the outline of a tool defines the shape of a worm thread. Different approaches focused on using CAD modelling in the development of worm threads grinding processes are presented in publications [1–8, 10–22]. It should be noted that solids or surface models are very often the basis for other works in engineering practice, e.g. as comparative standards in measuring systems, for geometric or strength simulation using FE-based numerical methods. This paper presents the method and results regarding the development of

a grinding wheel's outline in grinding of the defined worm thread. The proposed approach enables modelling of grinding wheels geometry, which is applicable in grinding of worms characterized by various thread outlines.

Methodology of grinding wheel model development

The modelling method of a grinding wheel, characterized by complex geometry, concerns the simulation in a CAD environment. In order to complete the mentioned modelling tasks, a CAD model of a worn thread must be developed in advance. Modelling work was performed by the use of the SolidWorks software.

The investigations were completed using the worm thread defined by the following parameters:

m = 4 – axial module
z = 1 – number of start thread
q = 10 – diameter rate
γ = 5,71º – lead angle
α = 20º – axial outline angle
d = 40 – pitch diameter of worm
p_z = 12,56 mm – axial pitch
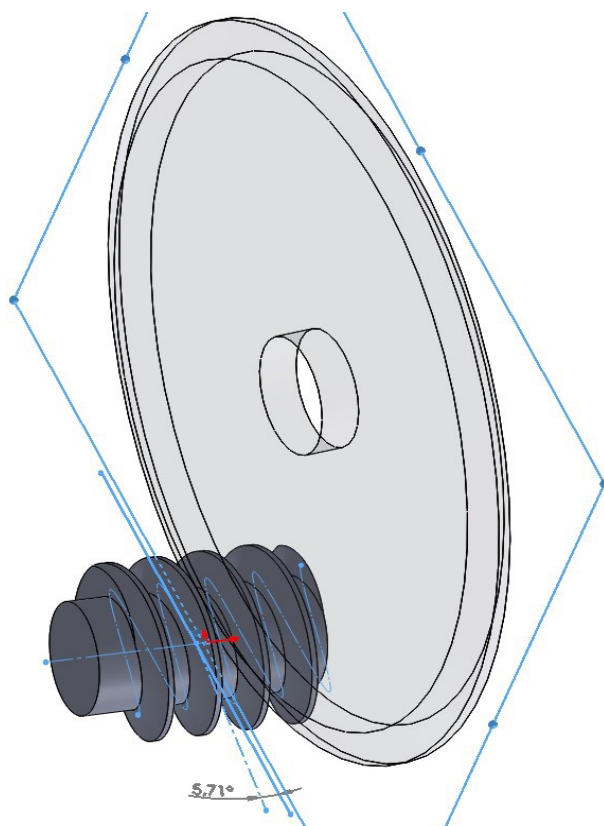h_a = 4 – tooth head height
h_f = 4,8 – tooth foot height

Fig. 1. Grinding wheel – worm thread setup

Preparation of a stock of grinding wheel is also necessary. It is used to create the required outline. Diameter and width of grinding wheel are important. These dimensions should correspond to the real

dimensions. The shaped worms will be characterized by the concave outline of thread and their radiuses are as follows: R_1= 30, R_2 =50 mm. The machining process will be performed by the use of grinding wheels which diameters equal D_1 = 200 mm and D_2 = 150 mm. Both models must be properly positioned in the modelling space. The proper orientation of grinding wheel and worm thread's axis is crucial. The first step is to set up the grinding wheel model in a worm's hob correctly using the defined lead angle. This was done by using an additional reference line related to the structural element of the screw model. The structural element is a line which is tangent to the helix projected onto the plane forming the thread. The point of tangency is fixed on the axis of worm. This ensures that the reference line is correctly positioned, (Fig. 1). Based on the pitch diameter of worm and the thread height, the nominal diameters of grinding wheel were pre-defined as follows D_{N1} = 192 mm and D_{N2} = 142 mm. According to the worm threads machining technology with the use of enveloped tool, the nominal diameter of grinding wheel, must be tangent to the pitch diameter of worm. The tangent points were determined in the research model using the auxiliary sketches.

In the next step, the grinding wheel was transferred from the center of the hob towards the thread's surface. Monitoring of the penetration depth of models enables to determine the "cutlayer" of grinding wheel (Fig. 2). Similarly, the cut-outs will be defined on the other side of the grinding wheel using another model of worm. This approach will let obtain the tool's symmetry and determine its width, including the nominal one (Bn).
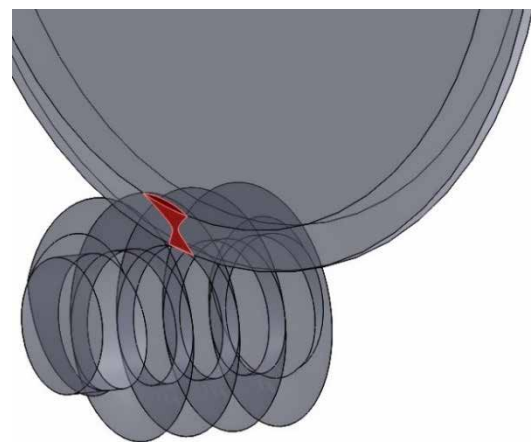
Fig. 2. The position of the grinding wheel shaped with the use of a worm

In comparison to the kinematic system of the machine tool such as thread grinders, the presented approach requires worm turning around wheel's perimeter. As a result, the contact of the grinding wheel with the thread is simulated during its rotational movement (Fig. 3). At this stage, the worm models "penetrate" the grinding wheel. The outline of the cutting surface is obtained by subtracting these worms by means of a function, which is

Fig. 3. The worms arranged on the perimeter of the grinding wheel

Fig. 4. The cutting surface of the grinding wheel obtained after the screw removal operation

based on the principle of Boolean algebra. The tool forming process is not continuous but discrete. The accuracy of the model is dependent on parameters of simulation, and more specifically – on the density of the distribution of the w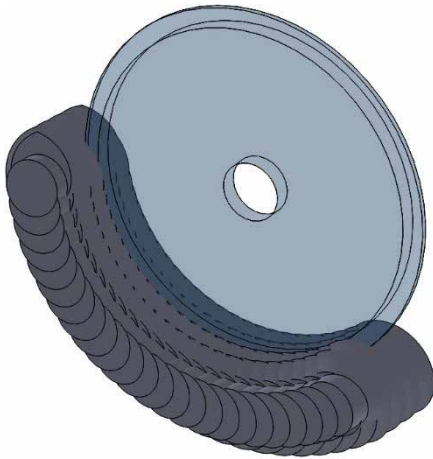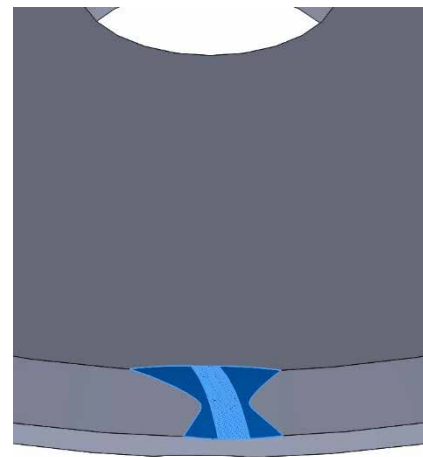orm models on the circumference of grinding wheel. Visualization of the process was presented in Fig. 3. As the final result, the model of tool is created (Fig. 4). It will be used to prepare the NC (Numerical Control) program for a grinding wheel dressing process. Due to PC computational efficiency, the range of models which are used for creation of wheel's shape was reduced to the necessary area – needed to define outline.

Outlines of grinding wheels were obtained by the use of presented approach. It is presented in Fig. 5. Grinding wheel models were developed for worms with a concave thread outline. There are fragments of the cross-sections of the grinding wheels used in machining of a worm. The radius of $R_1 = 30$ mm is presented in Fig. 5a. whereas Fig. 5b presents a worm characterized by radius $R_2 = 50$ mm. The functionality of any CAD software allows to collect the dimensional data of model, e.g. in the form of a two-dimensional drawing. A fragment of such a drawing (Fig. 6) shows the outline of one of the grinding wheel with marked dimensions. The information on the outline geometry will be helpful in NC program development for further application on CNC (Computerized Numerical Control) machine tool, and in the measurements of outline of a fabricated grinding wheel.
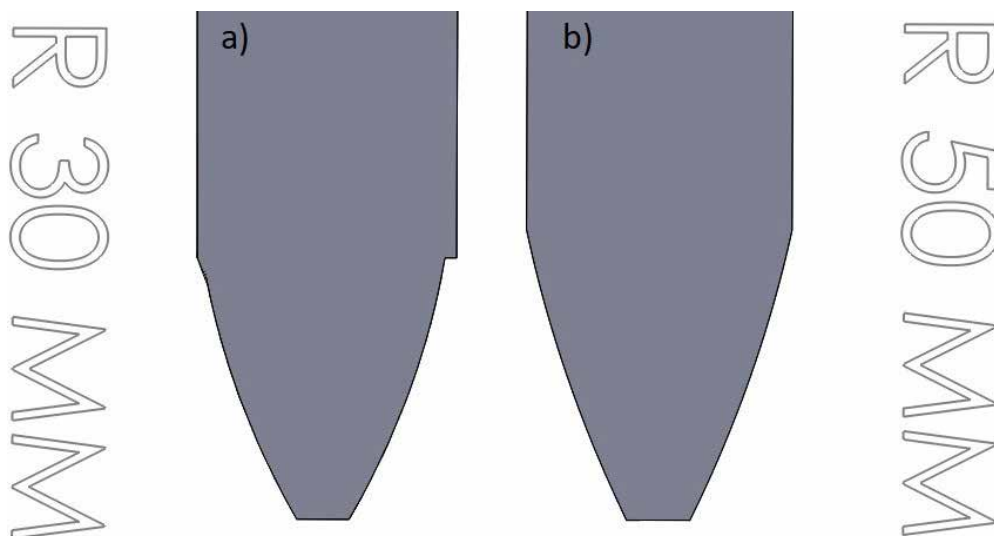

Fig. 5. The outline of a grinding wheel for a worm with the concave thread outline and the defined concavity radius: a) $R = 30$ mm, b) $R = 50$ mm
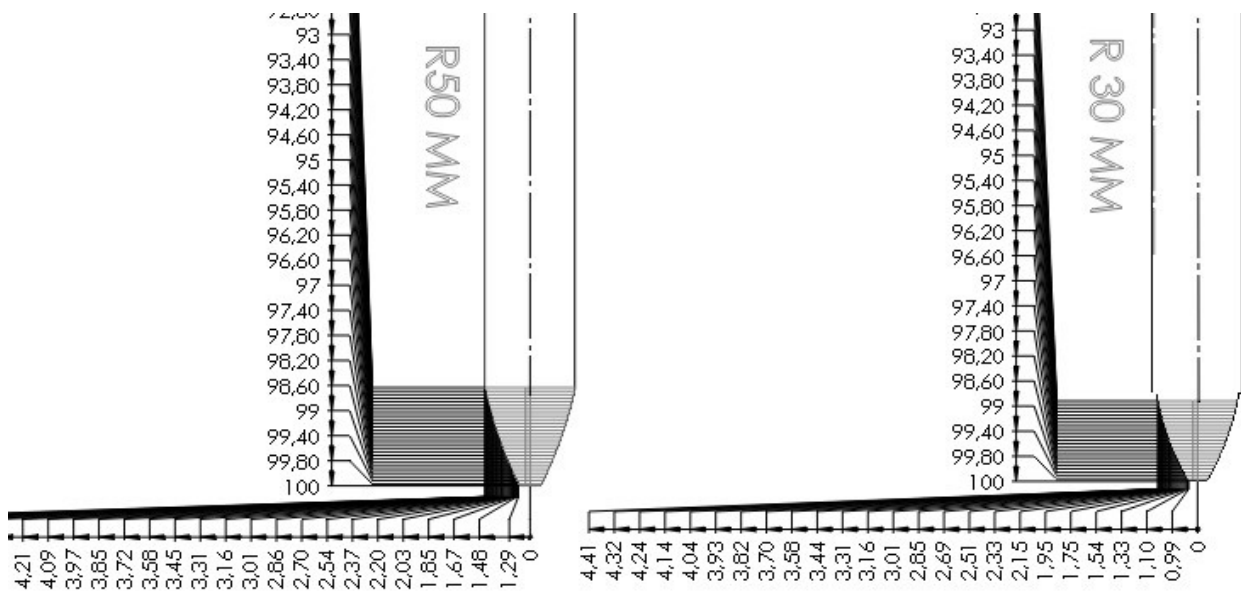
Fig. 6. The drawing of grinding wheel outline with marked dimensions

The outlines presented in Fig. 5 refer to a grinding wheel with the outer diameter of 200 mm. Preparation of a single tool model does not, however, end the design work. An active surface of wheel is subjected to natural wear during grinding. In order to retrieve the desired cutting properties of grinding wheel, it is necessary to dress it periodically. Subsequent dressings remove a certain layer of material. As the consequence of dressing process, a diameter of wheel decreases. This causes changes of its outline too. Due to the new diameter of grinding wheel which determines the new outline of active surface, the model must compensate these unavoidable changes in tool dimensions. A wear of diamond dressers is negligible. Therefore, the compensation of their dimensions can be skipped. On the basis of preliminary tests, the thickness of the abrasive layer, removed during dressing, is determined. This approach enables excessive loss of grinding wheel volume. An information concerning the expected diameter of a wheel after dressing may be used for program updates. It is also necessary to redefine the distance between the tool axis and the worm. Repeated Boolean operations generate a new shape of the active surface adapted to the new dimensions.

Summary

There are only few applications for development of the shape of selected element on the basis of a given model. The software developed by author of the publication [17], which is dedicated for modelling the outline of the thread worm and the cutting surface of the grinding wheel, is not commercial and is not easily accessible. However, it is possible to model these geometries using operations based on Boolean algebra available in CAD software. The abovementioned method was used for the aims of the study. A preliminary geometrical analysis of grinding wheel is hence enabled. The model is also the basis for a development of NC program which will be applied in dressing. The presented method allows to modify the outlines of the worms and ensure their "reflection" on the grinding wheel. It eliminates significant restrictions of envelope methods. These restrictions result from the lack of special tools with the required cutting edge. Roughing can be performed with simple tools (e.g. these which are generally available). Afterwards, it is possible to carry out finishing process using a properly prepared grinding wheel. The described modelling method allows to automate the grinding wheel design process and allows to control the correct preparation of the finished tool. The advantage of using CAD methods is a shortened design time. Grinding wheels, developed with the use of the presented method, will be research in the future.

References

[1] Balajti Z. 2012. „New Modelling of Computer Aided Design of Worms in the Same Axis". Manufacturing and Industrial Engineering 11(2): 26–29.

[2] Ivanov V., Nankov G., Kirov V. 1998. „CAD orientated mathematical model for determination of profile helical surfaces". International Journal of Machine Tools and Manufacture 38 (8): 1001–1015.

[3] Jagiełowicz P. 2018. „The direct solid method of geometry analysis of the globoidal worm gear with the rotary teeth". Mechanik 2: 162–165.

[4] Jagiełowicz P.E. 2015. „Modelowanie powierzchni globoidalnych w środowisku CAD". Mechanik 2: 1–7.

[5] Kacalak W., Budniak Z. 2015. „Modelowanie i analizy szlifowania powierzchni śrubowych w zintegrowanym

środowisku CAD/CAE". Inżynieria Maszyn R. 20, z. 1: 19–32.

[6] Kacalak W., Budniak Z., Szafraniec F. 2017. „Analysis of the Forming Process of Conical-Like Helical Surfaces with Roller Tools". International Journal of Applied Mechanics and Engineering 22: 101–110.

[7] Kacalak W., Budniak Z., Szafraniec F. 2016. „Analiza kształtowania powierzchni śrubowych w procesie szlifowania ściernicami krążkowymi z wykorzystaniem systemów CAD/CAE". Mechanik 10: 1368–1369.

[8] Kheifetc A.L. 2016. „Geometrically Accurate Computer 3D Models of Gear Drives and Hob Cutters". Procedia Engineering 150: 1098–1106.

[9] Marciniak T. 2013. Technologia przekładni ślimakowych. Łódź, Radom: Politechnika Łódzka; Instytut Technologii Eksploatacji - Państwowy Instytut Badawczy w Radomiu.

[10] Mohan L.V., Shunmugam M.S. 2004. „CAD approach for simulation of generation machining and identification of contact lines". International Journal of Machine Tools and Manufacture 44 (7–8): 717–723.

[11] Połowniak P., Sobolak M. 2015. „Modelowanie ślimaka globoidalnego w środowisku CAD". Mechanik 1: 71–74.

[12] Połowniak P., Sobolak M. 2016. „Modelowanie CAD zwoju ślimaka globoidalnego stożkopochodnego na podstawie modelu matematycznego". Mechanik 5–6: 486–487.

[13] Porzycki J., Wdowik R. 2012. „Wytyczne do opracowania systemu CAM dla szlifowania". Mechanik 2: CD.

[14] Porzycki J. 2004. Modelowanie szlifowania osiowego zewnętrznych powierzchni walcowych. Rzeszów: Oficyna Wydawnicza Politechniki Rzeszowskiej.

[15] Sabiniak H.G., Cichowicz R.A. 2014. „Metody CAD i CAE w komputerowym wspomaganiu projektowania zazębień ślimakowych". Zeszyty Naukowe Politechniki Śląskiej 82: 235–242.

[16] Skawiński P., Siemiński P., Pomianowski R. 2011. „Generowanie modeli bryłowych uzębień stożkowych za pomocą symulacji oprogramowanych w systemie 3D CAD". Mechanik 11: 922–924.

[17] Skoczylas L. 2010. „Automatyzacja procesu modelowania uzębienia kół przekładni ślimakowych". Technologia i Automatyzacja Montażu 1: 25–27.

[18] Skoczylas L. 2010. Synteza geometrii zazębienia walcowych przekładni ślimakowych ze ślimakiem o dowolnym zarysie. Rzeszów: Oficyna Wydawnicza Politechniki Rzeszowskiej.

[19] Skoczylas L., Wydrzyński D., Rębisz Ł. 2015. „Komputerowe wspomaganie obróbki uzębienia prototypów kół ślimakowych". Mechanik 12: 180–182.

[20] Sobolak M., Jagiełowicz P.E., Połowniak P. 2016. „Generowanie powierzchni zwoju ślimaka globoidalnego w środowisku CATIA z wykorzystaniem symulacji kinematycznej". Mechanik 5–6: 464–466.

[21] Twardoch K. 2014. „Cyfrowe modelowanie geometryczne zarysu zębów z zastosowaniem metodologii CAD". Zeszyty Naukowe Politechniki Śląskiej 82: 271–279.

[22] Wronkowicz A., Wachla D. 2014. „Model autogenerujący CAD zazębienia przekładni ślimakowej". Zeszyty Naukowe Politechniki Śląskiej 82: 291–300.

Leszek Skoczylas, DSc, PhD, Eng.
lsktmiop@prz.edu.pl

Artur Bełzo, MSc, Eng.
artur.belzo@prz.edu.pl

Roman Wdowik, PhD, Eng.
rwdowik@prz.edu.pl

Rzeszow University of Technology
al. Powstańców Warszawy 8, 35-959 Rzeszów, Poland

Z PRASY ZAGRANICZNEJ

Tytuły i streszczenia artykułów zamieszczonych w miesięczniku naukowo-technicznym „**Sborka v mashinostroenii priborostroenii**" (Wydawnictwo Maszynostrojenije, Moskwa, Rosja)

Sborka nr 8, 2019

1. Fixture for disassembly of the generator of the truck KamAZ-5320
Author: Dubovik E.A.

The paper proposes a kinematic and power calculation of the removable device for disassembly of the truck generator KamAZ-5320

2. The choice of the optimal precision operation the adaptive friction clutches
Author: Shishkarev M.P.

It is shown that the increase in the accuracy of the adaptive friction clutches leads to a decrease in the overall dimensions and weight of the drive and an increase in the self-mass of the clutch. Minimizing the total weight of the drive, including the clutch, is based on optimizing the actuation accuracy at a certain ratio of the drive and clutch weight. It is established that the minimum total weight of the machine drive depends on the composition of the drive, the initial mass of the clutch, the rate of change in its mass and the accuracy of operation, depending on the magnitude of the gain.

3. Physical and technical-economic features of the assembly process mounting joints of beams of a set of metal structures
Author: Rozinov A.Ya.

The technology of performing operations for assembling the shell plating joints and the beams of the set supporting it is analyzed. The scheme of application of the Assembly forces providing connection of beams of a set, and features of physics of action of these forces on the basis of the basic provisions of the theory of a bend and torsion of beams-strips and rod systems is considered. The mechanics of bending and torsion of the connected beams of the set is described taking into account the influence of welding of these beams to the surface of the sheathing. The resulting calculated expressions for the displacements of the ends of the joining beams of the set under the action of the assembly forces are given, as well as the results of the analysis of the technical and economic indicators of the traditional assembly technology for the joints of the set of metal structures and the method of changing this technology by mechanizing the process of joining the beams of the set.

4. Mechanical and tribological properties of UHMW-PE composites with chopped glass fibers functionalized with polyorganosiloxane reagents (part 1)
Authors: Panin S.V., Kornienko L.A., Huan TSitao, Buslovich D.G., Aleksenko V.O.

Mechanical and tribotechnical properties of ultrahigh-molecular weight polyethylene (UHMW-PE) composites filled with chopped fiberglass pretreated with three different silane-containing modifiers increasing adhesion of fiberglass to the polymer matrix in order were investigated. The choice of the filler and adhesion promoters for the ultrahighmolecular weight PE matrix is due to search of effective industrially manufactured fillers and surface modifiers for developing wear-resistant polymer composites for friction units in mechanical engineering. It is shown that coupling agents KH550 and Penta-1006 are more efficient industrially produced adhesion promoters for the fiberglass which provide high wear resistance of reinforced UHMW-PE composite for their stable operation in a wide range of velocities and loads.

5. Granule analyzing onto colloidal graphite for hot deformation lubricants
Authors: Petrov A.N., Tausenev D.S., Mizera S.V., Petrov M.A.

This article deals with researching of colloidal graphite to be used for hot deformation as powders or as lubricants. We have done these investigations by analyzers HELOS and QICPIC, Co. Sympatec GmbH, Germany. We have got results concerning sizes and shapes of graphite powders C1 and S12. We have researched technological properties of colloidal graphite C1 as ingredient for hot deformation lubricant.

6. Improvement of wear resistance of "duplex" coatings for cutting tools by ion mixing
Authors: Migranov M.Sh., Migranov A.M., Shekhtman S.R.

The results of the study of the ways of increasing the wear resistance of "duplex" coatings applied to the cutting tools, which, due to the preliminary diffusion of the tool surface saturation with nitrogen (known as ion nitrogen)

followed by physical deposition of the hard coating (Ti, Cr), the proposed coating contains an additional layer with an admixture of ions applied to the pre-nitrided surface of the high-speed coating before the deposition of the hard coating. Such multi-layer coatings significantly increase (3−4 times) the wear resistance of cutting tools compared to "duplex" coatings.

7. The heat propagation at imperfect heat exchange in crossection of two-dimensional medium
Author: Rapilbekova N.S.

The researches of heat propagation singularity in two-dimensional medium are carried out in case when natural condition of heat transfer is disturbed. Two condition of heat transfer are considered in this crossection: ideal and non-ideal conditions of heat exchange distinctive for many layer body.

Link: http://www.mashin.ru/eshop/journals/sborka_v_mashinostroenii_priborostroenii/2025/23/

Sborka nr 9, 2019

---

1. Automated assembly of connections based on micro-screws and technological features
Author: Berezin S.Ya.

The peculiarities of implementation of automated operations of screwing a separate class of screws with a thread diameter of less than one millimeter (micro-screws) in the threaded holes are considered. The types of technological equipment, including screwed heads, vibrating hoppers with feeders, manipulators of heads movement are given. Examples of the most well-known types of joints with micro-screws and calculation formulas for determining the geometric, power and speed parameters of the assembly are presented.

2. Assembling RFID tags work on metal surfaces based on special chips
Authors: Mikaeva S.A., Reznik A.A.

This article discusses the collected radio frequency label for operation on the basis of a special chip and the problem associated with the operation of radio frequency labels UHF range in close contact with different media. The principle of operation of RFID systems is explained, design features, assembly and reading of UHF RFID tags for metal objects are considered. Considered one of the possible options for improving RFID chip designed to work on metal.

8. Boundary lubrication as protection for tribocoupling against wear and scuffing at hard work
Authors: Buyanovsky I.A., Samusenko V.D.

The modern understanding of the most hard mode of lubrication of frictional units at which the rubbing surfaces are not separated by a continuous layer of lubricant, and protection against scuffing and the increased wear is carried out by the boundary layers representing products of interaction of active components of the lubricant environment with material of friction surfaces are considered. The phenomenology of process of boundary lubrication, to mechanisms of formation and destruction of boundary layers and their influence on friction and wear of the contacting bodies under various conditions of realization of boundary lubrication are taken into account.

3. Evaluation of corrosive effects on fatigue automotive materials
Authors: Pachurin G.V., Kuz'min N. A., Goncharova D. A., Filippov A. A., Nuzhdina T. V.

The influence of the corrosive environment on the laws of fatigue resistance of automotive structural steels is considered. The factors affecting the resistance to fatigue failure are identified: the environment and its aggressiveness; frequency, shape of the cycle and asymmetry of the loading cycle. Using the curves of the current deflection under cyclic loading fixing the moment of crack initiation and determining the speed of its subsequent propagation to justify the choice of materials, increase resource, reduce the consumption of materials for machines and manufacturing technology, taking into account the conditions of their operation and to improve maintainability of the cars.

4. The conditions of the automated coordination of the assembly components' mutual position
Authors: Kyznetsova S.V., Simakov A.L.

The formalized description of the details' overlapping process at assembly with using of the multitudes' theory is offered. The necessary and sufficient conditions of the automated coordination of the assembly components' mutual position are formulated and proved. The necessary

condition of the automated coordination is realization of purposeful moving of details' connecting surfaces on program trajectories of overlapping by the assembly device. The sufficient condition of the automated coordination is the monotone decrease of orientation's error of connecting surfaces at detail's moving on the program trajectory of overlapping.

5. Mechanical and tribological properties of UHMW-PE composites with chopped glass fibers functionalized with polyorganosiloxane reagents (part 2)
Authors: Panin S.V., Kornienko L.A., Huan TSitao, Buslovich D.G., Aleksenko V.O.

Mechanical and tribotechnical properties of UHMW-PE based composites with different initial size of the polymer powder filled with chopped glass fibers functionalized with silane-containing modifier KH550 to increase adhesion to the polymer matrix were studied. It is shown that the various initial size of the powder at an equivalent molecular weight determines the pattern of glass fiber distribution in the matrix, and, as a consequence, the mechanical and tribotechnical properties of the composites. It was revealed that glass fiber reinforced composite based on fine powder UHMW-PE grade GUR-2122.

6. Wave character of deformation at sliding friction
Author: Medeljaev I.A.

Elastic and plastic stress waves, temperature waves are considered as a source of wave processes during sliding friction. It is shown that the dynamic nature of friction and vibration of the technical system determine the wave character of deformation and vibration in the friction unit.

7. Geometrical adaptation of cutting wedge for increased wear resistance tool
Authors: Migranov M.Sh., Migranov A.M.

Results of research of increase of wear resistance of the tool by geometrical adaptation of the form of the cutting wedge at machining by cutting and milling of various materials on machinability are given. The possibility of increasing the wear resistance of the cutting tool by 75...90 % while ensuring and improving the quality of the treated surface layer is confirmed.

8. Diagnosis of the possibility of reducing unproductive labor costs and the mechanization of the process of assembling the outer skin joints, reinforced with stiffeners
Authors: Rozinov A.Ya., Logunov V.V.

The traditional schemes of assembling the joining of cladding and beams of reinforcing ribs are presented, their shortcomings are indicated. A model of improving the assembly process and graphs of the relative values of deviations of the edges of the joined skin and the ends of the beams of reinforcing ribs are given. The calculation of the forces of the assembly of the plating joints and the joints of the beams of reinforcing ribs is given. Variants of the schemes of mechanized application of these forces are given, as well as data on the reduction of labor costs as a result of the rejection of the use of temporarily welded elements and a change in the sequence of work.

---

1. A prioritized planning algorithm of trajectory coordination based on time windows for multiple AGVs with delay disturbance
Authors: Ruochen Tai, Jingchuan Wang, Weidong Chen

This paper proposes a prioritized path planning algorithm based on time windows to solve the delay problems of multiple AGVs. The architecture is a unity consisting of three components which are focused on scheduling AGVs under normal operations, delays of AGVs, and recovery of AGVs. In the components of scheduling AGVs under normal operations and recovery, this paper adopts a dynamic routing method based on time windows to ensure the coordination of multiple AGVs and efficient completion of tasks. In the component for scheduling AGVs under delays, a dynamical prioritized local path planning algorithm based on time windows

is designed to solve delay problems. The introduced planning principle of time windows would enable the algorithm to plan new solutions of trajectories for multiple AGVs, which could lower the makespan. At the same time, the real-time performance is acceptable based on the planning principle which stipulates the parameters of local time windows to ensure that the computation of the designed algorithm would not be too large.

The simulation results demonstrate that the proposed algorithm is more efficient than the state-of-the-art method based on homotopy classes, which aims at solving the delay problems. What is more, it is validated that the proposed algorithm can achieve the acceptable real-time performance for the scheduling in warehousing applications.

2. Tolerance–reliability analysis of mechanical assemblies for quality control based on Bayesian modeling
Authors: Yinhua Liu, Shiming Zhang, Guoping Chu

The purpose of this paper is to present a new efficient method for the tolerance–reliability analysis and quality control of complex nonlinear assemblies where explicit assembly functions are difficult or impossible to extract based on Bayesian modeling.

In the proposed method, first, tolerances are modelled as the random uncertain variables. Then, based on the assembly data, the explicit assembly function can be expressed by the Bayesian model in terms of manufacturing and assembly tolerances. According to the obtained assembly tolerance, reliability of the mechanical assembly to meet the assembly requirement can be estimated by a proper first-order reliability method.

The Bayesian modeling leads to an appropriate assembly function for the tolerance and reliability analysis of mechanical assemblies for assessment of the assembly quality, by evaluation of the assembly requirement(s) at the key characteristics in the assembly process. The efficiency of the proposed method by considering a case study has been illustrated and validated by comparison to Monte Carlo simulations.

The method is practically easy to be automated for use within CAD/CAM software for the assembly quality control in industrial applications.

Bayesian modeling for tolerance–reliability analysis of mechanical assemblies, which has not been previously considered in the literature, is a potentially interesting concept that can be extended to other corresponding fields of the tolerance design and the quality control.

3. An integrated production-distribution planning with a routing problem and transportation cost discount in a supply chain
Authors: Behzad Karimi, Mahsa Ghare Hassanlu, Amir Hossein Niknamfar

The motivation behind this research refers to the significant role of integration of production-distribution plans in effective performance of supply chain networks under fierce competition of today's global marketplace. In this regard, this paper aims to deal with an integrated production-distribution planning problem in deterministic, multi-product and multi-echelon supply chain network. The bi-objective mixed-integer linear programming model is constructed to minimize not only the total transportation costs but also the total delivery time of supply chain, subject to satisfying retailer demands and capacity constraints where quantity discount on transportation costs, fixed cost associated with transportation vehicles usage and routing decisions have been included in the model.

As the proposed mathematical model is NP-hard and that finding an optimum solution in polynomial time is not reasonable, two multi-objective meta-heuristic algorithms, namely, non-dominated sorting genetic algorithm II (NSGAII) and multi-objective imperialist competitive algorithm (MOICA) are designed to obtain near optimal solutions for real-sized problems in reasonable computational times. The Taguchi method is then used to adjust the parameters of the developed algorithms. Finally, the applicability of the proposed model and the performance of the solution methodologies in comparison with each other are demonstrated for a set of randomly generated problem instances.

The practicality and applicability of the proposed model and the efficiency and efficacy of the developed solution methodologies were illustrated through a set of randomly generated real-sized problem instances. Result. In terms of two measures, the objective function value and the computational time were required to get solutions.

4. Quantifying the complexity of subassemblies in a fully automated assembly system
Authors: Yicong Gao, Chuan He, Bing Zheng, Hao Zheng, Jianrong Tan

Complexity is the main challenge for present and future manufacturers. Assembly complexity heavily affects a product's final quality in the fully automated assembly system. This paper aims to propose a new method to assess the complexity of modern automated assembly system at the assembly design stage with respect to the characteristics of both manufacturing system and each single component to be mounted. Aiming at validating the predictive model, a regression model is additionally presented to estimate the statistic relationship between the real assembly defect rate and predicted complexity of the fully automated assembly system.

The research herein extends the S. N. Samy and H. A. ElMaraghy's model and seeks to redefine the predictive model using fuzzy evaluation against a fully automated assembly process at the assembly design stages. As the evaluation based on the deterministic scale with accurate

crisp number can hardly reflect the uncertainty of the judgement, fuzzy linguistic variables are used to measure the interaction among influence factors. A dependency matrix is proposed to estimate the assembly complexity with respect to the interactions between mechanic design, electric design and process factors and main functions of assembly system. Furthermore, a complexity attributes matrix of single part is presented, to map the relationship between all individual parts to be mounted and three major factors mentioned in the dependency matrix.

5. A constraint programming approach to type-2 assembly line balancing problem with assignment restrictions
Authors: Mehmet Pinarbasi, Hacı Mehmet Alakas, Mustafa Yuzukirmizi

Main constraints for an assembly line balancing problem (ALBP) are cycle time/number of stations and task precedence relations. However, due to the technological and organizational limitations, several other restrictions can be encountered in real production systems. These restrictions are called as assignment restrictions and can be task assignment, station, resource and distance limitations. The purpose of the study is to evaluate the effects of these restrictions on ALBP using constraint programming (CP) model.

A novel CP model is proposed and compared to mixed-integer programming (MIP) as a benchmark. The objective is to minimize the cycle time for a given number of stations. The authors also provide explicit anthology of the assignment restriction effects on line efficiency, the solution quality and the computation time.

Assembly line is a popular manufacturing system in the making of standardized high volume products. The problem of assembly line balancing is a crucial challenge in these settings and consists of assigning tasks to the stations by optimizing one or more objectives. Type-2 AR-ALBP is a specific case with the objective function of minimizing the cycle time for a given number of stations. It further assumes assignment restrictions that can be confronted due to the technological limitations or the strategic decisions of the company management. This is especially encountered in rebalancing lines.

6. A genetic algorithm approach for balancing two-sided assembly lines with setups
Authors: Yilmaz Delice

This paper aims to discuss the sequence-dependent forward setup time (FST) and backward setup time (BST) consideration for the first time in two-sided assembly lines. Sequence-dependent FST and BST values must be considered to compute all of the operational times of each station. Thus, more realistic results can be obtained for real-life situations with this new two-sided assembly

line balancing (ALB) problem with setups consideration. The goal is to obtain the most suitable solution with the least number of mated stations and total stations.

The complex structure it possesses has led to the use of certain assumptions in most of the studies in the ALB literature. In many of them, setup times have been neglected or considered superficially. In the real-life assembly process, potential setup configurations may exist between each successive task and between each successive cycle. When two tasks are in the same cycle, the setup time required (forward setup) may be different from the setup time required if the same two tasks are in consecutive cycles (backward setup).

Algorithm steps have been studied in detail on a sample solution. Using the proposed algorithm, the literature test problems are solved and the algorithm efficiency is revealed. The results of the experiments revealed that the proposed approach finds promising results.

7. A novel hybrid control approach for modular automation system: a case study of sensorless interior permanent magnet in-wheel motor
Authors: Yong Li, Yanjun Huang, Xing Xu

Sensorless interior permanent magnet in-wheel motor (IPMIWM), as an exemplar of modular automation system, has attracted considerable interests in recent years. This paper aims to investigate a novel hybrid control approach for the sensorless IPMIWM from a cyber-physical systems (CPS) perspective.

The control approach is presented based on the hybrid dynamical theory. In the standstill-low (S-L) speed, the rotor position/speed signal is estimated by the method of the high frequency (HF) voltage signal injection. The least square support vector machine (LS-SVM) is used to acquire the rotor position/speed signal in medium-high (M-H) speed operation. Hybrid automata model of the IPMIWM is established due to its hybrid dynamic characteristics in wide speed range. A hybrid state observer (HSO), including a discrete state observer (DSO) and a continuous state observer (CSO), is designed for rotor position/speed estimation of the IPMIWM.

The hardware-in-the-loop testing based on dSPACE is carried out on the test bench. Experimental investigations demonstrate the hybrid control approach can not only identify the rotor position/speed signal with a certain load but also be able to reject the load disturbance. The reliability and the effectiveness of the proposed hybrid control approach were verified.

The proposed hybrid control approach for the sensorless IPMIWM promotes the deep combination and coordination of sensorless IPMIWM drive system. It also theoretically supports and extends the development of the hybrid control of the highly integrated modular automation system.

8. A framework for tolerance design considering systematic and random uncertainties due to operating conditions
Authors: Saeed Khodaygan

The purpose of this paper is to present a novel Kriging meta-model assisted method for multi-objective optimal tolerance design of the mechanical assemblies based on the operating conditions under both systematic and random uncertainties.

In the proposed method, the performance, the quality loss and the manufacturing cost issues are formulated as the main criteria in terms of systematic and random uncertainties. To investigate the mechanical assembly under the operating conditions, the behavior of the assembly can be simulated based on the finite element analysis (FEA). The objective functions in terms of uncertainties at the operating conditions can be modeled through the Kriging-based metamodeling based on the obtained results from the FEA simulations. Then, the optimal tolerance allocation procedure is formulated as a multi-objective optimization framework. For solving the multi conflicting objectives optimization problem, the multi-objective particle swarm optimization method is used. Then, a Shannon's entropy-based TOPSIS is used for selection of the best tolerances from the optimal Pareto solutions.

The proposed method can be used for optimal tolerance design of mechanical assemblies in the operating conditions with including both random and systematic uncertainties. To reach an accurate model of the design function at the operating conditions, the Kriging meta-modeling is used. The efficiency of the proposed method by considering a case study is illustrated and the method is verified by comparison to a conventional tolerance allocation method. The obtained results show that using the proposed method can lead to the product with a more robust efficiency in the performance and a higher quality in comparing to the conventional results.

9. 3D modelling of a frame assembly using deep learning and the Chu–Liu–Edmonds Algorithm
Authors: Hao Cao, Rong Mo, Neng Wan

The proposed method is to generate the 3D model of frame assemblies based on their topological model automatedly. It was a very demanding task and there was no appropriate automated method to facilitate this work.

The proposed method includes two stages. The first stage is decisive. In this stage, a deep learning network and the Chu–Liu–Edmonds algorithm are used to recognize contact relations among parts. Based on this recognition, the authors perform a geometrical computation in the second stage to finalize the 3D model.

The authors verify the feasibility of the proposed method using a case study and find that the classification rate of the deep learning network for part contact relations is higher than 75 per cent. Furthermore, more accurate results could be achieved with modification by the Chu–Liu–Edmonds algorithm. The proposed method has lower computational complexity compared with traditional heuristic methods, and its results are more consistent with existing designs.

The proposed method expands the application of machine learning into a new field. It would be more useful than simple machine learning in industry. The proposed method is better than general heuristic algorithms. It outputs identical results when the inputs are the same. Meanwhile, the algorithmic complexity in worst situation is better than general heuristic algorithms.

10. Ease of product assembly through a time-based design methodology
Authors: Anoop Desai

This paper aims to present a design methodology to enable product design for ease of assembly. It is corroborated by means of a case study. The methodology is based on standard time data. This enables quick computation of assembly time as well as comparing different design options for ease of assembly.

Component design that is easy to assemble is likely to take less time and vice versa. Assembly time is a function of product design attributes such as geometric shape, weight, center of gravity, type of material, number of fasteners and types of fasteners. The methodology uses standard data to achieve its objective. Numeric scores are developed for each design feature based on the aforementioned design attributes. This enables not only computation of assembly time for a brand new product but also comparison of two or more alternative design configurations from the point of view of ease of assembly.

The amount of time to assemble a product before the product is ever designed is facilitated by this system. Assembly time is a direct function of product design attributes. Process time is calculated using standard data, specifically, the Methods Time Measurement (MTM) system. This is accomplished by converting design features into time measurement units (TMUs). Assembly cost can then be easily computed by using assembly time as the basis. The computation of assembly time and cost is important inasmuch as its role in influencing productivity. This is of obvious value not only to the designer but the company as a whole.

11. Research on software synchronization method of real-time ethernet distributed motion control system
Authors: Zhengyu Huang, Lingyu Chen, Lianchao Zhang, Shixun Fan, Dapeng Fan

This paper aims to analyze the key factors influencing the synchronization performance of distributed motion control system and to improve the synchronization performance for peripherals control of this system.

This paper deals with the software synchronization problems of distributed motion control system based on real-time Ethernet. First, combined with communication and control tasks, the key factors affecting synchronization performance of system are analyzed. Then, aiming at key factors and considering the synchronization of system bus, protocol conversion and task scheduling, a software synchronization method based on CANopen protocol and real-time Ethernet is proposed. Finally, the feasibility of this method is verified by establishing distributed motion control system and testing the synchronization performance of terminal control signals of slaves.

Based on this method, the results show that the synchronization accuracy for peripherals control of all slaves could be about 100 ns.

This research provides high-precision synchronization method, which could lay a foundation for the application of distributed motion control system in the field of assembly automation, such as multi-axis assembly robots control.

In distributed motion control system, many factors affect the synchronization performance. At present, there is no synchronization method that could comprehensively consider these factors. This paper not only analyzes the key factors influencing the synchronization performance of system but also proposes a synchronization method. Therefore, the method proposed in this paper has certain theoretical value and engineering significance.

12. Effective design and development of hybrid ABC-CSO-based capacitor placement with load forecasting based on artificial neural network
Authors: Sarika Sharma, Smarajit Ghosh

This paper aims to develop a capacitor position in radial distribution networks with a specific end goal to enhance the voltage profile, diminish the genuine power misfortune and accomplish temperate sparing. The issue of the capacitor situation in electric appropriation systems incorporates augmenting vitality and peak power loss by technique for capacitor establishments.

This paper proposes a novel strategy using rough thinking to pick reasonable applicant hubs in a dissemination structure for capacitor situation. Voltages and power loss reduction indices of distribution networks hubs are shown by fuzzy enrollment capacities.

A fuzzy expert system containing a course of action of heuristic rules is then used to ascertain the capacitor position appropriateness of each hub in the circulation structure. The sizing of capacitor is solved by using hybrid artificial bee colony–cuckoo search optimization.

Finally, a short-term load forecasting based on artificial neural network is evaluated for predicting the size of the capacitor for future loads. The proposed capacitor allocation is implemented on 69-node radial distribution network as well as 34-node radial distribution network and the results are evaluated.

Simulation results show that the proposed method has reduced the overall losses of the system compared with existing approaches.

13. Gamification of assembly planning in virtual environment
Authors: Samir Garbaya, Daniela M. Romano, Gunjeet Hattar

The purpose of this paper is to study the effect of the gamification of virtual assembly planning on the user performance, user experience and engagement.

A multi-touch table was used to manipulate virtual parts and gamification features were integrated into the virtual assembly environment. An experiment was conducted in two conditions: a gamified and a non-gamified virtual environment. Subjects had to assemble a virtual pump. The user performance was evaluated in terms of the number of errors, the feasibility of the generated assembly sequence and the user feedback.

The gamification reduced the number of errors and increased the score representing the number of right decisions. The results of the subjective and objective analysis showed that the number of errors decreased with engagement in the gamified assembly. The increase in the overall user experience reduced the number of errors. The subjective evaluation showed a significant difference between the gamified and the non-gamified assembly in terms of the level of engagement, the learning usability and the overall experience.

The effective learning retention after training has not been tested, and longitudinal studies are necessary. The effect of the used gamification elements has been evaluated as a whole; further work could isolate the most beneficial features and add other elements that might be more beneficial for learning.

The research reported in this paper provides valuable insights into the gamification of virtual assembly using a low-cost multi-touch interface. The results are promising for training operators to assemble a product at the design stage.

14. Robust scheduling in two-stage assembly flow shop problem with random machine breakdowns: integrated meta-heuristic algorithms and simulation approach
Authors: Sahar Tadayonirad, Hany Seidgar, Hamed Fazlollahtabar, Rasoul Shafaei

In real manufacturing systems, schedules are often disrupted with uncertainty factors such as random machine breakdown, random process time, random job arrivals or job cancellations. This paper aims to investigate robust scheduling for a two-stage assembly flow shop scheduling with random machine breakdowns

and considers two objectives makespan and robustness simultaneously.

Owing to its structural and algorithmic complexity, the authors proposed imperialist competitive algorithm (ICA), genetic algorithm (GA) and hybridized with simulation techniques for handling these complexities. For better efficiency of the proposed algorithms, the authors used artificial neural network (ANN) to predict the parameters of the proposed algorithms in uncertain condition. Also Taguchi method is applied for analyzing the effect of the parameters of the problem on each other and quality of solutions.

Finally, experimental study and analysis of variance (ANOVA) is done to investigate the effect of different proposed measures on the performance of the obtained results. ANOVA's results indicate the job and weight of makespan factors have a significant impact on the robustness of the proposed meta-heuristics algorithms. Also, it is obvious that the most effective parameter on the robustness for GA and ICA is job.

Robustness is calculated by the expected value of the relative difference between the deterministic and actual makespan.

15. Particle swarm optimization-based optimal real Gabor filter for surface inspection
Authors: Hao Wu, Xiangrong Xu, Jinbao Chu, Li Duan, Paul Siebert

The traditional methods have difficulty to inspection various types of copper strips defects as inclusions, pits and delamination defects under uneven illumination. Therefore, this paper aims to propose an optimal real Gabor filter model for inspection; however, improper selection of Gabor parameters will cause the boundary between the defect and the background image to be not very clear. This will make the defect and the background cannot be completely separated.

The authors proposed an optimal Real Gabor filter model for inspection of copper surface defects under uneven illumination. This proposed method only requires a single filter by calculating the specific convolution energy of the Gabor filter with the image. The Real Gabor filter's parameter is optimized by particle swarm optimization (PSO), which objective fitness function is maximization of the Gabor filter's energy average divided by the energy standard deviation, the objective makes a distinction between the defect and normal area.

The authors have verified the effect with different iterations of parameter optimization using PSO, the effects with different control constant of energy and neighborhood window size of real Gabor filter, the experimental results on a number of metal surface have shown the proposed method achieved a well performance in defect recognition of metal surface.

16. Local-global method to predict distortion of aircraft panel caused in automated riveting process
Authors: Di Yang, Weiwei Qu, Yinglin Ke

The riveting process is a metal forming process involving complex elastic-plastic deformation, which will induce a compressive residual stress field and cause local distortions in the connecting areas. Regarding to the aircraft panel assemblies with plenty of rivets, the global deformation is inevitable and undesired, leading difficulties to downstream assembly processes. This paper aims to present a new method for the local distortion calculation and the global deformation prediction of sheet panel assemblies during the automated riveting process.

In this paper, a simplified algebraic study is presented to analyze the local distortion of single countersunk rivet joint with the consideration of the barrel-like shape of the driven head and the through-thickness variations along the rivet shank. Then, an equivalent rivet unit is proposed based on the result of the algebraic study and embedded into the global-level model for the prediction of the overall distortions of riveted panels.

The algebraic study is able to reach a more precise contour of the deformed rivet than the traditional assumption of cylindrical deformations and rapidly determine the equivalent coefficients of the riveting unit. The result also shows an industrial acceptable accuracy of the prediction for the global deformations of the double-layered panel assemblies widely used in the aircraft panel structures.

17. Automatic press-fit assembly of small precision interference fitting parts: armature of electro-hydraulic servo valve
Authors: Xingyuan Wang, Zhifeng Lou, Xiaodong Wang, Yue Wang, Xiupeng Hao, Zhize Wang

The purpose of this paper is to design an automatic press-fit instrument to realize precision assembly and connection quality assessment of a small interference fitting parts, armature.

In this paper, an automatic press-fit instrument was developed for the technical problems of reliable clamping and positioning of the armature, automatic measurement and adjustment of the attitude and evaluation of the connection quality. To compensate for the installation error of the equipment, corresponding calibration method was proposed for each module of the instrument. Assembly strategies of axial displacement and perpendicularity were also proposed to ensure the assembly accuracy. A theoretical model was built to calculate the resistant force generated by the non-contact regions and then combined with the thick-walled cylinder theory to predict the press-fit curve.

The calibration method and assembly strategy proposed in this paper enable the press-fit instrument to achieve good alignment and assembly accuracy. A reasonable range of press-fit curve obtained from theoretical model can achieve the connection quality assessment.

This instrument has been used in an armature assembly project. The practical results show that this instrument can assemble the armature components with complex structures automatically, accurately, in high-efficiency and in high quality.

This paper provides a technical method to improve the assembly quality of small precision interference fitting parts and provides certain methodological guidelines for precision peg-in-hole assembly.

18. Robotic hand-arm system for on-orbit servicing missions in Tiangong-2 Space Laboratory

Authors: Yiwei Liu, Shipeng Cui, Hong Liu, Minghe Jin, Fenglei Ni, Zhiqi Li, Chongyang Li

The purpose of this study is to develop a robotic hand–arm system for on-orbit servicing missions at the Tiangong-2 (TG-2) Space Laboratory.

The hand–arm system is mainly composed of a lightweight arm, a dexterous hand, an electrical cabinet, a global camera, a hand–eye camera and some human–machine interfaces. The 6-DOF lightweight arm and the 15-DOF dexterous hand adopt the modular design philosophy that greatly reduces the design cycle and cost. To reduce the computational burden on the central controller and simplify system maintenance, an electrical system which has a hierarchical structure is introduced.

The prototypical operating experiments completed in TG-2 space laboratory demonstrate the performance of the hand–arm system and lay foundations for the future applications of space manipulators.

The main contributions of this paper are as follows a robotic hand–arm system which can perform on-orbit servicing missions such as grasping the electric drill, screwing the bolt, unscrewing J599 electrical connector has been developed; a variable time step motion plan method is proposed to adjust the trajectories of the lightweight arm to reduce or eliminate the collision force; and a dexterous hand uses the coordinated grasp control based on the object Cartesian stiffness to realize stable grasp. To solve the kinematic mapping from the cyber glove commands to the dexterous hand, a fingertip-position-based method is proposed to acquire precise solutions.

INFORMATION FOR AUTHORS

Please submit to the editorial office author's application form with contact details, a title of the proposed article, number of pages, illustrations and tables and a brief abstract. After receiving information about the acceptance of the proposed paper submit the entire text prepared according to the editorial instructions as well as a complete declaration form.

Submitted articles are subjected to editorial assessment and receive a formal editorial identification number used in further stages of the editorial process. Every submitted article is reviewed. Publication is possible after receiving positive reviews (see review procedure).

The editorial office does not pay royalties.

GUIDELINES FOR PREPARING PAPERS

• Articles for publication in Assembly Techniques and Technologies should have scientific and research character and deal with current issues of the industry.

• Articles must be original, not previously published (if the article is a part of another work i.e. PhD thesis, Habilitation etc. the information about that should be placed in the reference section) .

• The article should involve a narrow topic but treated thoroughly without repeating general knowledge information included in the widely known literature.

• If the problem is extensive break it into articles for separate publications.

• Articles should be of a clear and logical structure: the material should be divided into parts with titles reflecting its content. The conclusions should be clearly stated at the end of the paper.

• The article should be adequately supplemented with illustrations, photographs, tables etc. however, their number should be limited to absolute necessity.

• The title of the article should be given in Polish and English as well as the abstract and key words.

• The article should not exceed 8 pages (1 page – 1 800 characters).

• The article should include mailing and e-mail addresses of the author(s).

• The article should be electronically submitted in * doc or * docx format. Equations should be written in the editors, with a clear distinction between 0 and O. If the equations exceed the width of column (8 cm) they must be moved, otherwise use double width column (16 cm).

• The editorial staff does not rewrite the texts or prepare illustrations. Apart from doc, * docx formats it is recommended to submit the source files of illustrations (in *.eps, *jpg or * tif format).

• Drawings and graphs must be clear, taking into account the fact that the width of the columns in the magazine is 8 cm, width of the single column - 17 cm, height of the column - 24.5 cm.

• The text on the drawings cut to the size must be legible and not less than 2 mm.

• The authors are required to give at the end of the article a full list of sources used for the paper. The text must include citation references to the position of cited work in the bibliography. The bibliography prepared according to the references in the text must include: books – surname and first letter of the author's name, title, publisher, year and a place of publication (optionally page numbers), magazines – author's name and surname, title of the article, title of the magazine, number, year and optionally page numbers. The bibliography should present the current state of knowledge and take into account publications of world literature.

• The authors guarantee that the contents of the paper and the drawings are originally their property (if not, the source should be indicated). The authors who submit the paper, will receive the following documents from the Publisher SIGMA-NOT to be signed by them:

   - The declaration on granting a licence

   - The licence agreement

   - The Authors' agreement

   on the right of the Publisher to:

   a) Preservation and reproduction of the article, via production of its copies by paper and electronic way,

   b) Turnover of the copies on which the article has been preserved – by introduction to market, lending or lease of the copies,

   c) Making available to the public, including the Internet pages,

   d) Dissemination as a whole or of its parts for advertisement and/or promotional purposes.

• The editorial staff will document all forms of scientific misconduct, especially violations of the rules of ethics applicable in science.

WYDAWNICTWO *SIGMA-NOT*

ponad **70** LAT NA RYNKU

34 TYTUŁY

125 000 PUBLIKACJI

WYGODNY DOSTĘP
DO ARTYKUŁÓW FACHOWYCH

Nowy

PORTAL INFORMACJI TECHNICZNEJ

www.sigma-not.pl

Zmieniamy się dla Ciebie